Politecnico di Torino

Politecnico di Torino

Corso di Laurea in Ingegneria Biomedica
A.a. 2022/2023
Sessione di Laurea Ottobre 2023

Use of a prostaglandin analog to improve blood flow and tendon regeneration in a rabbit model

Relatori:
Prof. Danilo Demarchi
Prof. Carly S. Filgueira

Candidati:
Davide Magliano, s289351
Marco Mussato, s289344

This thesis is the culmination of a collaborative academic inquiry conducted in partnership with my esteemed colleague, Davide Magliano, from Politecnico di Torino. The research undertaken and the consequent findings presented herein are the fruits of our joint intellectual labour, and as such, the merit is equally attributed to both contributors.

Abstract

Around 30% of musculoskeletal consultations result from tendon and ligament injuries, which translates to a notable health concern with 4 million new cases globally every year. Current medical treatments, such as nonsteroidal anti-inflammatory drugs (NSAIDs), corticosteroids, biologics, and, for severe injuries, surgical remedies, often fall short in restoring optimal tendon function, leading to elevated medical costs, prolonged recovery, and significant productivity loss. Tendons are notoriously slow at healing when compared to other parts of the body. This is because mature tendons are characterized by their dense structure and reduced vascularization. Accelerating the healing process and enhancing regeneration can be achieved by augmenting blood circulation, thus facilitating the delivery of oxygen and essential nutrients while aiding in the clearance of waste products and controlling immune responses. This research focuses on promoting patellar tendon repair by inducing vasodilation, using localized, intra-articular injection of an FDA-approved small molecule drug, Remodulin, in the knee to improve blood flow and accelerate regeneration. A 10-week in vivo study in New Zealand white (NZW) rabbits is presented, consisting of two study groups, a control group (n=4, weekly saline injections) and a treatment group (n=4, weekly Remodulin injections), whereby a right patellar tendon injury was induced in the animals from both groups. We demonstrate sequence optimization for image acquisition on a 7T magnetic resonance (MR) scanner for the rabbit patellar tendon. Importantly, scan time was constrained to within an hour to ensure the animals' well-being under anesthesia. This limitation makes it challenging to achieve sufficient resolution and high signal-to-noise ratio (SNR) while accommodating all intended acquisitions. Acquired images, taken bi-weekly, are instrumental in generating parametric maps that quantify the tendon's healing process using T1, T2, and dynamic contrast enhanced (DCE) sequences. We also present a specialized MATLAB code and user interface developed to

facilitate the image analysis, which involves image uploading, segmentation, parametric map computation, and quantitative data extraction. The sequence optimization and MATLAB code and user interface presented here could be applicable to other longitudinal MR studies of musculoskeletal repair. The next phase of this project involves micro-CT and histological analyses to compare osteophytes in the post-injury knee and assess fibrosis for a cellular view of drug effects on tendon repair. Future studies include exploring therapeutic effects to prevent post-traumatic osteoarthritis progression and alternative delivery methods to optimize tendon healing and repair.

Introduction

Tendon Injury

Tendons are strong, flexible, fibrous tissues responsible for connecting muscles to bones, allowing for efficient motion and force transmission. Unfortunately, these vital structures are prone to injury and degeneration, which can significantly impact an individual's quality of life and result in substantial economic costs for society.[1,2] Tendon injuries are a common type of musculoskeletal injury that frequently result from overuse or age-related degeneration. While damaged tendons can eventually recover, their healing process is often slow and may not fully restore their original strength and structure. As a result, the recurrence rate of tendon injuries is high, and affected individuals may experience prolonged periods of disability and reduced mobility.

Soft tissue injuries, including tendon injuries, account for almost half of all joint injuries in the United States each year.[3] Tendinopathy, which refers to a range of tendon-related conditions, is the most commonly occurring type of tendon injury. It can affect tendons located throughout the body, such as the Achilles tendon, patellar tendon, epicondylitis, and rotator cuff.[4] Individuals who engage in activities that involve repetitive strain or overuse, such as sports or manual labor, are at an increased risk of developing tendon injuries. Additionally, the natural aging process, coupled with the reduced ability of tissues to repair and regenerate, makes older individuals more susceptible to such injuries. Given the aging population and the growing number of individuals participating in physical activities, the incidence of soft tissue injuries, including tendon injuries, is likely to increase, leading to higher healthcare costs and patient morbidity.[3] The economic burden of tendon injuries is significant, as it includes the cost of

treatment, rehabilitation, and lost productivity. Therefore, effective prevention and management strategies for tendon injuries are essential to reduce the morbidity and economic burden associated with such injuries. Such strategies may include targeted exercise programs, protective equipment, and prompt medical intervention to prevent or minimize the extent of tendon injuries. Unfortunately, however, most treatment goals focus on controlling pain and reducing inflammation and swelling of injured tissue. There still remains an unmet medical need for treatment strategies that help in tendon/ligament healing.

Tendon Anatomy and Biology

Tendons, pervasive and structurally dense connective tissue formations, are integral in facilitating the transmission of muscular forces to skeletal structures, thereby enabling joint articulation. They predominantly consist of type I collagen fibers, accompanied by other collagen variations such as type III in the endotenon and epitenon, types IV and V within the vasculature, and type X near entheses in the mineralized fibrocartilage. This intricate configuration of collagen endows the tendon with its robustness, pliability, and durability.[5]

At the microscopic level, tendons exhibit a hierarchical organization. Collagen fibrils, which have a diameter ranging from 100 to 500 nm, are clustered together to form collagen fibers. These fibers are further arranged into subfasicles and subsequently into tertiary fiber bundles. The endotenon, a sheath of connective tissue, envelops subfasicles and fascicles, while the epitenon encompasses the entire tendon, supplying vascularization, lymphatic drainage, and innervation. Tenocytes, spindle-shaped tendon fibroblasts situated between collagen fibers, are essential for the synthesis and maintenance of the tendon's extracellular matrix (ECM).[5,6]

The ECM of tendons is composed of diverse elements that contribute to their structural and functional properties. Proteoglycans, including decorin and aggrecan, and glycosaminoglycans offer hydration, lubrication, and support to the tendon by sustaining the

spacing and alignment of collagen fibrils. Elastin fibers and various glycoproteins also contribute to the functional stability of collagen fibers and aid in the resistance of tensile forces.[6] The elaborate composition and organization of tendons are responsible for their extraordinary mechanical attributes. The parallel alignment of collagen fibrils within collagen fibers enables tendons to tolerate high tensile loads. The crimped or sinusoidal pattern discernible in tendons under light microscopy allows them to extend by 1% to 3% and absorb abrupt mechanical loads. Furthermore, the hierarchical organization and interaction between collagen fibrils at the macroscopic scale determine the overall robustness and integrity of tendons.[5,6]

Comprehending tendon biology is imperative for diagnosing and managing tendon-associated conditions. Alterations in tendon structure and composition may predispose individuals to tendinopathy, a spectrum of disorders characterized by mechanical, degenerative, and overuse-induced injuries, as well as enthesial inflammation. Tendon lacerations, either partial or complete, can result from tendinopathy or trauma. Advanced imaging techniques, such as magnetic resonance imaging (MRI) and ultrasound (US), are critical in assessing the normal and aberrant tendon structures and evaluating tendon pathologies.[6] Unfortunately, tendinopathy can easily go undetected until it manifests as a full blown rupture, providing further evidence for the importance of advanced imaging for injury evaluation and tracking.

In conclusion, tendons display a complex hierarchical organization, primarily composed of collagen fibers and tenocytes embedded within an ECM. The structural and compositional properties of tendons facilitate force transmission and joint stability and movement. A thorough understanding of tendon morphology and biology is crucial for the diagnosis, treatment, and rehabilitation of tendon-related disorders, thereby ensuring optimal patient care and outcomes.

Tendon Pathophysiology

Tendon pathologies, including inflammatory enthesitis and tendinopathy, represent a complex spectrum of diseases that vary significantly in their underlying etiology and clinical presentation. Inflammatory enthesitis, an inflammation of the entheses, or the points where tendons, ligaments, fascia, or the joint capsule attach to the bone, is a defining feature of spondylarthritis. Histological changes linked with this condition may include destruction of fibrocartilage by macrophages, infiltration of lymphocytes within bone, paucity of lymphocytes near the insertion site, and infiltration of macrophages. Tendinopathy, conversely, arises due to mechanical stress, degeneration, and overuse, leading to structural disorganization of collagen, increased mucoid, proteoglycan, and water content, and the enhanced expression of protective factors such as insulin-like growth factor 1 and nitric oxide synthetase. [3,6]

The human tendon is designed to tolerate high mechanical stresses and can change its structure in response to loading by producing more collagen and activating metalloproteinase. These modifications modify the tendon's mechanical strength, viscoelastic characteristics, and stress susceptibility. However, the tremendous forces exerted on tendons during repetitive activities and extensive use in sports often lead to overuse injuries. On the histological level, these injuries are characterized by collagen degeneration, fiber disorientation, thinning, increased cellular activity, changes in tenocyte shape, increased vascular in-growth, and a shift towards a fibrocartilaginous composition. Furthermore, the tendon's appearance changes from a glossy white to a gray-brown amorphous state, indicating a notable loss of integrity and structure. Common signs of tendon degeneration include fibrin deposits, calcifications, and lipid accumulations. This condition is primarily caused by an imbalance between matrix production and deconstruction brought on by mechanical loads and stressors.[5]

On MRI, healthy tendons typically appear dark due to the alignment of collagen and water molecules. However, when injured, tendons can exhibit various changes: tendinosis may

present as an enlarged tendon with increased signal intensity on certain sequences; tendon tears can manifest as areas of heightened signal intensity indicating the tear's extent and orientation; other injuries may cause tendons to gather fluid, alter in size, or change in signal intensity, ranging from low to very high depending on the injury severity and MRI sequence used.[7]

Major structural alterations, including increased amounts of fibronectin, tenascin C, GAGs, aggrecan, and biglycan, as well as overexpression of collagen type I and type III mRNA, are associated with tendon problems on a molecular level. The tendon extracellular matrix (ECM) is also weakened by the actions of several matrix metalloproteinases (MMPs), disintegrin and metalloproteinases (ADAMs), disintegrin and metalloproteinases with thrombospondin motifs (ADAMTSs), and tissue inhibitors of metalloproteinases (TIMPs). Notable are the presence of growth factors like TGF-β and platelet-derived growth factor (PDGF), insulin-like growth factor-1 (IGF-1), prostaglandin E2, interleukin-1, increased expression of cyclooxygenase-2, and neurotransmitters like glutamate and substance P.[5] These mediators can effect tendon ECM degradation, which can in turn, influence the mechanical properties of tendon. The discussion of these mediators elucidates their contributory role in tendon extracellular matrix (ECM) degradation, significantly impacting the tendon's mechanical properties. By understanding these molecular interactions, the pathway towards developing targeted therapeutic interventions for tendon disorders is broadened, aligning with the broader objective of improving tendon health, especially in populations like athletes where tendinopathy is prevalent. [8]

After an injury, the tendon repair and regeneration process initiates through three distinct stages: tissue inflammation, cell proliferation, and remodeling. In the inflammatory stage, a clot forms at the wound site, initiating the release of chemotactic factors that attract inflammatory cells. These cells begin synthesizing various ECM components, including collagen and proteoglycans. The remodeling stage, which begins 6-8 weeks post-injury, is

characterized by a rise in type I collagen synthesis, a decrease in type III collagen, a reduction in cellularity, and a reduction in matrix formation, all of which increase the mechanical strength of the regenerated tissue.[3,6] Growth factors are essential in controlling these processes. Examples of these factors are transforming growth factor-β (TGF-β), insulin-like growth factor-1 (IGF-1), platelet-derived growth factor (PDGF), and vascular endothelial growth factor (VEGF).[2,5]

Additionally, aging significantly impacts the structural properties and metabolism of tendons, making them more susceptible to microdamage, degenerative changes, and decreased healing capability. Chronic tendon disorders, either due to the accumulation of tissue microdamage or the reduced regenerative capacity associated with aging, further exacerbate these complications. As we age, the rate of collagen synthesis decreases while the concentration of cross-linking in the collagen matrix increases, which may contribute to a loss of tensile strength. Further, the rate of cellular metabolism and proliferation decreases, leading to a decline in the tendon's repair capacity.[2]

As evident, the healing process of tendon injury is complex and understanding the mechanisms of tendon degeneration and healing at the molecular, cellular, and tissue levels is pivotal for effective disease management and the development of novel treatment strategies. This understanding can also facilitate the discovery of therapeutic targets and the development of tissue engineering approaches to improve tendon repair and regeneration, thereby enhancing patient outcomes in cases of tendon injuries and diseases.

High Risk Individual

Tendinopathy is a common type of overuse musculoskeletal injury that can cause significant morbidity and disability in the affected population. It is defined as a repeated strain until tiny tears form. While the prevalence of tendinopathy is relatively low in the general

population, specific groups, such as athletes, manual labor personnel, and individuals with comorbidities, are at a higher risk of developing this condition.[4] Athletes, in particular, are highly vulnerable to tendinopathy due to the high-intensity nature of their sports and the frequent and repeated strain or overuse placed on their tendons. The prevalence of tendinopathy among athletes ranges from 10% to 40%[4,9], depending on various factors such as age, type of sport, type of athlete, and hours of training. Manual labor personnel are also at significant risk due to the highly repetitive movements required by their daily tasks and poor workplace ergonomics.[4]

Individuals with comorbidities such as advanced age, obesity, and wheelchair use are also at a higher risk of developing tendinopathy. These conditions result in reduced flexibility, increased load, and stress on the tendons, which can ultimately lead to the development of tendinopathy. Effective interventions, such as targeted exercise programs, ergonomic interventions, and close monitoring of individuals with comorbidities, are necessary to prevent or manage tendinopathy effectively.

Overall, tendinopathy is a prevalent musculoskeletal injury that affects specific groups of the population, and its incidence is likely to increase with an aging population and growing participation in physical activities. Implementing effective prevention and management strategies could help reduce the morbidity and economic burden associated with this condition. Traditional pharmaceutical treatment modalities aimed at controlling inflammation may not be the most effective options and while a short course of NSAIDs may be reasonable for pain treatment, there is no clear evidence that they are effective for chronic tendinopathy.[10]

Unmet medical needs

Tendon injuries bring a significant burden to individual patients, impairing their quality of life, and effect our entire healthcare system. Despite advances in understanding tendon

biology and the biological mechanisms that regulate repair, the development of effective treatment strategies for tendon injuries remains a significant challenge.[3] Current treatment options for tendon injuries are limited, and there is no gold standard approach for their management.[2] Conservative measures, such as rest, ice, compression, and elevation, are often used as the first-line treatment, but their efficacy is often limited. In more severe cases, surgical intervention is often required, and the effectiveness of such intervention remains unclear.[11] Unfortunately, surgical interventions can result in significant morbidity and require a prolonged recovery period.[12]

Pharmacological treatments, such as nonsteroidal anti-inflammatory drugs (NSAIDs), are commonly used to manage pain and inflammation associated with tendon injuries. However, the efficacy of these treatments is still unclear, and they are often associated with adverse effects, such as gastrointestinal disturbances, cardiovascular events, and renal dysfunction.[10] Furthermore, there is no specific pharmacological treatment available that can promote tendon healing or regeneration.[13] Recent research has shown promising results with tissue engineering, gene therapy, and biological treatments for tendon injuries. These emerging treatments have shown the potential to promote tendon healing and regeneration, reducing the need for surgical intervention and prolonged recovery periods. However, there is still a lack of high-quality clinical evidence to support the use of these treatments.[11,12]

In conclusion, developing effective treatments for tendon injuries remains an urgent need. Further research is needed to identify optimal surgical techniques and pharmacological treatments. Emerging treatments, such as tissue engineering, gene therapy, and biological treatments, hold great promise for the future of tendon injury management, but further clinical trials are needed to establish their efficacy and safety. Developing a personalized treatment approach is also crucial in effectively treating tendon injuries and improving patient outcomes.

Need to study tendon injuries

Tendon injuries are a significant burden on the healthcare system and can have a negative impact on patient outcomes. These injuries can increase healthcare utilization, leading to increased healthcare costs, placing a burden on the healthcare system. Tendon injuries can also limit an individual's productivity, resulting in lost wages and decreased economic productivity. Moreover, these injuries can lead to discomfort and limitations on activities, ultimately leading to decreased quality of life.[14]

To effectively address tendon injuries, several challenges must be overcome. Tendons have a limited ability to repair and regenerate due to their limited blood supply, making it difficult to treat these injuries effectively. Furthermore, the limited evidence to support the use of certain treatments over others and a lack of consensus on the most effective treatment approach make it challenging to determine the best course of treatment for individual patients. Additionally, limited access to specialized care for tendon injuries, particularly in remote or underserved areas, can further exacerbate the challenges associated with treating these injuries.[3] To address these challenges, further research is necessary to identify optimal treatment approaches, when to intervene, and methods to improve access to care. Collaborations between healthcare providers and policymakers could help facilitate these efforts. Developing new approaches for the prevention and management of tendon injuries, as well as improving access to specialized care for those who need it most, could help reduce healthcare utilization and increase productivity, ultimately leading to improved quality of life for individuals with tendon injuries.

Moreover, it is essential to educate patients, particularly those at high risk, on ways to prevent tendon injuries. This may involve emphasizing the importance of proper warm-up and stretching techniques, using proper equipment, and engaging in activities that promote tendon

health. By focusing on prevention and early intervention, we may be able to reduce the incidence and severity of tendon injuries and improve patient outcomes.

In conclusion, tendon injuries pose a significant challenge to the healthcare system and can have a negative impact on patient outcomes. Addressing these challenges will require further research and collaboration between healthcare providers and policymakers. Developing new approaches for the prevention and management of tendon injuries, improving access to care, and educating patients on ways to prevent these injuries could ultimately improve patient outcomes and reduce the burden of tendon injuries on the healthcare system.

The Rabbit Model: Benefits of Its Anatomy Over Other Animals

Given the complexity of studying tendinopathy, as described above, the selection of an appropriate animal model is crucial. The use of rabbits as an animal model for the study of tendinopathy presents a distinct set of advantages and challenges. The larger size of rabbit tendons compared to those of rats, for example, allows for easier manipulation during surgical procedures and provides larger samples for histopathological and molecular analysis. This is a significant benefit, as these analyses play a critical role in evaluating the organizational and compositional parameters of tendinopathy, as outlined previously.[15] Further, clinically available imaging equipment is more adaptable for study with larger animals than rodents.

However, the care and maintenance of rabbits require specialized knowledge and meticulous attention. Rabbits are susceptible to postoperative complications and certain health issues, which can threaten their survival during the course of a study. Thus, while rabbits may offer specific advantages as an animal model for tendinopathy, these potential complications necessitate a thorough understanding of rabbit physiology and behavior to ensure their well-being and the reliability of the study.[15]

Despite these challenges, the use of rabbits in tendinopathy studies can still be preferable over other large animals such as dogs or horses, which are less practical due to their size and associated costs. Additionally, rabbits present a more robust set of biological tools available for study, including a wealth of genetic and physiological information. It is also worth noting that rabbits, like humans, are mammals, which implies a certain level of anatomical and physiological similarity that makes them a more suitable model than non-mammalian species.[15]

While rabbits offer several advantages, they cannot fully replicate the human condition of tendinopathy due to inherent differences in anatomy, physiology, and biomechanics. Like all animal models, rabbits may only be able to reproduce certain aspects of human tendinopathy. Therefore, it is important to use a combination of modalities to assess efficacy and to consider supplementing rabbit models with other experimental approaches to fully understand the complexity of tendinopathy.[15]

In conclusion, the choice of rabbit as an animal model for tendinopathy studies is largely justified by their anatomical and physiological similarities to humans, the practicality of their size and cost, and the wide range of biological tools available for study. However, the care and welfare of the rabbits, as well as the inherent limitations of using any animal model, must be considered when designing and conducting these studies.

Standard treatments and their limitations

Palliative Treatments

Palliative treatments for tendon injuries, including nonsteroidal anti-inflammatory drugs (NSAIDs) and other approaches, aim to alleviate pain and inflammation. The choice of administration route, such as intralesional injection, systemic methods, or topical application, significantly influences treatment effectiveness and safety. Each approach has its benefits and

considerations, making it essential to select the most suitable method based on factors like the injury's severity, location, patient tolerance, and the therapeutic agent's pharmacokinetics.

NSAIDs

NSAIDs (nonsteroidal anti-inflammatory drugs) are often prescribed to manage pain and reduce swelling in tendon and ligament injuries. They work by inhibiting the production of prostaglandins, which are responsible for inflammation. However, their impact on healing is multifaceted. While they can inhibit the proliferation and migration of tendon cells, NSAIDs tend to promote collagen synthesis. Studies on animals have yielded mixed results, with some showing no significant difference in tendon strength after NSAID use, while others indicated reduced strength.[16,17] These drugs can decrease adhesion formation, improving range of motion, but their effects on joint laxity following ligament injury require further study. Overall, NSAIDs' effects on tendon and ligament healing are complex and still not fully understood, necessitating further research to clarify their impacts.[18] Moreover, adverse effects in the gastrointestinal tract and kidney can reduce patient compliance, limiting the use of these drugs.

Corticosteroids

Corticosteroid injections remain a subject of controversy in treating tendinopathy. Although some studies have suggested potential benefits such as pain relief, due to their anti-inflammatory properties and improved function, there are significant concerns, including side effects and the risk of tendon rupture associated with these injections.[19–21] To mitigate risk of rupture, corticosteroid injections are often administered alongside normal saline under the guidance of ultrasound imaging. This technique aims to induce local mechanical changes, primarily targeting the new blood vessels and accompanying nerves that are common in tendinopathy and often a source of pain. By disrupting these structures, the injections may

alleviate discomfort and improve patient outcomes. The utility and safety of corticosteroids in tendinopathy management are still debated due to inconsistent evidence and varying study outcomes. Further research is needed to clarify short-term versus long-term benefits as well as their role and risks, ensuring patients receive effective and safe care.[22]

Therapeutic Interventions

In the domain of therapeutic intervention for tendon injuries and tendinopathy, a wide range of approaches is employed, reflecting the absence of a gold standard for treatment. This multitude of options underscores the complexity of managing tendon injuries and highlights the need for tailored solutions that suit individual patient needs and the specific characteristics of their condition. These approaches include scaffolds (autografts, allografts, xenografts, bioengineered scaffold materials), biologics (growth factors, stem cells, gene therapy, platelet-rich plasma), small molecules (nitroglycerine, curcumin), and minimally invasive techniques.

Scaffolds

Scaffolds play a pivotal role in the realm of therapeutic intervention for tendon injuries and tendinopathy. When native tissue proves insufficient to bridge a torn tendon or ligament, autografts, allografts, or xenografts can serve as viable alternatives. However, these graft-based reconstructions often yield suboptimal results due to factors such as donor site morbidity, immunological rejection, and poor graft integration, contributing to re-tears in a substantial number of cases.[2] The gold-standard is autografts, which despite their immediate structural support ultimately undergo graft remodeling that can result in diminished mechanical properties and adhesion formation.[23]

To address the challenges associated with graft remodeling, particularly in the context of tendinopathy treatment, the exploration of bioactive molecules such as cells and growth

factors has been underway. For instance, alginate scaffolds have been designed to encapsulate and accurately release bioactive molecules like fibroblasts or type I collagen, with a notable achievement being the controlled release of Transforming Growth Factor Beta 1 (TGF-β1) to promote cell proliferation, showcasing a potential pathway to enhance graft remodeling.[24] Moreover, the advancement of biomimetic scaffolds, which are paired with bioactive growth factors, aim to replicate the natural tendon tissue environment, thereby fostering better healing and potentially improving graft remodeling outcomes.[25] The functionalization of scaffolds with bioactive molecules is also a significant stride, where synthetic biomaterial scaffolds are modified with biological properties such as cytokines or anti-inflammatory drugs, either during or immediately post scaffold preparation, to promote better outcomes in tendon repair and regeneration.[26] Furthermore, tissue engineering strategies have emerged, combining cells, scaffolds, and bioactive molecules, as seen in the treatment of patellar tendinopathy, aiming to enhance the remodeling and healing of tendon grafts, with the expression of factors like Vascular Endothelial Growth Factor (VEGF) during graft remodeling showcasing the potential of this integrative approach.[27] Through these examples, it's evident that the intersection of bioactive molecules and scaffold technology holds promise in addressing the complexities of graft remodeling in tendinopathy treatment. Additionally, synthetic non-degradable materials, including silk, have emerged as potential candidates. Silk exhibits enzymatic degradability over an extended period, making it an attractive option for tendon repair. Silk scaffolds have demonstrated promise in large animal models and can attain mechanical properties comparable to native tendons. Other synthetic scaffold materials include polystyrene, poly-l-lactic acid, polyglycolic acid, and poly-dl-lactic-co-glycolic acid (PLGA), and degradable polyesters.[28] However, the adoption of synthetic grafts in clinical practice remains a challenge.[27] The wide array of scaffold options reflect the absence of a gold standard in tendon injury treatment,

emphasizing the need for further research as well as potential personalized solutions tailored to individual patient needs and condition characteristics.

Injection of biologics

The injection of biologics offers a promising avenue in the therapeutic intervention for tendon injuries and tendinopathy. Various cell types, including tenocytes, dermal fibroblasts, and mesenchymal stem cells (MSCs), are being explored for their potential in tendon tissue engineering. Tenocytes, renowned for their role in ECM synthesis and collagen fiber formation, have shown promise in improving mechanical strength and matrix deposition in tendon defects.[27] Dermal fibroblasts, a readily accessible alternative cell source, have demonstrated similar potential in enhancing tendon engineering and healing. MSCs from different tissues, such as bone marrow and adipose, offer multilineage differentiation potential and have been applied to promote tendon tissue repair, showing increased collagen production and tenogenic differentiation.[27]

Bioactive molecules, including growth factors, have been investigated for their potential in enhancing tendon healing. Growth factors like IGF-1, TGF-beta, bFGF, and PDGF-BB have been associated with collagen synthesis and matrix production, and their application has shown promise in accelerating the healing process. These factors stimulate cell proliferation, migration, and the expression of tendon-specific genes, offering potential benefits in tendon tissue engineering.[27]

The local administration of structural proteins and bioactive compounds can be achieved with minimally invasive techniques by injecting biopolymers, such as collagen or fibrin gels. Making sure that these materials polymerize into ordered scaffolds that support tendon repair is still a difficulty. The creation of aligned injectable gels could be a promising step toward replicating the architecture of original tissue.[2]

Platelet-Rich Plasma (PRP) is another bioactive component derived from the patient's own blood that is being explored for its potential in promoting tendon healing. PRP is rich in growth factors and cytokines, which is proposed to accelerate the healing process and enhance tissue regeneration. Several ongoing studies are investigating the use of PRP in tendon healing, although the exact mechanisms involved are still not fully understood.[5,22,27] Indeed, the efficacy of PRP treatment on injured tendons is highly controversial and there are many factors that can influence outcomes.[29]

Additionally, autologous blood injection and the use of substances like polidocanol are being explored as potential treatments for tendinopathy. These approaches aim to induce healing by providing cellular and humoral mediators or by targeting areas with neovascularization outside the tendon, which may be involved in pain generation.[22] The multitude of approaches within the realm of biologic injection highlights the complexity of managing tendon injuries and the ongoing efforts to find tailored solutions that promote effective healing.

Small molecules

In the realm of small molecules, two promising options for managing tendinopathies are nitroglycerin and curcumin. Nitroglycerin, primarily known for angina relief, has shown potential in promoting tendon healing through nitric oxide (NO) release, reducing pain, and improving function in affected patients, exhibiting a broader role in inflammation research. The study of Ali et al. explored NO's role in tendon healing using injured tendon models in rats and humans. NO, delivered via glyceryl trinitrate (GTN) patches, demonstrated significant positive effects in clinical trials on patients with various tendinopathies, including Achilles tendinopathy, tennis elbow, and supraspinatus tendonitis. Enhanced tendon healing was observed in animal models, and increased collagen synthesis was noted in cultured human cells

with NO addition.[30,31] Curcumin, primarily recognized for its anti-inflammatory properties, has been examined for its therapeutic potential in tendon healing across several studies. Utilizing injured tendon models in rats, researchers have explored the effects of curcumin on tendon injuries. In one particular study, an Achilles tendon injury model was employed, where tendon injuries were surgically created and repaired under anesthesia.[32] The administration of curcumin, although the exact method wasn't detailed, demonstrated significant improvements in tendon healing properties, as evidenced by extensive deposition of well-organized collagen fibers, decreased Malondialdehyde (MDA) levels, and enhanced biomechanical properties of the regenerated tendon tissues.[33] Another investigation highlighted the utilization of controlled-release curcumin, a formulation aimed at prolonging the delivery of curcumin, showcasing its ability to promote tenogenesis and inhibit osteogenesis in a pathological microenvironment, hinting at a new therapeutic strategy for tendon diseases.[34] While these studies predominantly involved animal models, specifically rats, they underscore the promising potential of curcumin in promoting tendon healing and possibly managing musculoskeletal injuries. Moreover, curcumin's anti-inflammatory properties have been noted to suppress common inflammatory mediators in tendinopathies, extending its promise to the management of other musculoskeletal injuries like ligament and meniscus damage, common in sports medicine, although its effectiveness at cellular and molecular levels warrants further exploration.[35]

However, delivering small molecules, such as curcumin, effectively to these tissues, especially those with limited blood supply, presents a challenge. Options like intra-articular injection and trials comparing curcumin with other treatments, such as steroid injections, warrant exploration. Additionally, understanding curcumin's pharmacokinetics, including dose-response relationships and potential synergistic effects with other compounds, is crucial for its clinical application.[30,31]

In conclusion, nitroglycerin and curcumin offer exciting small molecule prospects for managing tendinopathies, each through distinct mechanisms. Nitroglycerin enhances tendon healing via nitric oxide, while curcumin's anti-inflammatory properties hold promise for musculoskeletal conditions. Research into optimal delivery methods and potential synergies with existing treatments will be key to realizing their therapeutic potential in musculoskeletal medicine.

Minimally invasive approach

The minimally invasive approach for acute Achilles tendon repair, as discussed by Alcelik *et al*[36], and elucidated further through various sources, is a surgical procedure that aims to repair the ruptured Achilles tendon while minimizing the incision size, thereby reducing trauma to surrounding tissues and promoting a quicker recovery. The procedure begins with a small incision, typically about an inch long, made at the site where the tendon ends are located, significantly smaller compared to the one made in traditional open surgery, thus the term "minimally invasive." A specially designed suture device is then maneuverer up and around the tendon, guiding the sutures into the tendon and pulling them through the small incision. The sutures are then pressed to "lock" into the tendon, ensuring they are securely in place before being tied so that the tendon ends meet, achieving the correct length of the tendon which is crucial for proper functionality. Once the sutures are securely tied and the correct length of the tendon is achieved, the wound is closed. About a week post-surgery, patients begin motion exercises which aid in reducing tendon adhesions and aligning the collagen fibers of the tendon into a stronger configuration, with more motion, gentle strengthening, and eventually walking and running integrated into the therapy program over time. This rehabilitation phase is crucial for restoring functionality and strength to the tendon and surrounding muscles. This approach is particularly advantageous as it aims to reduce common complications associated with

traditional open surgery such as wound healing issues and scar adhesions. By potentially reducing post-operative pain and facilitating a quicker return to normal activities, minimally invasive surgery is beneficial in decreasing the chance of wound complications and re-tearing, while promoting a more rapid return to full activity. This technique is noted for enabling quicker functional recovery due to reduced trauma to adjacent soft tissues, which potentially leads to less post-operative pain and a faster return to normal activities.[36]

A comparative study revealed that minimally invasive surgery (MIS) had a shorter surgery duration, lower rate of post-operative wound necrosis, fewer infections, and less scar tissue adherence compared to open surgery. However, the latter had a lower rate of sural nerve palsy and postoperative palpable knot, showcasing each method's unique advantages and drawbacks.[37]

Moreover, MIS often results in shorter hospital stays and improved functional outcomes, marking significant benefits over traditional open surgical procedures. Yet, it's technically demanding and might not be suitable for all tendon pathologies or patients, with concerns regarding inadequate surgical exposure potentially leading to suboptimal outcomes in some cases. [36,38]

Imaging modalities for diagnosis

Introduction and comparison

Imaging modalities are indispensable tools for improving the diagnosis of different tendon injuries. In this chapter, we discuss various imaging modalities, such as computed tomography (CT), ultrasound (US), and magnetic resonance imaging (MRI), that can be utilized to identify tendon injuries.

Computed tomography is an imaging technique that uses X-rays and computer processing to create detailed cross-sectional images of the body. The benefit of CT is that it can

produce detailed pictures of bone and soft tissue structures. However, because CT has a limited ability to distinguish between various types of soft tissues[39] and exposes the patient to ionizing radiation, it might not be the optimal method for diagnosing tendon injuries.

Ultrasound (US) is a non-invasive imaging technique that uses high-frequency acoustic waves. US has the advantage of using non-ionizing radiation, is portable, and can be performed in an outpatient setting. Additionally, it allows for dynamic imaging of tendons at multiple angles and under stress. However, US has some limitations in the diagnosis of tendon injuries. Ultrasound waves are unable to penetrate through bone and gas, which can act a barrier to the underlying tissues, such as some ligaments and deep-lying tendons, including the cruciate ligaments of the knee or those in the pelvis.[40]

Magnetic resonance imaging is a non-invasive imaging modality that uses non-ionizing electromagnetic radiation to create cross-sectional images of the body in any plane. MRI is considered the gold standard for the diagnosis of tendon injuries, as it provides high-resolution images of both bone and soft tissue structures. However, MRI is more expensive than other imaging modalities, and it is not as widely available.

In conclusion, each imaging technique can effectively diagnose tendon injuries with its own advantages and limitations. CT provides detailed images, but it exposes the patient to ionizing radiation. Ultrasound is non-ionizing and portable but cannot image the tendon underneath bones and gas. MRI is considered the gold standard for the diagnosis of tendon injuries, but it is more expensive and less widely available.

Computed Tomography

Computed tomography is a radiological technique that allows for 3D visualization of anatomical structure. It was created to overcome some of the limitations of traditional radiography, such as:

- information related to a single projection
- difficulty observing different bones and soft tissues close together
- shielding effect of dense tissues (such as bones)

CT works by rotating an x-ray tube around the body that acquires planar x-rays images and the detectors come to form a complete ring around the patient. The data are then reconstructed to produce a distribution of the linear attenuation coefficient in the body, that forms a map of tissues and various internal structures. CT scans have the advantage of being quick and non-invasive, making them well-suited for emergency situations. However, CT scans utilize ionizing x-ray radiation that can increase the risk of cancer and other health problems through repeated exposure. Furthermore, CT is not ideal in evaluating soft tissues such as tendon and ligaments since it is not able to differentiate between healthy and injured soft tissues due to minor differences in the attenuation coefficient.

Ultrasound

Ultrasound imaging is a popular non-invasive method that relies on the principles of high-frequency acoustic waves (1-2 MHz < f < 20 MHz) and their reflection off internal body structures. The system is based on the direct piezoelectric effect, in which an acoustic wave from a transducer is reflected off tissue, converting mechanical energy into electrical energy. The mechanical energy reflected from the tissues is sensed by the sensors that transform it into electrical energy, exploiting the direct piezoelectric effect. The safety profile of ultrasound imaging has led to its widespread use in clinical settings. Unlike other imaging modalities such as CT, ultrasound utilizes non-ionizing radiation, which does not carry the same risks of ionizing radiation exposure.

Because of this safety aspect, ultrasonography is the recommended method for monitoring conditions over time and in situations where ionizing radiation exposure could be dangerous, such as for pregnant women or young patients. Also, the high temporal resolution of

ultrasonography, which can record up to 300 pictures per second, enables efficient monitoring of dynamic events. However, ultrasonography is not without its limits when it comes to diagnosing tendon injuries. These limitations include operator dependence and the inability to see some tendons and ligaments that are hidden or covered by bone. Despite its drawbacks, ultrasonography is still utilized in many clinical situations because it has a better safety profile than CT imaging.

Magnetic Resonance Imaging

Magnetic resonance imaging (MRI) is a non-invasive imaging technique based on nuclear magnetic resonance. It creates high-quality cross-sectional images of the body in any plane using a strong magnetic field and nonionizing electromagnetic (radiofrequency) radiation. Current advancements in MRI technology have concentrated on increasing the image resolution and reducing the scanning time. One such advancement is the creation of high-field MRI devices that employ more powerful magnetic fields to generate higher-resolution images.

The superior ability of MRI to detect soft tissue and osseous injuries confirms that it is the most comprehensive imaging modality. MRI is useful for the diagnosis of a wide range of medical conditions, including tumors, neurological disorders, and cardiovascular diseases. Compared to other imaging modalities, such as CT or X-ray, MRI's superior soft tissue contrast enables the detection of small changes in tissue composition and structure.

Despite its benefits, MRI has several limitations. Access to this modality may be constrained in some settings because of its high cost, need for specialized equipment, and shortage of trained personnel. Additionally, owing to the potential risk of magnetic field interference, MRI may not be appropriate for patients with certain medical conditions, such as pacemakers or metallic implants.

Numerous studies have shown how well MRI can assess tendon injuries, such as tendinitis, partial or total tears, and degenerative changes. According to Miller *et al.,* the sensitivity of US for detecting both lateral and medial epicondylitis ranged from 64 to 82%, while the sensitivity of MRI was between 90 and 100%.[41] Similar to this, when comparing the sensitivity of US and MRI, US was demonstrated to be an effective diagnostic tool for identifying partial and full-thickness Achilles tendon tears with high sensitivity and specificity, but MRI was generally considered to be more sensitive in detecting partial tears. [3,14]

MRI is an important diagnostic tool for evaluating tendon injuries and has become an essential imaging modality in the evaluation of musculoskeletal injuries because of its ability to provide detailed information about the tendon structure, surrounding soft tissue, and bone.

Impact of magnetic field strengths on image quality: 1.5T vs 3T vs 7T.

MRI systems with varying magnetic field strengths, such as 1.5T, 3T, and 7T, provide different levels of image quality. The magnetic field strength influences the signal-to-noise ratio (SNR), a key factor in determining image quality. Higher field strengths yield higher SNR, producing images with enhanced detail and contrast resolution, which allows for improved visualization of anatomical structures and detection of pathological changes. However, higher field strengths can also result in susceptibility artifacts and challenges related to radiofrequency power deposition and magnetic field homogeneity, potentially affecting image quality.

Factors influencing MRI system selection

The choice of a particular MRI system depends on factors including clinical application, patient population, cost, and resource availability.

Clinical application: Specific MRI applications may necessitate different magnetic field strengths for optimal image quality and diagnostic capabilities. For example, 3T MRI systems

are often preferred for neuroimaging, musculoskeletal imaging, and prostate imaging, while 7T MRI systems may be required for specialized applications or advanced research.

Patient population: MRI system selection can depend on the patient population. For example, 1.5T MRI systems may be suitable for general clinical practice and pediatric imaging, while 3T and 7T MRI systems might be more appropriate for populations with complex or subtle pathologies needing higher resolution imaging.

Cost: Financial considerations significantly impact MRI system choice. Higher field strength MRI systems generally have higher initial and operational costs and may require specialized infrastructure and maintenance, leading smaller healthcare facilities or budget-conscious institutions to choose lower field strength systems like 1.5T MRI machines.

Availability of resources: The selection of a MRI system can be influenced by the accessibility of resources, such as trained personnel, technical support, and compatible software. For instance, 7T MRI systems may require specialized technicians and physicists and customized software, which might not be readily available in all healthcare settings, limiting high-field MRI system adoption.

Advantages of 7T MRI systems

Improved image quality

One of the most significant benefits of a 7T MRI system is the remarkable improvement in image quality when compared to 1.5T and 3T systems. The higher magnetic field strength of 7T MRI results in several advantages that contribute to enhanced image quality. Firstly, the increased SNR allows for more precise visualization of small anatomical structures and better differentiation between closely related tissue types. This heightened level of detail enables clinicians to identify and characterize subtle pathological features, ultimately enhancing diagnostic accuracy. Secondly, the higher field strength facilitates advanced imaging

techniques, such as improved chemical shift imaging and superior susceptibility-weighted imaging. These methods allow for more accurate tissue characterization and provide additional information that can be critical for diagnosis and treatment planning. Lastly, the higher magnetic field strength allows for reduced acquisition times while maintaining or improving image quality. This advantage is particularly critical for patients with movement disorders, claustrophobia, or those undergoing dynamic imaging studies that require multiple scans in a single session. Faster acquisition times result in a more streamlined scanning process, minimizing the impact of patient motion on image quality and reducing the likelihood of patient discomfort or anxiety during the scanning procedure.

Enhanced diagnostic capabilities

The superior image quality provided by 7T MRI leads to enhanced diagnostic capabilities across various medical disciplines, offering several advantages in the clinical setting. Firstly, the increased SNR allows for the improved detection of subtle pathologies that may be challenging to identify at lower field strengths. These include tiny lesions, microhemorrhages, and early-stage tumors, which are crucial for early diagnosis, treatment, and monitoring of a wide range of medical conditions, ultimately leading to better patient outcomes. Secondly, the higher resolution facilitated by 7T MRI enables more accurate visualization of small anatomical structures. This advantage is particularly beneficial when examining complex regions such as blood vessels, nerves, and intricate brain structures, where greater detail is required for accurate diagnosis and treatment planning. Lastly, the advanced imaging capabilities of 7T MRI allow for more precise assessments of disease progression and treatment response. This is vital in various clinical scenarios, including surgical planning, monitoring therapeutic interventions, and identifying potential complications or disease

recurrence. The enhanced diagnostic capabilities provided by 7T MRI contribute to improved clinical decision-making, leading to more targeted and effective patient care.

Improved research capabilities

7T MRI systems offer significant advantages for research purposes across various disciplines, providing researchers with several key benefits. Firstly, the advanced imaging capabilities of these systems, facilitated by the increased SNR and higher resolution, allow for more precise and sensitive studies of tissue structure and function. This enables the investigation of complex biological processes and the assessment of subtle changes that may not be detectable with lower field strength systems, leading to a better understanding of various disorders and the development of novel therapeutic strategies. Secondly, 7T MRI facilitates improved quantitative imaging techniques, such as T1 and T2 mapping, which allows for the evaluation of tissue properties and assessment of their integrity. This advantage is invaluable for investigating the structural changes associated with various medical conditions, including degenerative diseases, tissue regeneration, and response to treatment. Additionally, improved quantitative imaging plays a crucial role in monitoring the efficacy of treatments and understanding their impact on tissue organization and function. Lastly, the higher resolution and increased SNR provided by 7T MRI enable researchers to explore subtle changes and processes in various fields of research, contributing to the advancement of medical knowledge. By offering enhanced visualization of small anatomical structures and more accurate characterization of tissue properties, 7T MRI systems equip researchers with powerful tools for delving into the intricacies of various biological systems, driving the progress of medical research. In conclusion, the advantages of 7T MRI systems extend beyond clinical applications, providing researchers with advanced tools for investigating a wide range of biological processes and contributing to the advancement of medical knowledge in various disciplines.

Challenges

There are, however, challenges associated with higher field strengths that can potentially affect image quality. One particular challenge is the increased susceptibility to artifacts, such as those caused by differences in magnetic susceptibility between tissues or the presence of metal implants in the body. These artifacts can compromise the overall image quality and may require additional post-processing techniques or specialized sequences to mitigate their effects. Another challenge related to higher field strengths is the issue of radiofrequency (RF) power deposition. As the magnetic field strength increases, so does the amount of RF energy absorbed by the body, which can cause heating of tissues. This necessitates the use of specific absorption rate (SAR) monitoring and the implementation of safety guidelines to ensure that RF energy levels remain within safe limits. Additionally, the design and optimization of RF coils become more complex at higher field strengths, which can impact image quality and necessitate the use of parallel imaging techniques or multi-channel coil arrays. Finally, achieving magnetic field homogeneity becomes more challenging as the field strength increases. Inhomogeneities in the magnetic field can lead to spatial variations in signal intensity and image distortion, particularly in larger field-of-view (FOV) acquisitions. To address this issue, advanced shimming techniques and field mapping methods may be required to optimize field homogeneity and maintain image quality.

In summary, while higher magnetic field strengths offer the potential for improved image quality and diagnostic capabilities, they also present challenges related to susceptibility artifacts, radiofrequency power deposition, and magnetic field homogeneity. To fully harness the benefits of high-field MRI systems, these challenges must be carefully addressed through the development and implementation of appropriate hardware, software, and imaging techniques.

MRI: Different analytical methods of study

T2 sequence

MRI T2 sequence is a specialized imaging technique that uses the T2 relaxation time of tissues to create detailed images. The core principle is measuring the spin-spin relaxation time, which indicates how quickly transverse magnetization decays to 37% of its initial value. This decay is influenced by the interactions between water protons and their surroundings, allowing T2 mapping to effectively differentiate between various tissue types. By focusing on T2 relaxation time, this method reveals subtle differences in tissue properties, providing insight into the diversity within the examined area[42,43].This technique is particularly notable for its ability to produce high-resolution images, a feature essential for the detailed visualization of tendon structures. Enhanced resolution facilitates a thorough examination of the tendon, uncovering its anatomy and any pathological deviations, thereby fostering a more comprehensive and accurate evaluation of the tissue. Beyond its capability for qualitative insights, T2 mapping excels in delivering quantitative data on tissue properties, a feature pivotal for the objective comparison of tissue characteristics. This quantification enables clinicians and researchers to discern variations in tissue composition and structure, a critical aspect for monitoring pathological progression and appraising therapeutic efficacy[42,43].

T2 mapping demonstrates particular effectiveness for tendon tissue due to its ability to differentiate between complex structures within the tendon. This specificity allows for a detailed analysis of collagen fiber arrangement, extracellular matrix composition, and water content distribution within the tendon, providing valuable insights into the tendon's health and condition. The sensitivity of T2 mapping enables the detection of subtle changes in the tendon during the healing process. This capability is vital for identifying early signs of tendon healing

or degeneration, allowing for timely intervention and adjustment of treatment strategies to optimize healing outcomes.

Delving deeper into its applications, T2 mapping offers a unique perspective into the interaction between collagen structure and water content in tendons. By assessing the distribution and mobility of water molecules within the tendon, T2 mapping sheds light on the microstructural changes occurring during the healing process, providing insights into the collagen network's integrity and the overall health of the tendon tissue. The insights gained from T2 mapping are invaluable for monitoring the progress of tendon healing. By providing both qualitative and quantitative data on tendon structure and composition, this technique allows clinicians and researchers to assess the efficacy of different treatment approaches, tailor interventions based on individual healing trajectories, and optimize patient outcomes.

Variable Flip Angle T1 sequence

Variable Flip Angle (VFA) T1 sequence is an advanced imaging modality that leverages varying flip angles to compute the T1 relaxation time of tissues, generating meticulous images. The fundamental principle revolves around measuring the spin-lattice relaxation time, reflecting the time taken for longitudinal magnetization to return to its original state. This characteristic decay, governed by the interactions between hydrogen protons and the surrounding environment, enables VFA T1 mapping to distinctly differentiate among diverse tissue types. Noteworthy for its potential to yield high-definition images, VFA T1 mapping is indispensable for the precise visualization of tendon architectures. The enhanced resolution promotes an in-depth exploration of the tendon, unveiling its anatomical structure and any pathological deviations, thereby promoting a more holistic and accurate assessment of the tissue. Beyond qualitative insights, its application has proven particularly promising in the evaluation of tendon tissues, where it facilitates a meticulous analysis of the matrix

composition, providing valuable insights into both the morphological and functional characteristics of these critical connective tissues. This quantitative data is invaluable for the accurate diagnosis and effective monitoring of various tendon-related disorders, such as tendinopathies. The sensitivity of VFA T1 mapping facilitates the detection of subtle alterations in the tendon during the healing phase. The insights rendered by VFA T1 mapping are instrumental for monitoring the progress of tendon healing. By supplying both qualitative and quantitative data on tendon structure and composition, this technique empowers clinicians and researchers to gauge the efficacy of various treatment regimens, tailor interventions based on individual healing trajectories, and optimize patient outcomes. Through the amalgamation of qualitative imagery and quantitative data, VFA T1 mapping emerges as a potent tool in advancing the understanding and treatment of tendon-related ailments.

Dynamic Contrast Enhanced MRI

Dynamic Contrast Enhanced MRI (DCE-MRI) is a pivotal, non-invasive imaging modality employing contrast agents to dynamically visualize and evaluate tissue vasculature in real-time. This technique stands out for its technical advantages, particularly its ability to provide high-resolution images and quantitative assessments of tissue perfusion and vascular permeability, which are instrumental for accurate diagnoses and insightful evaluations. The quantitative nature of DCE-MRI also paves the way for a more nuanced understanding of tissue vascularization, which is often crucial in deciphering various pathological conditions.

In the realm of tendon tissues, DCE-MRI has emerged as a significant tool. It facilitates precise visualization of tendon vascularity, a key aspect often implicated in various tendon disorders. By employing DCE-MRI, clinicians and researchers can assess the extent of vascularity and the nature of vascular changes in tendon tissues. This is indispensable for

diagnosing tendinopathies, monitoring treatment responses, and devising effective treatment strategies, which is a leap forward in managing tendon-related disorders.

A deeper examination into the applications of DCE-MRI reveals a vast spectrum of use cases extending beyond tendon tissues. In oncology, it is a robust tool for tumor detection, characterization, and monitoring treatment responses by evaluating tumor vascularization—a critical indicator of tumor aggressiveness and treatment efficacy. Similarly, in neurology, DCE-MRI assists in assessing disorders like stroke and multiple sclerosis by providing insights into altered blood-brain barrier permeability and cerebral perfusion. Furthermore, in cardiovascular medicine, it contributes to the evaluation of myocardial perfusion and viability, playing a crucial role in managing cardiovascular diseases.

The value of DCE-MRI is profound in both clinical and research domains. Clinically, it supports early diagnosis, aids in treatment planning, and monitors treatment efficacy, which is invaluable for patient care. In research, DCE-MRI is a useful tool that provides valuable insights into how diseases affect the body. Its wide range of uses and ability to capture clear images quickly makes it a strong choice for medical imaging, helping to improve patient care and advance medical research. Through its various applications and technical benefits, DCE-MRI plays an important role in modern medical imaging and research, helping to connect diagnostic assessments with treatment plans.

Research models for tendon evaluation

Achilles tendon

The Achilles tendon is the largest and strongest tendon in the human body and connects the calf muscles to the heel bone. It plays a crucial role in walking, running, and jumping. In recent years, advancements in imaging techniques have allowed researchers to study the Achilles tendon's microstructure, healing processes, and pathologies more effectively. In this

subchapter, we discuss several studies that employed various MRI techniques to assess the Achilles tendon and its associated conditions.

Dallaudière *et al*.[44] investigated the use of 3D-ULtrashort Echo Time (UTE) magnetic resonance imaging sequences to evaluate the Achilles tendon in a spondyloarthropathy (SpA) experimental mouse model. The purpose of this work was to investigate the potential of a 3D UTE sequence to quantitatively assess both diseased and normal rat Achilles entheses at 4.7T. In line with the histology results, the study discovered that 3D-UTE sequences were superior to lengthy TE T2 3D balanced steady-state free precession (bSSFP) sequences in determining the intrinsic anatomy of the Achilles enthesis and identifying early anomalies in clinical circumstances.

Furthermore, the healing process of the tendon has also been the subject of many studies. Fukawa *et al*.[45] conducted a study utilizing MR T2 mapping to investigate the tendon healing process in a rabbit Achilles tendon transection model. Their objective was to determine whether MR T2 mapping could be used to measure the healing of tendons treated with platelet-rich plasma (PRP). The researchers found that the T2 value of the healing area decreased over time in both the control and PRP groups, confirming tendon repair. However, PRP injection had no significant effect on the histological results of tendon repair.

Grosse *et al*. [46] explored the effects of repetitive tendon straining activity on T1 and T2* relaxation times using an ultrashort echo time (UTE)-MRI technique. This study compared healthy recreational long-distance runners with a control group. The researchers observed no significant differences in the mean T1 values between the two groups. However, they found that the mean T2* relaxation time was significantly higher in runners, particularly in the mid-portion of the Achilles tendon. This difference could potentially be attributed to adaptations in tendon microstructure and/or water content induced by repetitive mechanical loading.

Malmgaard-Clausen *et al*.[47] carried out a cross-sectional study with 90 participants, including 25 healthy controls and 65 tendinopathic patients. The purpose of this study was to compare the T2* values of patients with early tendinopathy to those of healthy controls and to examine the relationships that exist between T2*, clinical outcomes, tendon size, and mechanical characteristics. The research discovered no significant link between VISA-A and T2* or VISA-P and T2*, but a positive correlation between cross-sectional area (CSA) and T2* for both the patellar and Achilles tendons. According to the study's findings, structural alterations in the early stages of tendinopathy might be predicted by UTE T2* MRI acquired using a mono-exponential fitting model.

Szaro *et al*.[48] conducted a review of MRI techniques used to investigate various Achilles tendon pathologies. They highlighted the potential of diffusion tensor imaging (DTI) MRI to monitor regeneration, healing, remodeling, and treatment response in tendon pathologies. They also discussed the promising nature of T2-mapping in assess tendon healing, as T2 values in normal, healthy tendons are lower than those in wounded sections. This review also suggested that intravoxel incoherent motion (IVIM) MRI could be employed to assess the microcirculation and microvasculature properties of tendons during the healing process. Additionally, MR spectroscopy, specifically sodium MRI, can be used to evaluate glycosaminoglycan content, which is found at higher concentrations in pathological tendons.

Wengler *et al*.[49] contribute to the field by developing a novel intravoxel incoherent motion (IVIM) MRI protocol for the Achilles tendon, which addresses the limitations of low tendon T2/T2* values and low intratendinous blood volume and blood velocity. By implementing a stimulated echo-based diffusion preparation with readout-segmented echo-planar imaging (ste-RS-EPI IVIM) and specific tendon positioning at a 55° angle, this study demonstrates the potential to study the microvasculature and microcirculation of the human Achilles tendon.

In conclusion, the studies discussed in this subchapter highlight advancements in MRI techniques for assessing the Achilles tendon and its associated pathologies. These techniques have the potential to improve our understanding of tendon microstructure, healing processes, and disease progression. Further research and development of these imaging methods may lead to more accurate diagnosis and better treatment strategies for individuals with Achilles tendon injuries and conditions.

Rotator cuff

The rotator cuff plays a crucial role in shoulder function and stability. The use of advanced MRI techniques for evaluating rotator cuff pathologies has gained increasing attention in recent years. This subchapter focuses on studies that have utilized various MRI methods to investigate rotator cuff tendons, with the aim of improving our understanding of their anatomy, healing processes, and pathologies.

Ariyachaipanich *et al*.[50] highlighted the T2 mapping technique as an effective method for assessing collagen disorganization during early cartilage degeneration. T2 relaxation times can be mapped with color maps using mono- or bi-exponential fitting methods, allowing early lesion identification and characterization. This method has shown promising results in rotator cuff tendons. Recent advancements in MRI techniques now enable comprehensive imaging of the knee, these new sequences can identify structural and biochemical changes in bones and soft tissues during injury, early degeneration, and repair phases.

Trudel *et al*.[51] performed a study on rabbit supraspinatus tendons to generate T2 and T2* maps, and analyzed the effects of supraspinatus tendon tears at different time points after surgical repair. They used a 7T MRI scanner with a multi-echo spin-echo (MESE) CPMG sequence for T2 mapping and a 3D UTE sequence for T2* mapping. The study found that q-MRI could

identify disuse of the supraspinatus tendon after the tear and the benefits of the surgical repair procedure. However, the T2* maps did not generate reliable signals from relaxation time. The study concluded that q-MRI could be employed as a supportive tool for the preoperative and postoperative investigation of supraspinatus tendons, particularly when using ultra-high-field MRI at 7T. In a related study, Trudel *et al*.[52] examine the influence of bone-channeling intervention on enthesis reformation in rabbit supraspinatus tendons following surgical repair. Utilizing 7T MR and quantitative T2 imaging, this study successfully quantified enthesis reformation and the impact of channeling within the first four weeks post-surgery.

In summary, the studies presented in this subchapter demonstrate the potential of advanced MRI techniques for assessing the rotator cuff tendons and their related pathologies. These imaging methods can provide valuable insights into tendon healing, microstructure, and disease progression, ultimately contributing to the development of more effective diagnostic and therapeutic approaches for rotator cuff injuries and disorders.

Patellar tendon

The patellar tendon is an essential structure for knee function and stability, as it transmits forces from the quadriceps muscles to the tibia. Understanding pathological changes and healing processes in the patellar tendon is crucial for developing effective diagnostic and treatment strategies. This subchapter focuses on studies that have used various MRI techniques to investigate the patellar tendon, providing valuable insights into its anatomy, healing mechanisms, and pathologies.

Ariyachaipanich *et al*.[50] also investigated the Ultrashort Echo Time MRI (UTE MRI) technique in the patellar tendon. This technique can detect changes in collagen fibrillar architecture not visible on standard clinical pulse sequences, allowing for evaluation of tendons

and entheses. Animal studies have demonstrated the feasibility of this technique for the treatment of patellar tendons and quantitative assessment.

Fischer *et al.*[53] investigated the application of DCE-US and Dynamic Contrast-Enhanced MRI (DCE-MRI) methods to measure vascularization during tendon regeneration. Participants in this research included those who had surgery to address catastrophic ruptures of the Achilles, patellar, and quadriceps tendons. By measuring tissue microcirculation prior to, during, and following an intravenous contrast agent injection, the DCE-MRI method allows for the evaluation of the tendon regeneration process. The efficacy of these instruments for evaluating tendon regeneration quality was demonstrated by the study's finding of strong correlations between the quantification parameters of the two tested methods (DCE-US and DCE-MRI) at 6- and 12-weeks following surgery.

Gatehouse *et al.*[54] evaluate the use of ultrashort time-echo (UTE) sequences for imaging various tendons, including the patellar tendon. The study demonstrated that tendons exhibit a relatively high signal on subtraction images, indicating enhancement. The use of UTE sequences offers a high-signal alternative to traditional low-signal techniques. However, the authors noted that a more detailed assessment is required to determine the clinical relevance of UTE sequences, as this technique provides new possibilities for tendon imaging, and future research is expected to yield results of substantial interest.

Kijowski *et al.*[55] evaluated the patellar tendon's bi-component UTE-T2* characteristics in patients with patellar tendinopathy and healthy controls. The findings demonstrated a significantly smaller fraction of the patellar tendon's fast-relaxing macromolecular-bound water component (FF) and significantly higher T2* and T2F values in patients with tendinopathy. A decrease in collagen content and an increase in bulk water content within the injured tendon may be the cause of the decreased FF in tendinopathy patients. Moreover, it is possible that

patients with tendinopathy have higher T2F values because of microstructural disruption of the collagen fibers, which leads to reduced restriction of the water bound to the collagen.

Koff *et al*. [56] evaluated the effect of cyclic loading on the T2* values of fresh and frozen rabbit patellar tendons using UTE-MRI. The patellar tendons of 16 rabbit's lower limbs (eight fresh and eight frozen) were subjected to 100 cycles of 45 N load at approximately 1 Hz, after which they were scanned using a 3T system and a 2D fast-spin-echo (FSE) sequence. Histological analysis was performed using H&E staining to evaluate the collagen fiber structure. The results showed no significant difference in T2* values between fresh and frozen specimens before loading. However, both groups exhibited shorter T2* values and reduced T2*variability post-loading. In 11 of 16 tendons, the T2* values decreased, while the remaining tendons experienced minimal prolongation. Histological analysis confirmed the absence of damage and organized fiber structure. The shortening of the T2* values in the patellar tendons after loading is attributed to stronger spin-spin interactions, which may result from greater tissue organization and the presence of collagen fibril disruption.

Wengler *et al*.[49] examined how to evaluate the microcirculation and microstructure of patellar tendons in ten healthy individuals using stimulated echo readout-segmented echoplanar imaging (ste-RS-EPI) sequences. The goal of this study was to encourage early intervention in order to stop or reverse tendon deterioration. Using diffusion tensor imaging (DTI) and intravoxel incoherent motion (IVIM), several parameters were computed from the processed images. The findings showed that while IVIM-derived patellar tendon parameters showed greater variability due to factors like SNR, non-uniformity of tendon vasculature, and other physiological factors, ste-RS-EPI protocols were effective in assessing DTI-derived patellar tendon parameters. Additionally, the study showed that the patellar tendon's outer two thirds had higher microvascular blood flow and volume. In summary, the patellar tendon

microstructure and microcirculation may be effectively assessed using both DTI and IVIM techniques.

Krämer *et al*.[57] explored the use of ultrashort echo time imaging sequences to quantify both T1 and T2* in the quadriceps and patellar tendons. The study found that combining isotropic T1 and T2* mapping with bivariate histogram analysis enabled successful knee segmentation and visualization of relaxation parameter distribution across the entire tendon volume.

Liu and Kijowski[58] compared four different fitting methods for bi-component effective T2 (T2*) relaxation time analysis. This study recommended the method proposed by Gudbjartsonn *et al*.[59] for T2 analysis on human tendons due to its lower computational cost.

Papp *et al*.[60] assessed the applicability of three different methods for the quantification of the T2* relaxation time constant in the patellar tendon in humans: mono-exponential, bi-exponential, and a model provided by the fractional-order extension of the Bloch equation. The study recommended a fractional-order model when the image presented a low SNR.

Pownder *et al*.[61] carried out a pilot study to evaluate the connection between the UTE T2* metrics, histology, and biomechanical assessment and the produced mechanical strain on the patellar tendon. This study showed that the healing process of mechanically damaged tendons could be assessed using UTE q-MRI.

Van der Heijden *et al.*[62] using quantitative DCE magnetic resonance imaging (MRI), compared the changes in patellar bone blood perfusion between patients with patellofemoral pain (PFP) and healthy controls. The study discovered that although the differences between the patients' and the healthy control participants' values of perfusion parameters in the patellar bone were not statistically significant, it appears that the venous or arterial blood outflow is not reduced in people with PFP.

In conclusion, the studies discussed in this subchapter highlight the potential of advanced MRI sequences to evaluate the patellar tendon and its related pathologies. These imaging methods contribute to our understanding of tendon healing, the microstructure, perfusion, and disease progression. The findings of these studies can provide more accurate diagnoses and targeted treatment approaches for patellar tendon injuries and disorders, ultimately improving patient outcomes.

Other tendons

Chang *et al*.[63] reviewed various UTE sequences and their modifications to improve efficiency or contrast and provided quantitative analysis on the Achilles tendon, the patellar tendon and the menisci. They compared different UTE techniques such as 2D-UTE, 3D-UTE, the acquisition-weighted stack of spirals (AWSOS), and variable TE (vTE) sequences. This study highlighted the potential of UTE techniques for improving the contrast between adjacent musculoskeletal structures and their applications in bones, tendons, ligaments, and entheses, as well as their limitations and challenges..

Remodulin

Treprostinil, marketed under the brand name Remodulin, is a key therapeutic agent in the management of Pulmonary Arterial Hypertension (PAH), a condition marked by increased blood pressure in the pulmonary arteries.[64] The Food and Drug Administration (FDA) approved Treprostinil following rigorous clinical trials, highlighting its efficacy in alleviating PAH symptoms and improving patients' quality of life.[65]

A notable aspect of Treprostinil's therapeutic profile is its safety, with clinical studies showing minimal off-target effects, establishing its suitability for long-term PAH management. This

safety profile not only emphasizes Remodulin's significance in current therapeutic settings but also paves the way for investigating its utility in other medical domains.[64]

Belonging to the prostacyclin analogue class, Treprostinil shares a group with compounds known for their vasodilatory, antiplatelet, and anti-inflammatory attributes. When compared to other prostaglandins like Alprostadil, Treprostinil demonstrates a distinct pharmacological profile, marked by an extended half-life and diverse administration routes, rendering it a therapeutic advantage in managing chronic conditions like PAH. Its mechanism of action encompasses vasodilation and platelet aggregation inhibition, which lead to reduced pulmonary vascular resistance, thereby alleviating symptoms associated with elevated pulmonary arterial pressure. This dual-action proves beneficial in mitigating PAH progression and improving patients' overall well-being. Additionally, Treprostinil's inherent anti-inflammatory effects are crucial to its therapeutic efficacy. By modulating inflammatory responses, it not only addresses the symptomatic facets of PAH but also aids in altering the disease trajectory, thereby offering a holistic approach to patient management.

The exploration of Remodulin’s potential in tendon healing is grounded in its ability to modulate two key biological processes: blood flow and inflammation. Tendons, characterized by their relatively avascular nature, often face challenges in healing due to limited blood supply. Enhanced blood flow is crucial in tendon healing as it facilitates the delivery of essential nutrients, oxygen, and cells to the injury site, thereby fostering a conducive environment for tissue regeneration. Remodulin, with its vasodilatory properties, emerges as a candidate of interest in augmenting blood flow to injured tendons, thereby potentially expediting the healing process.

In addition to its impact on blood flow, Remodulin’s anti-inflammatory properties hold significant promise in the context of tendon healing. Inflammation is a double-edged sword in the healing process; while it is essential for initiating healing, prolonged inflammation can be

detrimental, leading to chronic pain and impaired function. Remodulin's ability to modulate inflammatory responses can potentially mitigate excessive inflammation at the injury site, thereby promoting a balanced and optimal healing environment. This dual action on both vascularization and inflammation positions Remodulin as a potential therapeutic agent in addressing the challenges associated with tendon healing.

The potential application of Remodulin in tendon healing brings forth a spectrum of benefits and challenges that warrant thorough exploration. One of the most anticipated benefits is the acceleration of the tendon healing process. By enhancing blood flow and modulating inflammation, Remodulin could potentially foster a more conducive environment for cellular activities essential for tissue regeneration. This acceleration in healing is not only pivotal for reducing recovery time but also for mitigating the risk of chronic complications associated with delayed or impaired healing.

However, the application of Remodulin in this new therapeutic area is not without challenges. While the drug exhibits a favorable safety profile in the treatment of PAH, its use for tendon healing necessitates a careful evaluation of possible side effects and risks. These may include local reactions at the administration site, systemic effects, or unforeseen complications arising from long-term use. Addressing these challenges requires a meticulous approach, involving dose optimization, monitoring strategies, and patient selection, to ensure that the benefits outweigh the risks and that patient safety remains paramount.

Study Aim

In the pursuit of addressing tendon and ligament injuries, this study emphasizes the essential role of optimizing 7T MR sequences. The need for such optimization is driven by the requirement to reconcile time constraints with the acquisition of high-resolution images, thereby safeguarding the well-being of the subjects' animals and ensuring the reliability of the

findings. Regular, bi-weekly image acquisition is integral, facilitating a systematic monitoring and assessment of healing trajectories and the efficacy of treatment interventions over time.

The generation of parametric maps, utilizing T1 and T2 sequences, and the DCE sequence, are another pivotal aspect of this research. This methodology is used for quantifying the healing process and providing an objective framework for assessing treatment outcomes. The combination of these varied sequences is optimized to have a detailed insight into the dynamics of healing, contributing to a comprehensive and rigorous evaluation of the applied therapeutic interventions. At the core of this research is the objective to assess the potential effectiveness of Remodulin in accelerating tendon healing. The methodologies developed and implemented, namely the optimization of the MRI sequences and protocol, are designed to evaluate whether Remodulin may be considered a potential therapeutic option. Emphasis is placed on a meticulous and comprehensive evaluation to ensure that any conclusions drawn are well-founded and indicative of the potential therapeutic applications of Remodulin in tendon repair. The potential implications of this research are noteworthy as no small molecule drug has been identified to aid in tendon repair. The methodologies and insights developed through this work aim to contribute to the existing body of knowledge, exploring new avenues for enhancing therapeutic strategies and bettering patient outcomes in treating tendon and ligament injuries.

Materials And Methods

Sequence optimization

Images were obtained utilizing a MAGNETOM Terra 7 T MRI scanner (Siemens Medical Solutions USA Inc., Malvern, PA). This high-resolution scanner was paired with a commercially available 1Tx/28Rx human knee coil (Quality Electrodynamics, Mayfield Village, OH). For optimal image acquisition, the coil was strategically placed at the isocenter of the MR unit. For all subsequent studies involving MRI acquisition, it is essential to note that isocenter coil placement was consistently employed to ensure standardized image acquisition conditions.

Preliminary sequence optimization with rabbit carcass

Before initiating MR imaging on live subjects, we utilized a skeletally mature frozen rabbit carcass to fine-tune our sequence for optimal resolution and SNR, aiming for a total MRI acquisition time of under one hour. The objective was to improve both the resolution and the SNR within the time constrain, making the images sharper and clearer.

Fat saturation, which can be a limitation in differentiating tendon structures, was intentionally removed. This facilitated the segmentation process of the tendon in the images.

Additionally, to maximize image quality within this timeframe, the edges of the field of view (FOV) were meticulously adjusted to avoid proximity to the patella, and phase oversampling was employed to prevent any overlapping of body parts with the patella, which could compromise the imaging. The rabbit carcass also helped to determine the most favorable positioning for the subjects. After a few tests, the supine position was selected, as it ensured that the patellar tendon area for both knees was as close to the coil's isocenter as possible.

Regarding the selection of imaging planes, the axial plane was chosen deliberately. Our main aim was to achieve maximum resolution on the plane where the defect was present. Given that the defect ran longitudinally to the patella, the axial plane presented the defect most visibly across every slice that represented the patella.

Optimization with a live rabbit for the DCE sequence

While the carcass provided invaluable insights for the T1 and T2 sequences, the Dynamic Contrast-Enhanced (DCE) sequence demanded tests on a skeletally mature live rabbit due to its inherent requirements. Our team strived to strike the right balance between temporal resolution and image quality. With the live rabbit, we focused our efforts on obtaining the highest possible temporal resolution, which is crucial for DCE sequences, without compromising on the overall image quality.

Pilot study

The pilot study's design was carefully deliberated upon in collaboration with our research team, the anatomopathologist, and the veterinarian team. The primary objective was to assess the tolerability and potential side-effects associated with the intra-articular (IA) injection of Remodulin in the stifle joint. In pursuit of this goal, a comprehensive sampling plan was established, comprising four critical time points for blood sample collection: baseline, one-hour post-procedure, seven days post-procedure, and fourteen days post-procedure. Following completion of a 14-day observation period, euthanasia of the two animal subjects occurred, and subsequent organ retrieval was performed. This methodological approach was instrumental in ensuring a thorough evaluation of the intervention's effects within the study's designated timeframe.

To implement this approach, the study was conducted utilizing two rabbits, namely Rabbit 1 (a 6-month-old male weighing 3.02 kg) and Rabbit 2 (a female approximately 2 years old, with a weight of 5.33 kg). All procedures were executed by the veterinary team in a dedicated sterile room on day 0 of the study.

The initial step involved sedating both rabbits using an intramuscular (IM) injection of 5 mg of Midazolam (1M), as depicted in *Figure 1 A*. Subsequently, the knees of both rabbits were carefully shaved to expose the target area and were meticulously disinfected using a 2% Chlorhexidine Gluconate solution. Prior to the administration of any injections, baseline blood samples were collected. This blood draw was carried out on the lower limb of the knee using a 23-gauge butterfly needle, as illustrated in *Figure 1 B*. The needle was connected to a 5 mL syringe for the collection of blood.

A total volume of 9 mL of blood was obtained during each procedure. This collected blood was then transferred into two red top tubes (BD Vacutainer® serum Blood Collection Tubes, 6.0 mL • 13 x 100 mm), with 3 mL of blood placed in each tube, as well as two purple top tubes (BD Vacutainer® K2 EDTA (K2E) 7.2mg Blood Collection Tubes, 4.0 mL • 13 x 75 mm), with 1.5 mL of blood allocated to each tube. This transfer was conducted using a 20-gauge needle. These meticulous procedures ensured the proper handling and documentation of blood samples for subsequent analysis.

A. 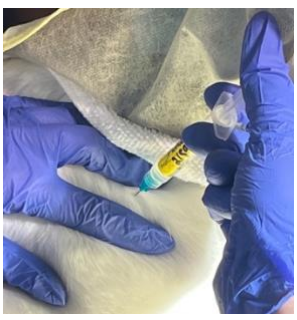 B.  C. 

Figure 1 . Depictions from Day 0 of the pilot study showing intramuscular sedation (A), blood collection (B), and intra-articular injection of Remodulin (C).

After the blood collection, the injection volumes were determined through collaborative discussions with veterinarians and the anatomical pathologist.

- For Rabbit 1, 51 µL of Remodulin (1 mg/mL) in 449 µL of saline was injected into the right knee, along with 500 µL of saline solution into the left knee. Rabbit 1 received the full dose in one knee to simulate the final study conditions and assess the drug's potential risks under a more hazardous scenario of a young rabbit receiving a full drug dose.
- For Rabbit 2, 25.5 µL of Remodulin (1 mg/mL) was combined with 474.5 µL of saline for both knees.

Following the initial injection, as shown in *Figure 1 C*, subsequent blood collections were conducted at one-hour intervals, as well as on the 7th and 14th days post-injection, employing the previously described blood collection procedure.

On each of these procedure days, 300 µL of anticoagulated whole blood and 250 µL of serum were dispatched to an external laboratory (IDEXX BioAnalytics, 2825 KOVR Drive, West Sacramento, CA) for comprehensive analysis, including a Research Comprehensive CBC and Expanded Tox Panel (non-rodent). Moreover, a pharmacokinetic analysis was performed utilizing Liquid Chromatography-Tandem Mass Spectrometry (LC-MS/MS) methodology. The analysis was carried out on serum samples, each with a total volume of 200 µL (100 µL for each rabbit). For the analytical process, 20 mg of a pure Remodulin compound were requisite to achieve accurate and precise quantification, facilitating a comprehensive understanding of the pharmacokinetic profiles of the substances under investigation.

The anticoagulated whole blood was directly drawn from the purple top tubes, while the remaining blood was processed to obtain plasma and serum. This process was facilitated using a centrifuge (Centrifuge 5810 R, Eppendorf AG, Barkhausenweg 1, 22339 Hamburg, Germany) under the following parameters: a temperature of 4°C, rotation at 2000 rpm, and a duration of 10 minutes. Post-centrifugation, the plasma and serum samples were meticulously transferred

to 2 mL cryovials, subsequently preserved in a -80°C freezer, with precise documentation of their storage locations for future reference.

Upon the completion of the 14-day observation period, both rabbits were euthanized, and their knees were harvested for comprehensive pathology assessment, where the soft tissues were removed and sections were taken of the joint cross section and of multiple areas of joint capsule. Various organs, including the liver, kidney, adrenal gland, spleen, thyroid, parathyroid, lungs, and heart, were carefully collected for further analysis. All these samples were preserved in plastic jars containing a 10% formalin solution to maintain their integrity for the investigations.

10-Week Final Study

In the 10-week final study, our primary objectives were threefold. Firstly, our primary goal was to evaluate the efficacy of the treatment. Secondly, we recognized the need to optimize 7T MR sequences, ensuring that the imaging captured the tendon healing process within our constraints. Lastly, we aimed to develop a specialized MATLAB code and user interface to streamline the analysis process, ensuring accurate and easily interpretable data extraction from the images.

The decision to span the study over a 10-week duration was based on our assessment that this timeframe would be sufficient to observe the tendon's healing process. While various durations were considered, 10 weeks was deemed optimal for our specific objectives and constraints. During this period, imaging was conducted bi-weekly, and injections were administered weekly, as shown *Figure* . This frequency was chosen with the well-being of the animals as a paramount concern. Each procedure required the animals to be sedated, and it was

essential to strike a balance between obtaining necessary data and ensuring the animals were not overly stressed or compromised.

A significant constraint we faced, as dictated by the veterinary team, was the one-hour scan limit, primarily instituted for the well-being of the rabbits. Given that rabbits are a sensitive species, they can react adversely to prolonged sedation. It's been observed that after about two hours under sedation, their breathing can become irregular, posing significant health risks. To navigate this constraint and still obtain quality data, we made a strategic compromise by reducing the image resolution to decrease the imaging time. However, we ensured our protocol still incorporated three essential sequences, striking a balance between time efficiency and data quality.

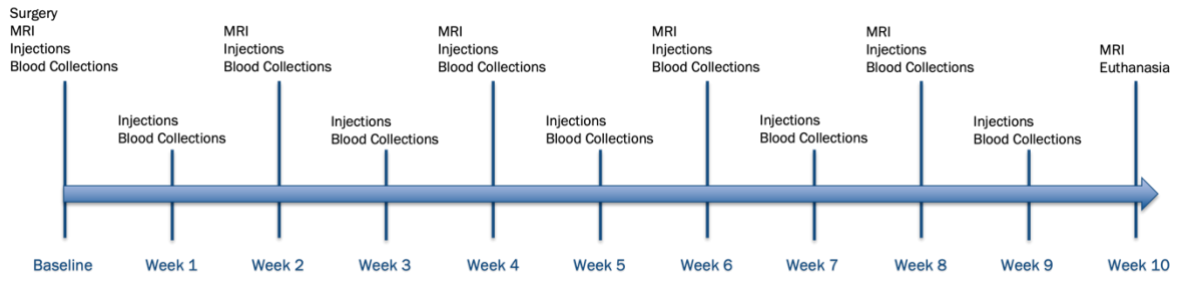

Figure 2. Study Timeline showing the procedures performed in each week.

Control Group: The control group consisted of four animals: one male and three females. Their average weight at the start of the study was 3.5 ± 0.54 kg. Each week, these animals received an intra-articular (IA) bolus injection of 500 µL of saline solution into the right knee.

Study Group: The study group also comprised four animals, with an even distribution of two males and two females. Their average weight at the commencement of the study was 3.36 ± 0.44 kg. These animals were administered a weekly intra-articular (IA) bolus injection consisting of 51 µL of Remodulin (with a vial concentration of 1 mg/ml) combined with 449 µL of saline solution, delivered to the right knee.

Surgical Procedure

The X-ray was performed before the surgery, using an XRpad 4336 MED digital x-ray detector system on a Minxray HF120/60HPPWV Power Plus, to assess the skeletal maturity of the rabbits, as shown in *Figure 3.*, which was confirmed by the veterinarian team. An MRI baseline acquisition was then carried out on each rabbit using the sequences described in the section below, to confirm the absence of abnormality in the musculoskeletal apparatus and to obtain baseline values for T1, T2, and DCE, providing a comprehensive pre-operative assessment of their condition. The surgery was then conducted by an orthopedic surgeon.

Figure 3. Radiographic confirmation of skeletal maturity, considering both chronological age and the sealed growth plates of New Zealand White rabbits. Coronal x-ray images of the right hind knee of rabbits 2110 (A), 2161 (B), 2166 (C), 2168 (D), 2163 (E), 2164 F (F), 2164 M (G) and 2167 (H).

The anesthesia protocol was administered which included Midazolam 5mg 1M, Ketamine 100mg 3M, Enrofloxacin 23.5 mg, and Buprenophine 0.56 mg. Once the rabbit was anesthetized, it was placed in the supine position on the operating table. The rabbit was intubated and monitored using ECG and pressure sensors.

Prior to making the skin incision, the knees of both rabbits were carefully shaved to expose the target area and were meticulously disinfected using a 2% Chlorhexidine Gluconate solution. A

longitudinal skin incision was then made on the medial edge of the patellar tendon on the knee. Subsequently, as shown in *Figure 5.* , the medial and lateral retinacula of the patellar tendon were cut. This was followed by separating the posterior surface of the tendon from the infrapatellar fat pad. A partial-thickness tendon substance, approximately 3 mm wide and 10 mm long, was resected from the central portion of the patellar tendon using a 15 surgical blade. This defect width was roughly equal to one-third of the tendon's width, as shown in *Figure* .

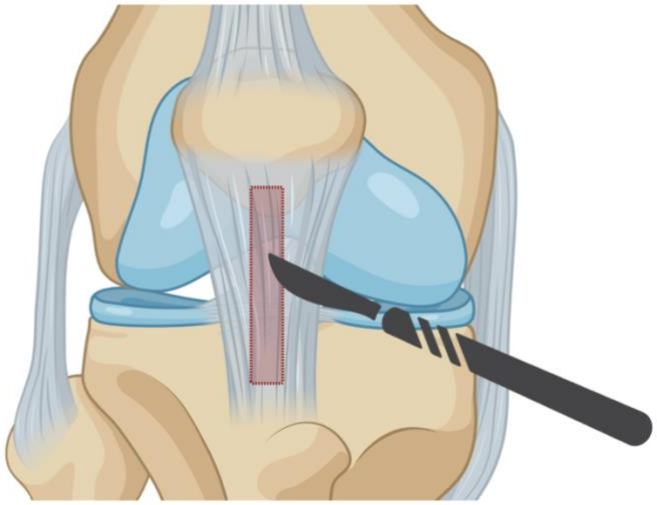

Figure 4. Schematic illustration of the defect in a human knee Created with BioRender.com.

The overlaying subcutaneous tissues and skin were then closed with 3-0 nylon sutures and metal staples, The combination of metal staples and sutures was chosen to ensure that any saline solution injected into the resected portion would not leak out from the skin incision and to guarantee wound healing, even in the event the rabbit might remove the metal staples itself.

The design of the procedure was such that postoperative immobilization was typically not required.

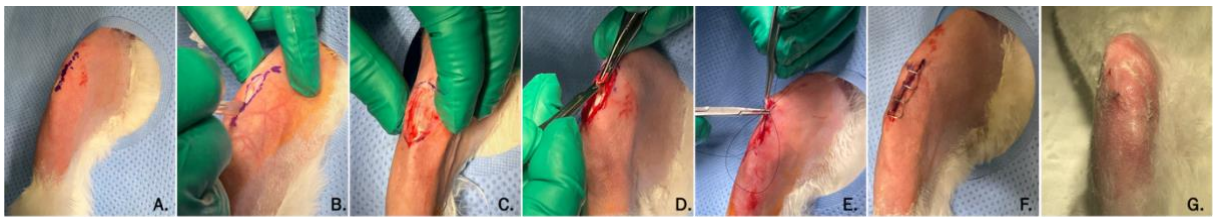

Figure 5. Patellar tendon partial resection procedure in the rabbit (A) surgical markings, (B) median knee incision, (C) exposure of superficial fascia, (D) tendon partial resection with a 15 surgical blade, (E) closure of superficial fascia with 3-0 nylon suture, (F) placement of staples, and (G) healed surgical site.

All rabbits were closely monitored post-surgery. The surgical techniques and equipment used were standardized to ensure consistency and optimal outcomes. The post-operative care involved observation of the rabbits, with specific attention to their recovery and the removal of staples within the stipulated time frame (7-10 days).

Injection Procedure:

During the preparation phase, the material for the procedure day included two red top tubes (BD Vacutainer® serum Blood Collection Tubes, 6.0 mL • 13 x 100 mm) and two purple top tubes (BD Vacutainer® K2 EDTA (K2E) 7.2mg Blood Collection Tubes, 4.0 mL • 13 x 75 mm). The veterinary team took charge of the administration of saline and drug injections. For the control group, 500 µL of saline solution was injected into the right knee.

Conversely, the experimental group received an injection of 51 µL of Remodulin mixed with 449 µL of saline solution into the right knee. Each rabbit then had a recovery period of one hour post-injection before blood collection, a critical window to ensure the rabbit's welfare and accurate blood collection. During this hour, the rabbits were closely observed. Blood processing began precisely an hour post-injection.

The veterinary technician collected about 3 mL of blood from each tube, amounting to 12 mL per rabbit. Plasma collection was prioritized, filling the purple-top tube first and gently shaking it to deter clotting. The red top tubes remained unshaken.

Typically, each rabbit's injection process took 15 minutes, with another 10 minutes for blood collection. Immediately after blood collection, the plasma was processed.
Conversely, the serum settled for roughly an hour before processing. Both plasma and serum underwent centrifugation (Centrifuge 5810 R, Eppendorf, Eppendorf AG Barkhausenweg 1, 22339 Hamburg, Germany) with specific parameters: 4 °C temperature, 2000 rpm rotation speed, and a 10-minute duration. After centrifuging, the plasma and serum were placed into 2 mL cryovials (Greiner Bio-One, cryo.s, 2 ml, pp, round bottom, external thread, natural screw cap writing area, starfoot, natural, sterile). These samples were stored in a -80°C freezer, with their precise location carefully documented for later access.

Imaging Procedure

To ensure the acquisition of high-quality images, meticulous attention was given to the positioning of the rabbit. Once on the MRI table, the rabbit was oriented in a supine position. A collaborative effort between the veterinary and MRI technicians ensured the proper setup of essential sensors and probes, such as the ECG, SpO_2 sensor, ventilation, and temperature probe. A marker was strategically placed on the rabbit's right knee, serving as a consistent reference point across imaging sessions. The rabbit's lower limbs were aligned and secured, minimizing any potential movement during the imaging process. To improve the alignment, we developed a leg holder to optimally position rabbit's lower limbs in the MRI coil for better imaging resolution. The custom design, developed in SolidWorks, was 3D printed using a Formlabs 3B+ printer and BioMed Amber Biocompatible Photopolymer Resin via Formlabs' PreForm software with a layer thickness of 0.1 mm. The device, enhanced with a foam triangle and

Velcro, enabled easy placement and quick release of the rabbit, minimizing injury risk while hastening the imaging setup and release, as shown in *Figure*.

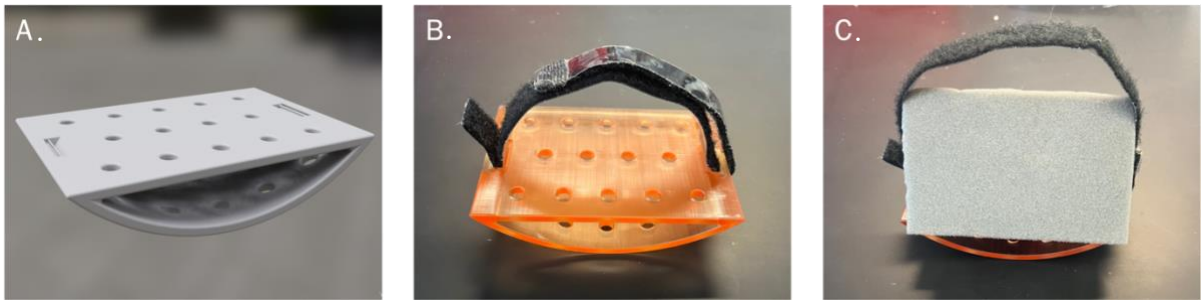

Figure 6. Set of images representing the 3D render of the leg holder (A), the 3D-printed version with Velcro (B) and the final version with added grey foam (C).

The coil, a pivotal component of the MRI, was then centered and aligned in relation to the rabbit.

With the setup complete, the MRI technician initiated the imaging protocol. The foundational sequences, T2 and T1, were captured first, providing essential baseline images of the rabbit's knee without the need for any external intervention. The final sequence employed in this study was the Dynamic Contrast Enhanced MRI (DCE-MRI).

Notably, the MRI machine utilized for this study, the MAGNETRON 7T, and the knee coil, remain consistent with those detailed in the sequence optimization paragraph, ensuring uniformity in the imaging setup throughout the research. Before delving into the specifics of the various sequences, it is essential to emphasize that all methods follow a shared process involving the loading of DICOM files and their storage in dedicated structures, facilitating image analysis across all approaches. Additionally, concerning the computational resources and libraries employed, it is relevant to note that the code has been predominantly developed in MATLAB (MathWorks), utilizing several MATLAB libraries, including the Image Acquisition Toolbox (Version 6.7.1, R2023a), the Image Processing Toolbox (Version 11.7, R2023a), and the Medical Imaging Toolbox (Version 1.1, R2023a). It is important to recognize that

compatibility extends beyond these versions, as the latest library iterations have also demonstrated comparable effectiveness and functionality.

To streamline the software utilization and enhance data presentation, a User Interface (UI) was developed for each sequence employed in the study: T1, T2, and DCE. Each UI facilitates the loading and segmentation of images, computation of requisite values, and the display of results both graphically and numerically, as shown in *Figure* .

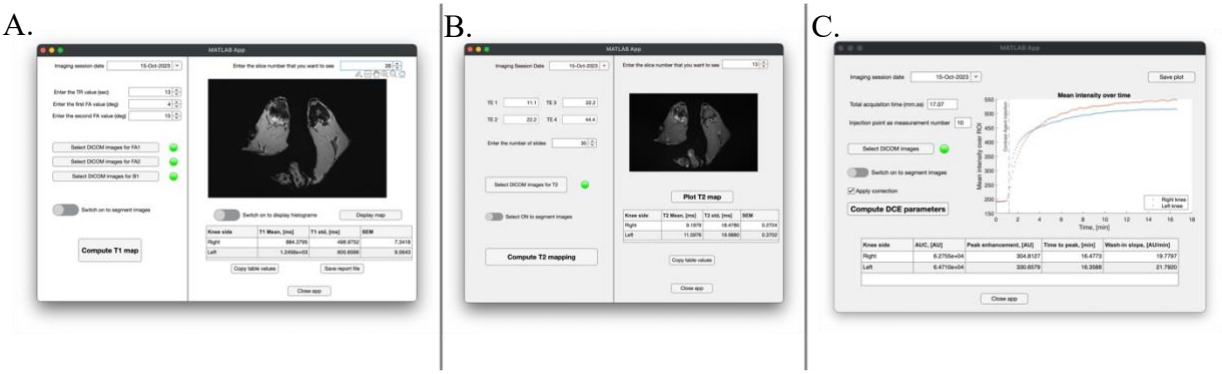

Figure 7. User Interface (UI) series. UI for T1 mapping (A), UI for T2 mapping (B), UI for DCE analyses (C).

T1

Sequence Parameters

The acquisition sequence was configured with the parameters listed in *Table 1*:

Parameter	**Value**
Repetition Time (TR)	13.0 ms
Echo Time (TE)	5.19 ms
Flip Angle (FA)	4°, 15°
Bandwidth	270 Hz/Pixel
Field of View (FOV)	160 mm

Voxel Size	0.2x0.2x1.5 mm
Signal-to-Noise Ratio (SNR)	1
Number of Slices	60
Averages	1
Total Acquisition Time	9.20 min
Water Suppression	None
Fat Suppression	None

Table 1. T1 sequence settings parameters.

Preprocessing

A total of 60 images were imported into MATLAB utilizing a developed user interface, employing the img_import and data_acquisition functions, detailed in Appendix A. The images were stored in two 512x512x60 matrices, each representing the images acquired with different flip angles (FA). Each matrix held 60 images, as depicted in *Figure 8*.

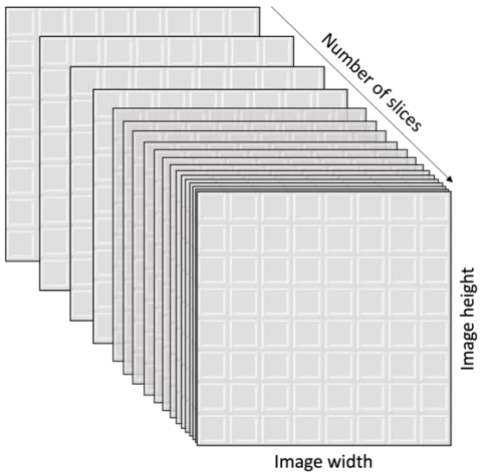

Figure 8. Matrix representation showcasing the image storage structure within the software. This configuration is consistently employed for both flip angle image loadings.

A crucial step in every acquisition is the segmentation of the patellar tendon over the knee. This segmentation is meticulously performed on the set of images acquired with the lower FA,

attributed to its superior resolution and clarity, thereby facilitating segmentation. The VolumeSegmenter tool, a built-in feature of the Medical Imaging Toolbox, was employed for this purpose. Segmentation was semi-automatically executed, leveraging the options provided by the tool, and the resultant segmentation was later utilized to compute the T1 value of the pixels within the patellar tendon. A result of this process can be seen in *Figure*.

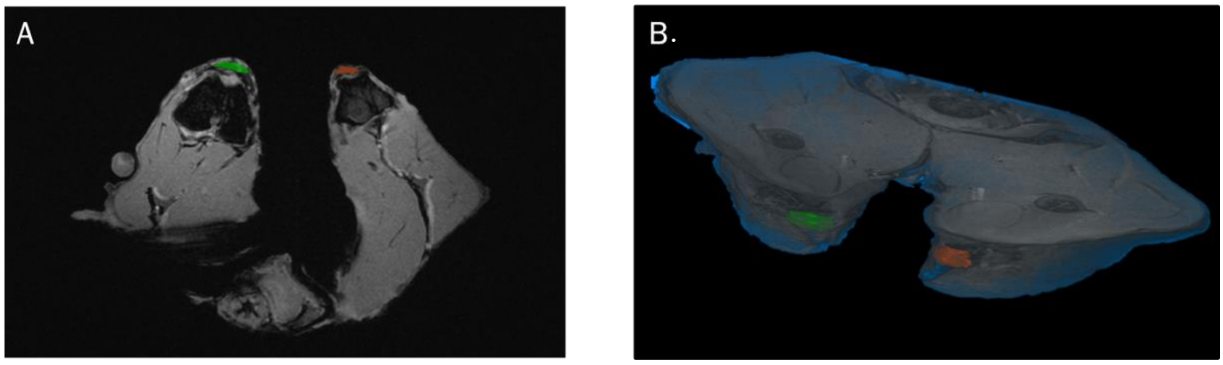

Figure 9. T1 image segmentation example with the right side highlighted in green (A) and 3D representation of the segmented region from the entire 3D reconstruction of the rabbit's scanned portion (B).

Variable Flip Angle (VFA) Technique Application

Parameter Setting: To compute the T1 value from the two sets of images, three primary parameters are essential: TR value, FA1, and FA2. Occasionally, a correction factor for the magnetic field B1 (f_{B1}) is necessitated for enhanced precision and reliability. However, in this instance, the correction was inherently incorporated into the acquisition protocol on the MRI machine side.

Algorithm Implementation: After the parameter setting, several steps were undertaken to compute the T1 value over the segmented region. Initially, the row and column indices of all pixels within the segmentation were extracted to optimize computational efficiency by focusing computations solely on the requisite region. Utilizing these indices, the value of a single pixel from both images (images with FA4 and FA15) was selected, and the ensuing *Equation 1* was applied to compute the value:

$$T1_{map} = \frac{2 \cdot TR \cdot (1/f_{B1}^2) \cdot \big((S1/FA1) - (S2/FA2)\big)}{(S2 \cdot FA2) - (S1 \cdot FA1)}$$

Equation 1. T1 computation using variable flip angle (VFA) technique.

as delineated in the *T1finalcomp* function in *Appendix A: Code Listings*. The value of the f_{B1} correction factor was designated to the value 1, aligning with the aforementioned justification. This process was iteratively applied over the segmented region, yielding a T1 value for each pixel. Subsequently, these T1 values were stored in a matrix mirroring the dimensions of the original, with zero values everywhere except within the segmented region, which was populated with values during the iteration of the code.

Post-Processing

Data Analysis: The derived T1 values were instrumental in computing the histograms of the T1 value distribution for both knees, with intensity normalization facilitating comparison as shown in *Figure 10 A*. Furthermore, these values were employed to calculate the mean, standard deviation (std), and the Standard Error of Mean (SEM) across the patellar tendon for

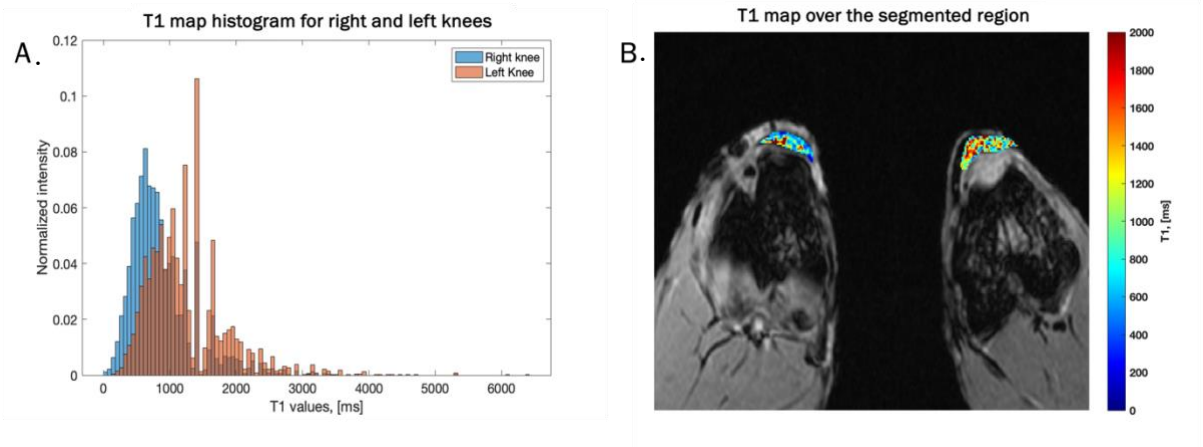

Figure 10. Histogram showcasing the distribution of T1 intensity (A). Heat map from the T1 analysis overlaid on the MRI's morphological image (B).

both the right and left knees. Ultimately, these values were utilized to generate a heat map overlaid on the original MRI image, visually representing the T1 value distribution within the patellar tendon. All images were complemented with a colorbar to enhance the interpretation of the displayed values, as shown in *Figure 10*.

T2

Sequence Parameters

The acquisition sequence was configured with the parameters listed in *Table 2*:

Parameter	**Value**
Repetition Time (TR)	3080.0 ms
Echo Times (TE)	11.1, 22.2, 33.3, 44.4 ms
Flip Angle (FA)	180°
Bandwidth	379 Hz/Pixel
Field of View (FOV)	160 mm
Voxel Size	0.2x0.2x1.5 mm
Signal-to-Noise Ratio (SNR)	1
Number of Slices	35
Averages	4
Total Acquisition Time	22:27 min
Water Suppression	None
Fat Suppression	None

Table 2. T2 sequence settings parameters.

Preprocessing

The user interface, using the data_acquisition_T2 function, detailed in Appendix A, enables to select the images for a specific rabbit in a 4-dimensional array, with dimensions corresponding to the x-y coordinates of the images, the slice number, and the echo time. A total of 140 images is selected, corresponding to the 35 slices acquired for each of the 4 echo times.

A crucial step in every acquisition is the segmentation of the patellar tendon over the knee. This segmentation is meticulously performed on the set of images acquired with the echo time (11.1 ms), attributed to its superior resolution and clarity, thereby facilitating segmentation. The VolumeSegmenter tool, a built-in feature of the Medical Imaging Toolbox, was employed for this purpose. Segmentation was semi-automatically executed, leveraging the options provided by the tool, and the resultant segmentation was later utilized to compute the T2 value of the pixels within the patellar tendon. A result of this process can be seen in *Figure 11*.

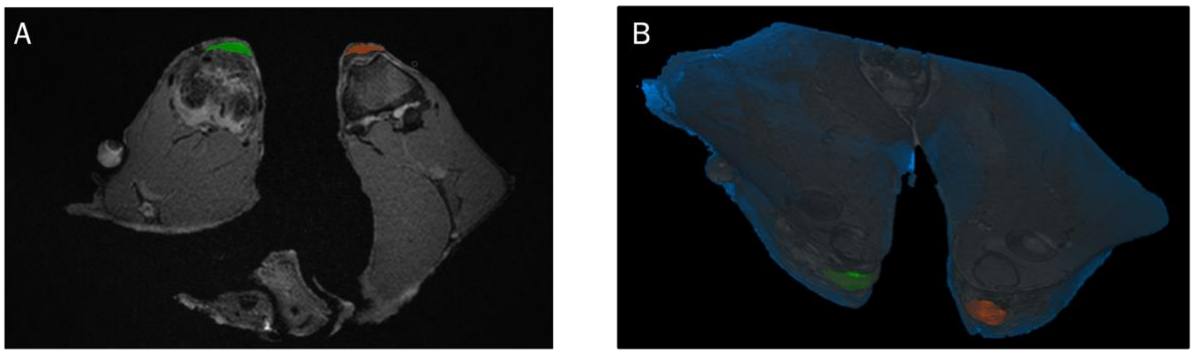

Figure 11. T2 image segmentation example with the right side highlighted in green (A) and 3D representation of the segmented region from the entire 3D reconstruction of the rabbit's scanned portion (B).

T2 Calculation

The T2 calculation process begins with the analysis of MRI images with the aim of creating T2 maps. The primary input to the function fit_T2_relaxation_curve is the 4D array containing MRI images. Additionally, a mask—a 3D binary array with dimensions matching

the MRI images—is used. This mask designates which pixels pertain to our region of interest (ROI) in each slice.

For every pixel inside the matrix, the function constructs a vector. This vector houses the pixel's values across different echo durations, as shown in *Figure 12*. Using these values, a fitting curve is computed.

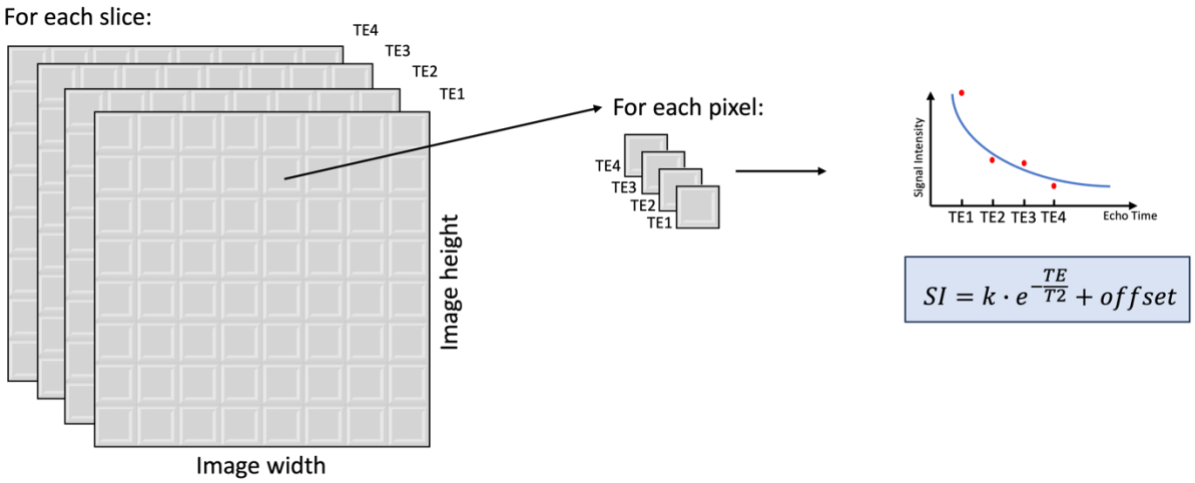

Figure 12. Graphic representation of one slice of the 4-dimensional matrix and the fitting function used to compute T2.

The fitting curve follows the *Equation 2*:

$$y = a \cdot e^{-bx} + c$$

Equation 2. Mono exponential decay equation.

Where a, b and c are the coefficients of the fitting curve.

The fitting is done using the NonlinearLeastSquares method, employing the Levenberg-Marquardt algorithm. Importantly, the coefficient *b* relates directly to the T2 value for that pixel, using *Equation 3*:

$$b = \frac{1}{T2}$$

Equation 3. T2 value computation.

In terms of validating the derived values, the function ensures that T2 values fall within the 0 to 100 ms range. Additionally, only fits with an r-square value above 0.90 are accepted, ensuring a high goodness of fit.

The function's output is a matrix that holds the T2 values for each pixel in the ROI, specifically within the patellar area determined during segmentation. From this matrix, we can create the T2 map for any desired slice. Typically, focus is placed on the mid-section of the patellar tendon. T2 maps are generated by color-coding each pixel based on its T2 value and then superimposing this colored map onto the original MRI image, as shown in *Figure 13*.

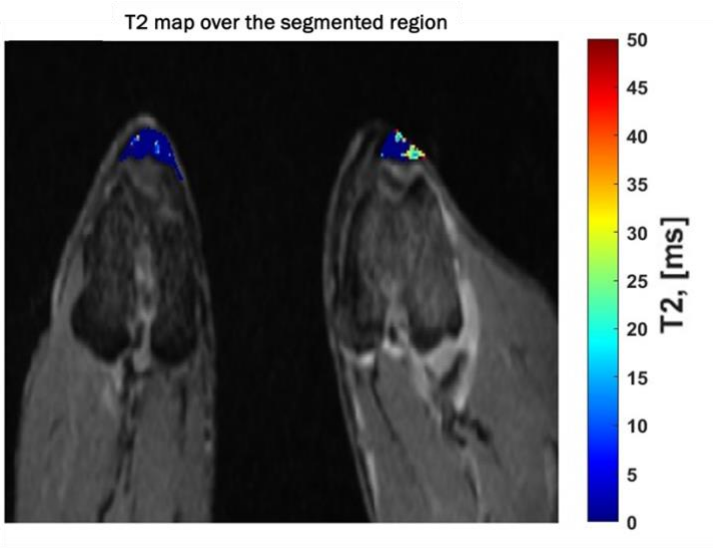

Figure 13. Heat map from the T2 analysis overlaid on the MRI's morphological image.

Once the T2 maps are generated, the next step involves calculating the mean T2 value for the chosen image. This is achieved by averaging the T2 values across the entire ROI, resulting in a singular, representative value.

DCE

Compared to the other sequences in the Dynamic Carats Enhance (DCE) sequence the use of the contrast agent is required. The contrast agent used was the Multihance (gadobenate dimeglumine injection, 529 mg/mL, Bracco Diagnostics).

Sequence Parameters

The acquisition sequence was configured with the parameters listed in *Table 3*:

Parameter	**Value**
Repetition Time (TR)	7.68 ms
Echo Time (TE)	1.88 ms
Bandwidth	300 Hz/Pixel
Field of View (FOV)	120 mm
Voxel Size	0.7 x 0.7 x 2 mm
Signal-to-Noise Ratio (SNR)	1
Number of Slices	24
Total number of measurements	144
Averages	1
Total Acquisition Time	17.07 min
Water Suppression	None
Fat Suppression	None

Table 3. DCE sequence settings parameters.

Injection procedure

For the injection the intravenous injection using the ear of the rabbit has been chosen, since is the easiest point where in intravenous access can be places in a rabbit and because it was a good place to facilitate the injection while the rabbit was places inside the machine.

The total quantity of contrast agent injected was dependent on the weight of the rabbit, that was taken before any procedure, to inject the proper quantity of contrast. The quantity was calculated using the following formula expressed in *Equation 4*:

$$\text{Dose (mL)} = \frac{\text{dosage (mmol/kg)} \cdot \text{weight (kg)}}{\text{molarity (mmol/mL)}}$$

Equation 4. Dosage computation.

Considering a dosage of 0.25 mmol/kg, a molarity of 0.5 mmol/mL and the weight expressed in kg.

The injection was manually performed by the veterinarian team during the DCE acquisition. To do so the line was primed with 6.2 mL of saline solution was connected to the intravenous access of the rabbit. After the injection a flush of 20 mL of saline solution was performed to be sure that the contrast agent was completely injected in the rabbit.

Moreover, in order to have a baseline of the intensity of the signal in the desired tissue, a total of 10 measurements (~1 min total) was waited before the injection.

Preprocessing

All the images resulting from the acquisition were imported in MATLAB for the analysis. Considering 24 images per measurement and a total of 144 measurement for the whole acquisition, a total of 3456 images were acquired in each session. A 512x512x24x144 matrix is utilized for storage. In the first two dimensions, a single image is represented, the third

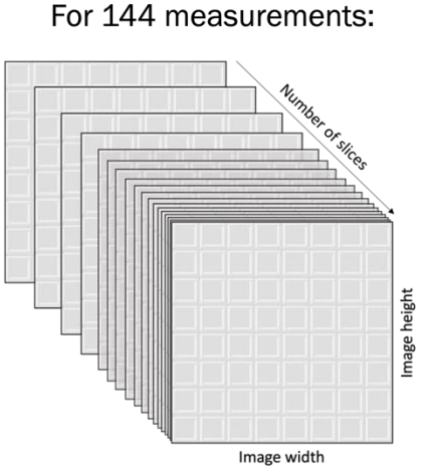

Figure 14. Graphic representation of one slice of the 4-dimensional matrix and the storage of the DCE images.

dimension is designated for the acquisition of measurements, and the fourth dimension accommodates the 144 measurements, as shown in *Figure 14*.

A crucial step in every acquisition is the segmentation of the patellar tendon over the knee. This segmentation is performed on the first set of 24 images acquired. The VolumeSegmenter tool, a built-in feature of the Medical Imaging Toolbox, was employed for this purpose. Segmentation was semi-automatically executed, leveraging the options provided by the tool, and the resultant segmentation was later utilized to compute the parameters related to the DCE.

Algorithm Implementation:

The required parameters for quantifying tissue perfusion and vascular characteristics are obtained through the computation of the uptake curve for the segmented area. This is achieved by essentially calculating the mean of the signal intensity for all the pixels within the segmented region. The resultant computation generates the curves depicted in *Figure 15*.

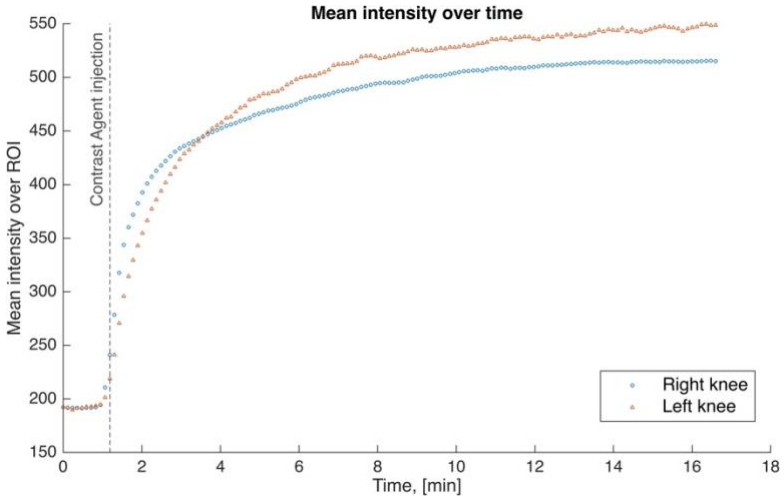

Figure 15. Mean intensity curves derived from the segmented DCE images.

Once the two DCE curves have been obtained, the following set of parameters were extracted:

1. **Area Under the Curve (AUC)**

The AUC is a measure of the total enhancement observed in the tissue. Mathematically, it is calculated using the trapezoidal role as represented by the *Equation 5*:

$$AUC = \int_{t_{\text{inj}}}^{t_{\text{end}}} \text{dce\_intensity}(t)\,, dt$$

Equation 5. AUC computation.

where (t_{inj}) is the time of injection, and (t_{end}) is the end time of the measurement.

2. **Initial Area Under the Curve (IAUC)**

IAUC is calculated similarly to AUC but is limited to the area under the curve up to the time of the peak enhancement. The formula for calculating IAUC is given by *Equation 6:*

$$IAUC = \int_{t_{\text{inj}}}^{t_{\text{peak}}} \text{dce\_intensity}(t)\,, dt$$

Equation 6. IAUC computation.

where (t_{peak}) is the time corresponding to the peak enhancement.

3. **Peak Enhancement**

Peak enhancement refers to the maximum enhancement observed from the time of injection. It is calculated as shown in *Equation 7*:

$$\text{Peak Enhancement} = \text{washin\_max} - \text{dce\_intensity}\left(t_{\text{inj}}\right)$$

Equation 7. Peak enhancement computation.

4. **Time to Peak**

Time to peak is the time taken from the injection to reach the peak enhancement. It is represented in *Equation 8*:

$$\text{Time to Peak} = t_{\text{peak}}$$

Equation 8. Time to peak computation.

5. **Wash-in Slope**

The wash-in slope is a measure of how quickly a tissue enhances, calculated by dividing the peak enhancement by the time to peak. The formula is given by the *Equation 9*:

$$\text{Wash-in Slope} = \frac{\text{Peak Enhancement}}{t_{\text{peak}} - t_{\text{inj}}}$$

Equation 9. Wash in slope computation.

The computed parameters with the uptake curve are then returned to the UI to be presented to the user.

Results

Pilot Study

This section delineates the findings from our pilot study, whose primary objective was to ascertain the feasibility and delineate the parameters of our main investigation.

Regarding the LS-MS/MS analyses, results one hour post-injection showed Rabbit 1 exhibited a concentration of 51.8 ng/mL, while Rabbit 2 displayed a concentration of 41.5 ng/mL. Notably, there was an absence of detectable Remodulin both at the intervals of 7 and 14 days post-injection.

In the anatomopathological assessment, the evaluator highlighted the conscientious effort made to devise a semi-quantitative assessment mechanism for the histological evaluation of these tissues. The assessment criterion was predicated on factors such as inflammation, stromal alterations, and vascular modifications, segmented on a five-point (0-4) continuum: normal, minimal, mild, moderate, and severe. Upon scrutiny, no palpable histological disparities were discerned amongst the subjects.

The microscopic diagnosis provided further insight. For Rabbit 1's right knee and left knee, the joint cross section and joint pouch showed evidence of multifocal synovial hypertrophy, both classified as minimal. For Rabbit 2, both the right and left knees revealed evidence of multifocal synovial hypertrophy, but they were classified as mild, with associated surface histiocytes observed.

T1

Utilizing 7T MR sequences, we analyzed T1 parametric maps to gauge potential changes in the tendon's molecular environment. The observed T1 values provide preliminary insights into the tendon's healing progression.

As illustrated in *Figure 16*, analysis of the T1 value over the 10-week study period reveals distinct trends between the control and experimental groups. Initially both groups start from a peak baseline value. However, the control group demonstrates a more rapid decline in T1 values in contrast to the experimental group, which exhibits a more gradual descent over the weeks. Additionally, there is a noticeable variance within the control group data points, as reflected by a consistently higher standard deviation at almost all time points, save for the initial one, when compared to the experimental group. Notably, neither graph suggests any tendency for the T1 values to revert to their baseline.

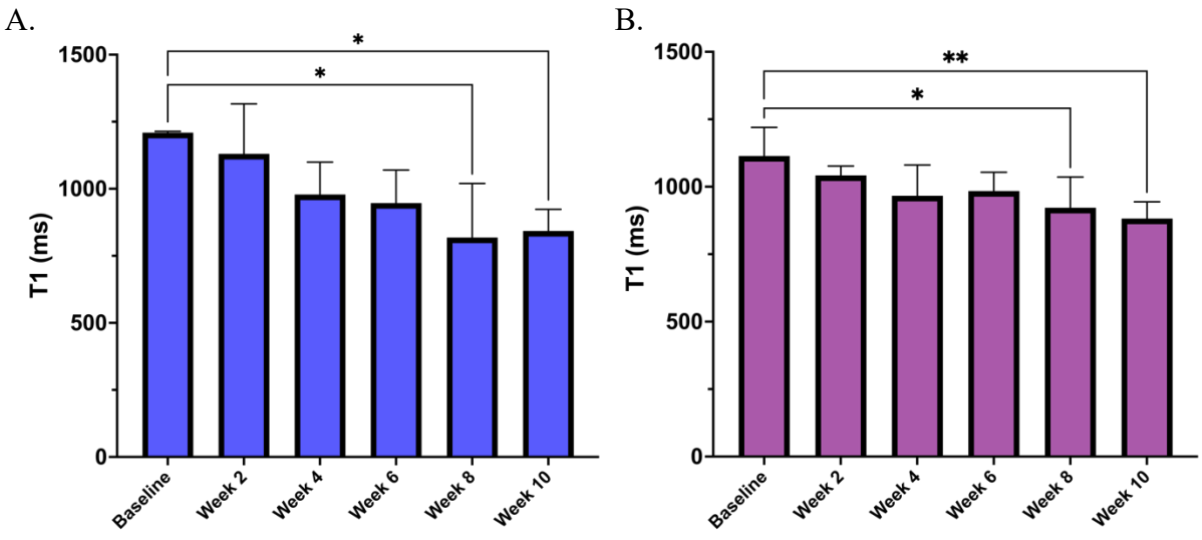

Figure 16. T1 values for the control group (A) and the experimental group (B).

T2

Alongside T1 parameters, we examined T2 parametric maps to infer the tendon's hydration and microstructural status. The T2 values offer a preliminary look at the differences in tendon recovery between the control and experimental groups.

As illustrated in *Figure 17*, both the control and experimental groups exhibited a noticeable surge during the initial four weeks, culminating in a peak at the fourth week. Following this apex, a subsequent decline in T2 values was observed in both cohorts. Notably, the descent in T2 values for the experimental group was more pronounced, evident by a steeper slope, especially when juxtaposed with the trajectory exhibited by the control group during the final three timepoints. This marked decline allowed the T2 values of the experimental group to converge more closely to baseline levels by the conclusion of the study relative to their control counterparts. An additional observation of interest is the consistently higher standard deviation in the experimental group throughout the study when contrasted with the control group, hinting at a greater variability in responses or measurements within the experimental cohort.

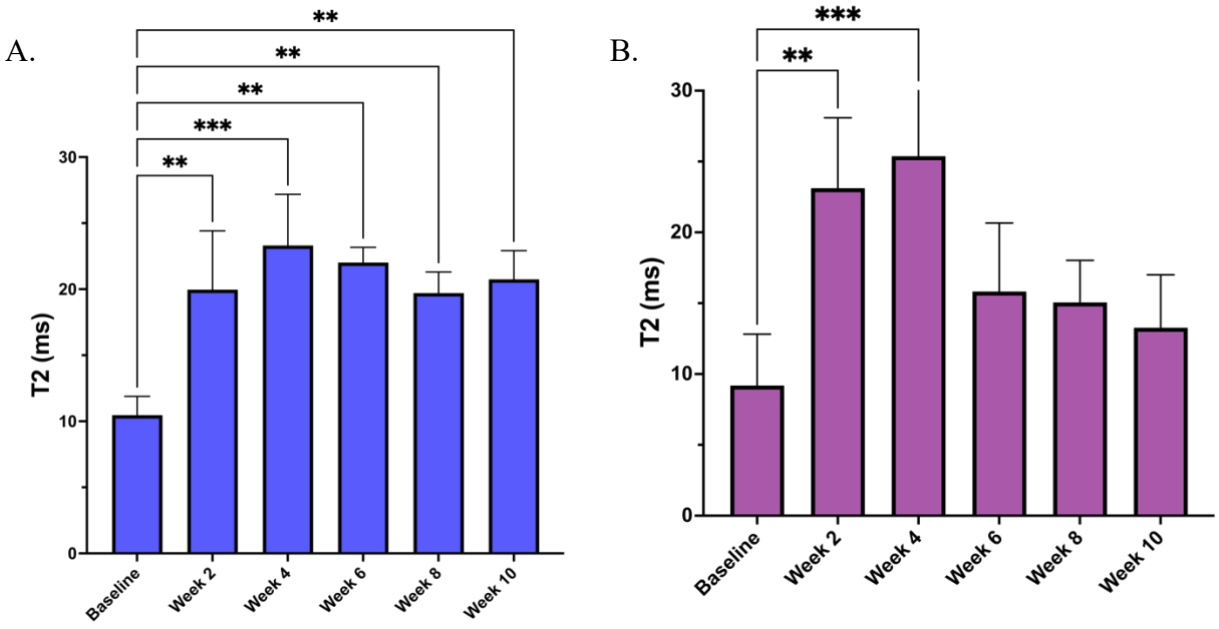

Figure 17. T2 values for the control group (A) and the experimental group (B).

DCE

By leveraging dynamic contrast enhanced (DCE) sequences, we aimed to evaluate tissue perfusion and vascular changes post-injury. The resultant DCE data aim to provide an initial understanding of blood flow dynamics within the healing tendon.

AUC

As shown in *Figure 18*, the AUC graphs for both control and experimental groups over the 10-week study duration show a notable trend. From baseline up to week 4, there's a clear rise in the AUC. Post week 4, however, a decline is evident until the study's conclusion. A sharper decrease is prominent for the experimental group in week 6, though the trajectories appear similar for both groups during the last two time points. Interestingly, by the study's end, the experimental group's AUC is nearing its baseline value, a shift not as pronounced in the control group.

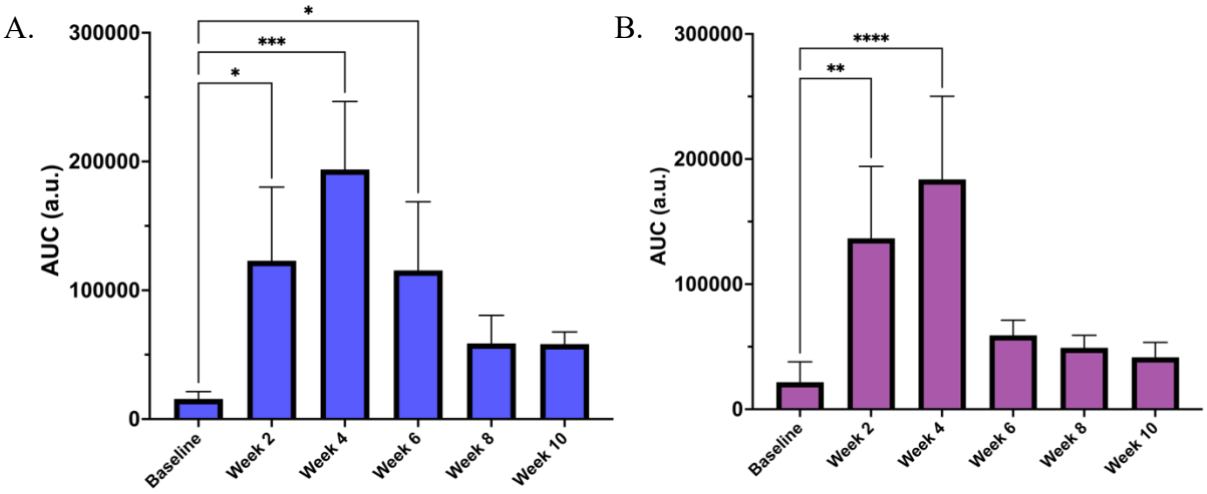

Figure 18. Area under the curve (AUC) values for the control group (A) and the experimental group (B).

IAUC

The IAUC graphs for both groups echo patterns observed in the AUC, as shown in *Figure 19*. Both groups demonstrate an upward trend in IAUC values up to week 4. Subsequent to that, a steady decline draws the values nearer to baseline by week 10. Notably, the experimental group displays a more pronounced ascent from baseline to week 4, and a subtler descent between weeks 6 to 10 when compared to the control group.

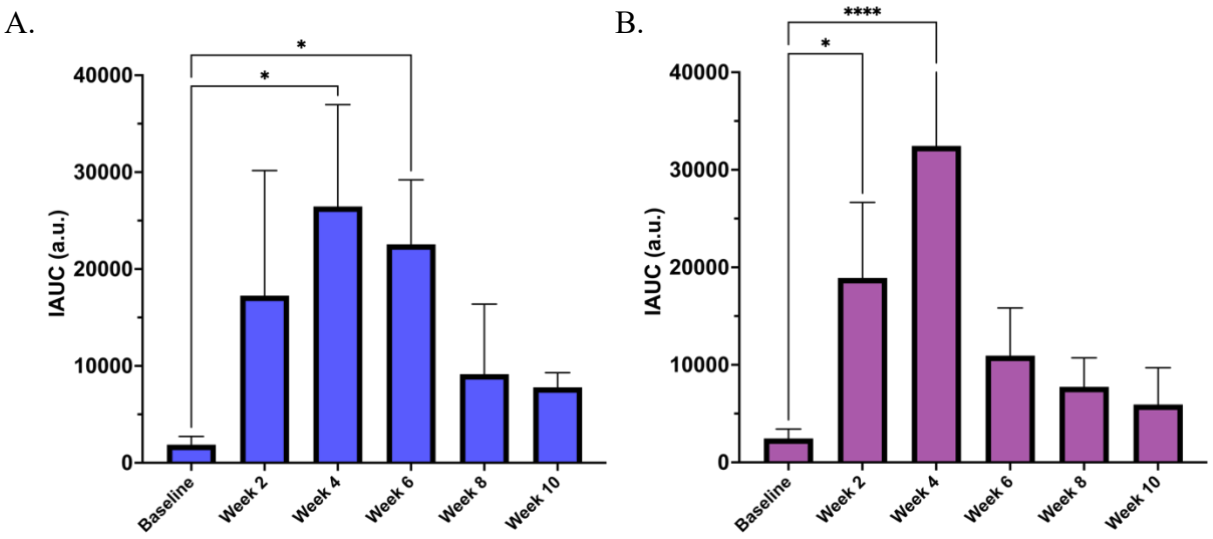

Figure 19. Initial area under the curve (IAUC) values for the control group (A) and the experimental group (B).

Peak Enhancement

Mirroring patterns discerned in the AUC and IAUC graphs, the peak enhancement trajectories share comparable trends, as illustrated in *Figure 20*. There's an upward surge in values leading up to week 4. Following this, the experimental group manifests a significant drop during week 6, later tapering gently towards week 10. In contrast, the control group's decline in week 6 is less pronounced, but the subsequent descent towards the study's conclusion is more marked.

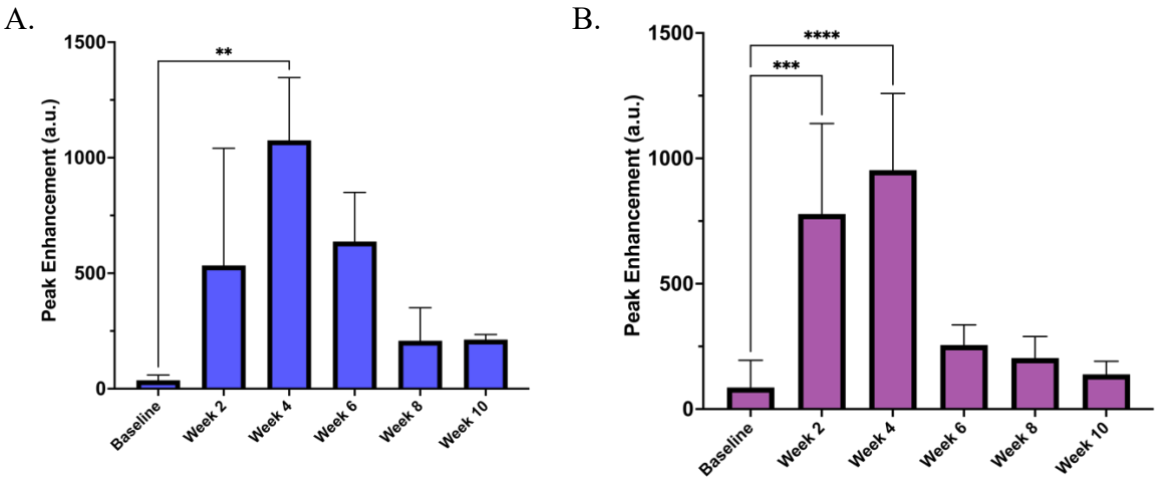

Figure 20. Peak enhancement values for the control group (A) and the experimental group (B)

Time To Peak

As shown in *Figure 21*, unlike the consistent trends evident in previous DCE data, the time to peak values for both groups present a more nuanced narrative. Over the course of the study, values largely remain steady, with only minor fluctuations from week to week. A notable divergence appears in the week-6 data for the control group, characterized by a distinct spike. Meanwhile, the experimental group exhibits a subtle ascent from baseline to week 4, followed by a gentle descent towards week 10. However, when factoring in the standard deviation, this perceived trend becomes less pronounced.

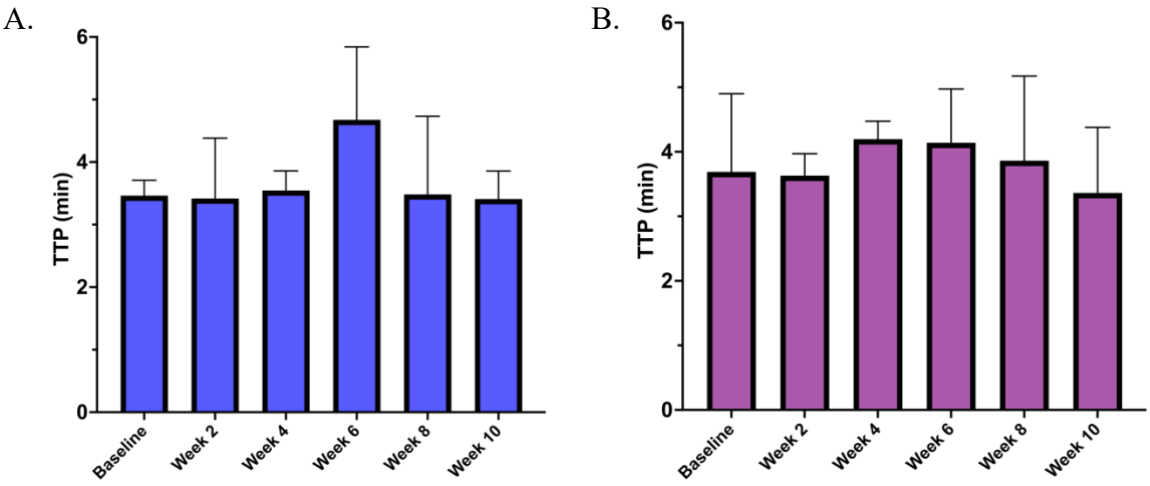

Figure 21. Time to peak values for the control group (A) and the experimental group (B).

Wash In Slope

The wash in slope, as depicted in the *Figure 22* for both control and experimental groups, demonstrates an upward trajectory from baseline to week 4. The control group registers incremental increases in both the baseline to week 2 and week 2 to week 4 intervals. Conversely, the experimental group evidences a notable surge between the baseline and week 2, but then stabilizes with negligible change up to week 4. Post the week 4 marker, there's a pronounced decline at week 6 for both sets, with the experimental group continuing on a descending path until week 10. The control group, however, experiences an additional dip at week 8, rebounding with a slight uptick by week 10. Summarily, after the significant week 4 ascent, both groups tend to gravitate back toward their baseline values as the study concludes.

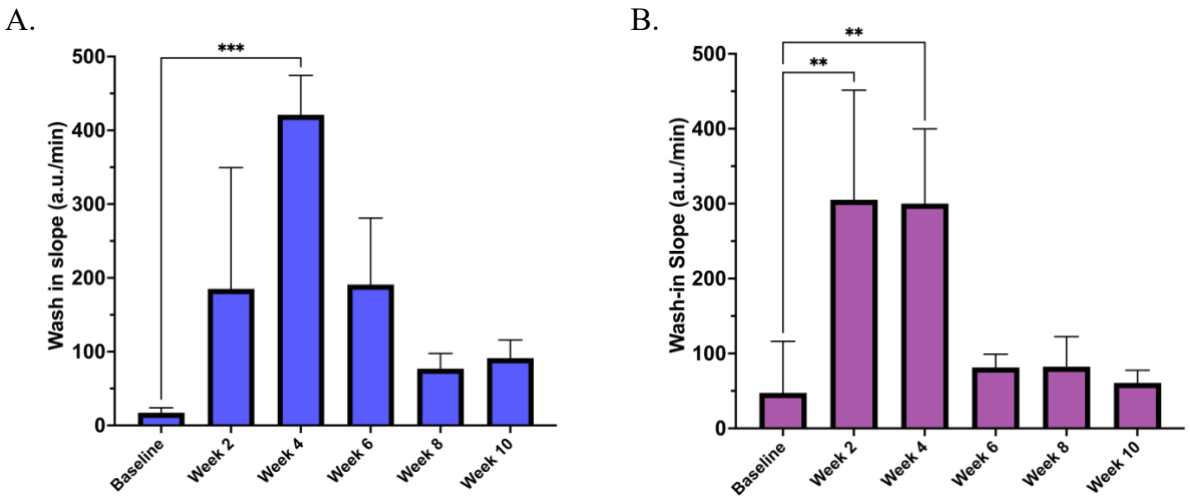

Figure 22. Wash in slope for the control group (A) and the experimental group (B).

Discussion

Pilot Study

Discussion

The pilot study was conceptualized to discern the feasibility, safety, and primary effects of intra-articular (IA) injection of Remodulin in the stifle joint of rabbits. With a comprehensive sampling and evaluation strategy in place, this study set the groundwork for deeper investigations into the clinical implications of this approach.

Upon analyzing the LS-MS/MS data, an immediate post-injection presence of Remodulin with concentrations of 51.8 ng/mL and 41.5 ng/mL in Rabbit 1 and Rabbit 2, respectively. Intriguingly, this detection was transient, with Remodulin becoming undetectable by the 7-day mark. This rapid decline could be indicative of an efficient metabolic or excretion process, or perhaps Remodulin's swift distribution and assimilation in tissue compartments. Adding further depth, the microscopic examinations did not reveal profound histological disparities between the subjects, emphasizing a relatively consistent tissue response to Remodulin.

Notably, synovial hypertrophy, which was multifocal and ranged from minimal to mild, was observed in both rabbits. The occurrence of this hypertrophy, along with the associated surface histiocytes, especially in the presence of Remodulin in Rabbit 2, hints at potential tissue reactions to the drug. While Rabbit 1 received a more concentrated dose in one knee, its reactions were not significantly intensified compared to the other, suggesting dose-independent tissue responses at the evaluated concentrations.

However, the appearance of cartilage fissures in Rabbit 2 and the consistent synovial hypertrophy observed could signify potential side effects of intra-articular Remodulin, though

further studies are needed to ascertain direct causality. Given that our aim was to assess tolerability and potential side-effects, these findings serve as crucial markers for risk assessment in subsequent larger-scale investigations.

The inherent limitations of this pilot study deserve attention. The pilot nature of this study, limited to two rabbits of differing ages and weights, might impact the generalizability of these findings. Rabbit 1, being younger and receiving a full dose in one knee, was envisioned to provide insights into a worst-case scenario. However, the age difference and weight disparities between the rabbits could introduce variables that might not have been fully accounted for in this preliminary study.

Looking ahead, the results underline the need for broader studies with larger cohorts to validate these findings. It would be prudent to investigate the rapid disappearance of Remodulin post-injection in greater depth, perhaps with more frequent sampling intervals in the immediate hours and days post-injection. Additionally, the potential tissue reactions to Remodulin warrant deeper exploration, possibly at varying dosages, to discern dose-dependent effects, if any.

In conclusion, this pilot study has shed light on the preliminary effects and potential concerns associated with intra-articular injections of Remodulin. While the findings provide a foundational understanding and pave the way for our 10-week study, it would be interesting to approach subsequent studies with a heightened focus on the observed tissue responses and pharmacokinetic behavior of Remodulin.

T1 Values

The potential of VFA T1 Mapping in gauging the molecular changes within tendons has been showcased in this study. It's pertinent to highlight that the fundamental principle of VFA T1 Mapping revolves around capturing the spin-lattice relaxation time, which is reflective of interactions between hydrogen protons and their surrounding environment. Such precision in imaging technique is expected to discern subtle tissue-specific changes.

Our observations hint at potential changes within the patellar tendon post-injury. As illustrated *Figure 16*, there appear to be certain distinctions in the T1 values between the control and experimental groups. Notably, specific time points indicated a statistically significant difference between the groups, with the one-way ANOVA indicating a p value < 0.05 at weeks 8 and the baseline in the experimental group, and a more pronounced significance (p value < 0.005) between week 10 and the baseline. This variance in values may suggest some disparities in the tendon's healing process.

A point to consider is the initial descent of the T1 values from a high baseline. The control group's decline, may be indicative of swift molecular changes post-injury, potentially related to an inflammatory or initial repair phase. In contrast, the experimental group’s more attenuated decrease might suggest a moderated healing process, possibly influenced by the drug under investigation. Whether this moderated process is advantageous in the long run, ensuring a more structured repair, is a hypothesis worthy of further exploration.

It's also worth noting the pronounced standard deviation observed in the control group. The variability could point towards a heterogeneous healing response within the control group. On the other hand, the experimental group's lower standard deviation signals a more uniform healing trajectory, perhaps facilitated by the intervention. Interestingly, there's no

evidence of either group's T1 values reverting to the baseline, a finding that demands further investigation.

The segmentation process and subsequent mathematical computations applied to deduce the T1 values from the MR images aim to establish a quantitative foundation. Given the role of these values in potentially offering glimpses into the tendon's structure, pathological deviations, and its healing phase, our methodology's preliminary findings present VFA T1 Mapping as a technique that may reveal changes not easily captured by traditional methods. However, its definitive reliability and sensitivity in understanding tendon healing still require comprehensive validation.

In conclusion, while the observed T1 values offer initial hints into tendon healing dynamics, the study also showcases the potential of VFA T1 Mapping in tendon research. Through the blend of qualitative and quantitative data on tendon composition, there's hope for refining treatment strategies and interventions for tendon-related conditions. However, the non-significant differences between control and experimental groups at other time points imply the need for further studies to cement the relevance and implications of observed T1 trends, especially in correlation with clinical outcomes.

T2 Values

T2 mapping is recognized for its profound ability to discern intricate distinctions in tissue properties, specifically for tendons. In our study, this advanced MRI technique shed light on the tendon's hydration and microstructural state throughout the healing process.

Observations from our results, shown in *Figure* 17, demonstrate that both the control and experimental groups experienced a pronounced increase in T2 values during the initial weeks. Notably, these alterations were statistically significant, with $p< 0.0005$ in the control group between the baseline and Week 4 and with a $p<0.0005$ in the experimental group between

the baseline and Week 4. This increase signifies an escalation in tendon hydration and changes in microstructure. Such a surge might be indicative of an inflammatory response post-injury, leading to an influx of water and inflammatory cells. This acute response is a typical phase in tendon healing, characterized by cellular infiltration and edema, both of which could lead to heightened T2 values. The observed peak at the fourth week, with $p<0.0005$ for both groups, might represent the climax of this inflammatory phase.

Following this peak, we noticed a decline in T2 values in both groups. This decreasing trend can be interpreted as the tendon transitioning from the inflammatory phase to the proliferative and remodeling phases of healing. During these phases, the water content in the tendon reduces, collagen fibers become more organized, and the extracellular matrix undergoes maturation. Such transitions would lead to a drop in T2 values as seen in our data.

One of the most interesting findings is the more pronounced descent in T2 values for the experimental group, bringing these values closer to the baseline by the end of our observation period, with the control gropu that presents a $p<0.005$ until the end of the 10 weeks. This suggests that the weekly intra-articular injections of Remodulin might accelerate the tendon's transition from the inflammatory phase, possibly by enhancing collagen fiber organization, improving extracellular matrix composition, or reducing prolonged inflammation. Our results show the potential efficacy of the drug in promoting expedited tendon repair by accelerating the healing trajectory, aligning with our initial hypothesis.

It's worth noting the higher standard deviation in T2 values within the experimental group throughout the study. This variability may imply a diverse response to the drug or potential variations in injury severity or individual healing rates among rabbits. While a larger sample size in future studies could elucidate this aspect further, the current variability underscores the importance of tailoring treatment interventions based on individual healing trajectories.

From a technical standpoint, the parameters and methodology employed ensured accurate and high-quality T2 data acquisition. The meticulous segmentation of the patellar tendon provided a consistent region of interest (ROI) for analysis. By emphasizing high resolution and clarity with the echo time of 11.1 ms and employing the VolumeSegmenter tool, our segmentation process potentially minimized errors that could arise from ROI delineation. Moreover, by leveraging the Levenberg-Marquardt algorithm for the NonlinearLeastSquares method, we ensured the precision of our T2 values, further supported by the strict criteria for fits having an r-square value above 0.90.

In conclusion, our results highlight the potential of T2 mapping as an helpful tool in monitoring tendon healing. The distinct patterns observed in the T2 values offer insight into the tendon's hydration and microstructural status, facilitating a deeper understanding of the tendon's repair process. The pronounced effect of the drug on accelerating tendon healing, as reflected by the T2 values, lays the groundwork for further exploration into its therapeutic potential in tendon repair and regeneration. Future studies focusing on varied animal models and larger sample sizes, coupled with micro-CT and histological analyses, will further consolidate our findings and help tailor interventions for optimal tendon recovery.

DCE

The dynamic nature of tissue recovery post-injury is a topic of great interest in the field of musculoskeletal research. Leveraging the capabilities of Dynamic Contrast Enhanced MRI (DCE-MRI), this study endeavored to provide a detailed insight into the vascular changes within the healing tendon.

Several parameters derived from DCE sequences were assessed, namely AUC, IAUC, Peak Enhancement, Time to Peak, and Wash-in Slope. These parameters provide unique insights

into tissue perfusion, highlighting the variations in blood flow dynamics over the course of tendon healing.

The AUC, as evidenced in our results in *Figure 18*, is indicative of the overall enhancement observed in the tendon tissue. The statistically significant rise in AUC values from baseline to week 4 for both control and experimental groups, with $p < 0.0005$ for the experimental and $p<0.005$ for the control group, could be emblematic of the acute phase of tendon healing, characterized by increased blood flow and nutrient delivery to the injured site. This phase usually involves inflammation and subsequent neovascularization, processes that might account for the increased AUC. The subsequent decline post-week 4, especially the sharper, statistically significant decrease in the experimental group ($p < 0.05$ on week 6 and $p>0.05$ until week 10, for the control group and $p>0.05$ until week 10 for the experimental group), may signify a transition into the proliferative phase, where tissue remodeling begins, necessitating reduced vascularity.

Similarly, the IAUC underscores the trends seen in AUC, reinforcing the findings, as shown in *Figure* 19. The more pronounced ascent from baseline to week 4 in the experimental group, which was statistically significant ($p < 0.0001$), could be attributed to higher blood flow in the experimental group compared to the control group where the p-value is <0.05.

Peak enhancement, similar to both AUC and IAUC, showed a statistically significant upward trajectory till week 4 (p value<0.005 for the control group and $p<0.00001$), as can be seen in *Figure 20*. The notable dip in the experimental group at week 6 might be an indication of rapid remodeling, possibly accelerated cellular activities, or alterations in the vascular structures that might require detailed histological assessments to validate.

In contrast to other parameters, Time to Peak introduces a unique perspective, exhibiting relatively steady values, as shown in *Figure* 21. The divergence at week 6 for the control group could hint at transient alterations in vascular flow dynamics or possible aberrations in the

healing process. However, the subtlety of the experimental group's trend and the overlap with standard deviation caution against deriving any definitive conclusions.

Lastly, the Wash-in Slope further illuminates the vascular dynamics at play, as in *Figure* 22. The upward trend in the experimental group till week 2, with a $p<0.005$ that remain stable, followed by stabilization suggests an early influx of nutrients and blood, possibly aligning with the immediate response to injury. The subsequent decline post-week 4 might be evocative of the healing tendon's reduced dependency on vascular support, hinting at a more mature tissue stage, this consideration is supported by the $p>0.05$ between the week6, week 8 and week 10 and the baseline.

To encapsulate, the insights drawn from the DCE sequences accentuate the intricate dance of tendon vascular dynamics post-injury. While the control and experimental groups both showcase similar trends, the intensity and timings of their responses carry nuanced differences that can potentially direct treatment and monitoring protocols. It's essential to integrate these findings with cellular and molecular studies to get a comprehensive understanding of tendon healing post-injury.

Future work might consider a deeper exploration into the specific factors influencing the vascular responses, potential interplay of molecular signaling pathways, and how these findings can be utilized to devise targeted interventions to expedite tendon healing without compromising tissue integrity.

Future Directions

This study has navigated the complexities of utilizing high-resolution 7T MR imaging to non-invasively monitor the healing process of induced patellar tendon injuries in a rabbit model. The development of a specialized MATLAB code for image analysis has streamlined the quantification of tendon repair, laying substantial groundwork for the next stages of this research. Moving forward, the future directions of this project are multifaceted and aim to build upon the current findings to offer more comprehensive insights into accelerated tendon repair strategies.

The forthcoming phase of research will employ micro-CT imaging and histological analyses. These methods will quantify osteophyte formation in post-injury knees, offering insights into the potential complications following tendon injuries. Histological analyses will enable the study of fibrotic tissue development at a cellular level, providing a deeper understanding of the tendon's healing landscape and the systemic effects of the drug being investigated. This approach will augment and possibly validate our MR findings, offering a more holistic view of the tendon repair process and the drug's impact on cellular activities and tissue morphology.

Building on the current image analysis framework, future work will involve refining the MATLAB code and user interface. Enhancements will focus on automating more components of the analysis process, incorporating machine learning algorithms for improved image segmentation, and expanding the code's capabilities to process data from upcoming micro-CT and histological studies. This advancement will expedite data processing, improve accuracy, and facilitate a more integrated analysis platform.

To enhance the robustness and applicability of our findings, subsequent studies could involve a larger cohort of animal subjects and introduce additional animal models. A more

substantial sample size will strengthen the statistical validity of the results, while varied animal models will allow the exploration of the therapy's efficacy across different biological contexts and tendon properties.

Future research will not limit itself to patellar tendons. Investigations could be extended to other tendon types to understand the universality of the observed therapeutic effects. Furthermore, the exploration of alternative drug combinations and delivery methods could be pivotal. Controlled release systems and combination therapies will be studied to identify protocols that optimize the balance between accelerated healing, reduced side effects, and overall tendon functionality post-recovery.

Beyond the biochemical and histological perspectives, long-term studies assessing the functional recovery of treated tendons will be integral. Advanced biomechanical testing methods will be used to evaluate the strength, elasticity, and functionality of healed tendons in comparison to untreated ones. Additionally, a comparative analysis between different treatment modalities, including NSAIDS, corticosteroids, and the drug under investigation, could be conducted to position our findings within the broader spectrum of available therapeutic options.

In conclusion, the next project phase will use micro-CT and histology to delve deeper into post-injury patellar tendon changes, validating our MRI findings. We also plan to expand our research scope, exploring varied tendons, alternative drug strategies, and larger, more diverse animal studies to enhance tendon recovery approaches.

Appendix A: Code Listings

T1 code:

T1map_app

```
classdef T1map_app < matlab.apps.AppBase

    % Properties that correspond to app components
    properties (Access = public)
        UIFigure                        matlab.ui.Figure
        GridLayout                      matlab.ui.container.GridLayout
        LeftPanel                       matlab.ui.container.Panel
        Lamp                            matlab.ui.control.Lamp
        Lamp_2                          matlab.ui.control.Lamp
        Lamp_3                          matlab.ui.control.Lamp
        ComputeT1mapButton              matlab.ui.control.Button
        Switch                          matlab.ui.control.Switch
        SelectDICOMimagesforB1Button    matlab.ui.control.Button
        SelectDICOMimagesforFA2Button   matlab.ui.control.Button
        SelectDICOMimagesforFA1Button   matlab.ui.control.Button
        EntertheseconFAvaluedegSpinner  matlab.ui.control.Spinner
        EntertheseconFAvaluedegSpinnerLabel  matlab.ui.control.Label
        EnterthefirstFAvaluedegSpinner  matlab.ui.control.Spinner
        EnterthefirstFAvaluedegSpinnerLabel  matlab.ui.control.Label
        EntertheTRvaluesecSpinner       matlab.ui.control.Spinner
        EntertheTRvaluesecSpinnerLabel  matlab.ui.control.Label
        ImagingsessiondateDatePicker    matlab.ui.control.DatePicker
        ImagingsessiondateDatePickerLabel  matlab.ui.control.Label
        RightPanel                      matlab.ui.container.Panel
        Switch_3                        matlab.ui.control.Switch
        DisplaymapButton                matlab.ui.control.Button
        CloseappButton                  matlab.ui.control.Button
        SavereportfileButton            matlab.ui.control.Button
        CopytablevaluesButton           matlab.ui.control.Button
        UITable                         matlab.ui.control.Table
        EntertheslicenumberthatyouwanttoseeSpinner  matlab.ui.control.Spinner
        EntertheslicenumberthatyouwanttoseeSpinnerLabel  matlab.ui.control.Label
        UIAxes                          matlab.ui.control.UIAxes
        ContextMenu                     matlab.ui.container.ContextMenu
        Menu                            matlab.ui.container.Menu
        Menu2                           matlab.ui.container.Menu
        ContextMenu2                    matlab.ui.container.ContextMenu
        Menu_2                          matlab.ui.container.Menu
        Menu2_2                         matlab.ui.container.Menu
    end

    % Properties that correspond to apps with auto-reflow
    properties (Access = private)
        onePanelWidth = 576;
    end

    properties (Access = private)
```

```
    TRval = 13;         % Repetition Time (TR) value
    FA1val = 4;         % First Flip Angle (FA1) value
    FA2val = 15;        % Second Flip Angle (FA2) value
    mri = [];           % MRI data
    statistics = [];    % Statistical data
    T = [];             % Temperature data
    printHisto = 0;     % Flag for printing histograms
    T1map = [];         % T1 map data
    slice2plot = 0;     % Slice number to plot
    allButtons = 0;     % Flag for all buttons
    labels = [];        % Labels data
    figureHandle = 0;   % Handle to the figure
end

% Callbacks that handle component events
methods (Access = private)

    % Code that executes after component creation
    function startupFcn(app, app1)
        % Set the value of a Spinner to TRval
        app.EntertheTRvaluesecSpinner.Value = app.TRval;

        % Set the value of a Spinner to FA1val
        app.EnterthefirstFAvaluedegSpinner.Value = app.FA1val;

        % Set the value of a Spinner to FA2val
        app.EntertheseconFAvaluedegSpinner.Value = app.FA2val;

        % Set the initial value of a Spinner to 1
        app.EntertheslicenumberthatyouwanttoseeSpinner.Value = 1;

        % Set the color of Lamp and Lamp_2 to red
        app.Lamp.Color = [1 0 0];
        app.Lamp_2.Color = [1 0 0];

        % Set the color of Lamp_3 to red
        app.Lamp_3.Color = [1 0 0];

        % Initialize the 'mri' structure with empty fields
        app.mri = struct("alpha1",[],"alpha2",[],"b1",[]);

        % Initialize the 'T' table with empty data
        app.T = table(["Right";"Left"],[0;0],[0;0],[0;0]);

        % Set variable names for the 'T' table columns
        app.T.Properties.VariableNames = ["Knee side","T1 Mean, [ms]","T1 std, [ms]","SEM"];

        % Set the data in the UITable to match the 'T' table
        app.UITable.Data = app.T;

        % Set the column names of the UITable to match the 'T' table variable names
        app.UITable.ColumnName = app.T.Properties.VariableNames;

        % Set the initial slice number to 1
        app.slice2plot = 1;

        % Find all uibuttons in the UIFigure and store them in 'allButtons'
        app.allButtons = findobj(app.UIFigure, 'Type', 'uibutton');

        % Set the visibility of UIAxes to 'off'
```

```
        app.UIAxes.Visible = 'off';

        % Set the value of ImagingsessiondateDatePicker to today's date
        app.ImagingsessiondateDatePicker.Value= datetime("today");

        % Set the options for the 'Switch' and 'Switch_3' components
        app.Switch.Items = {' ','Switch on to segment images'};
        app.Switch_3.Items = {' ','Switch on to display histograms'};

        % Get the screen size
        screenSize = get(groot,'Screensize');

        % Calculate the position to center the app within the screen
        position = app.UIFigure.Position;
        position(1) = (screenSize(3) - position(3)) / 2;
        position(2) = (screenSize(4) - position(4)) / 2;

        % Update the app's position to center it on the screen
        app.UIFigure.Position = position;

    end

    % Value changed function: EntertheTRvaluesecSpinner
    function EntertheTRvaluesecSpinnerValueChanged(app, event)
        % Update the TRval variable with the value from EntertheTRvaluesecSpinner
        app.TRval = app.EntertheTRvaluesecSpinner.Value;

    end

    % Value changed function: EnterthefirstFAvaluedegSpinner
    function EnterthefirstFAvaluedegSpinnerValueChanged(app, event)
        % Update the FA1val variable with the value from EnterthefirstFAvaluedegSpinner
        app.FA1val = app.EnterthefirstFAvaluedegSpinner.Value;

    end

    % Value changed function: EntertheseconFAvaluedegSpinner
    function EntertheseconFAvaluedegSpinnerValueChanged(app, event)
        % Update the FA2val variable with the value from EntertheseconFAvaluedegSpinner
        app.FA2val = app.EntertheseconFAvaluedegSpinner.Value;

    end

    % Button pushed function: SelectDICOMimagesforFA1Button
    function SelectDICOMimagesforFA1ButtonPushed(app, event)
        % Disable all buttons
        set(app.allButtons,'Enable','off');

        % Perform data acquisition for MRI with specified parameters and update app.mri
        app.mri = data_acquisition(app.mri,'T1',1,[app.TRval,app.FA1val]);

        % Set the color of Lamp to green to indicate successful acquisition
        app.Lamp.Color = [0 1 0];

        % Enable all buttons again
        set(app.allButtons,'Enable','on');

    end

    % Button pushed function: SelectDICOMimagesforFA2Button
```

```
function SelectDICOMimagesforFA2ButtonPushed(app, event)
    % Disable all buttons
    set(app.allButtons,'Enable','off');

    % Perform data acquisition for MRI with specified parameters and update app.mri
    app.mri = data_acquisition(app.mri,'T1',2,[app.TRval,app.FA2val]);

    % Set the color of Lamp_2 to green to indicate successful acquisition
    app.Lamp_2.Color = [0 1 0];

    % Enable all buttons again
    set(app.allButtons,'Enable','on');

end

% Button pushed function: SelectDICOMimagesforB1Button
function SelectDICOMimagesforB1ButtonPushed(app, event)
    % Disable all buttons
    set(app.allButtons,'Enable','off');

    % Perform data acquisition for MRI with specified parameters and update app.mri
    app.mri = data_acquisition(app.mri, 'T1',3,[]);

    % Set the color of Lamp_3 to green to indicate successful acquisition
    app.Lamp_3.Color = [0 1 0];

    % Enable all buttons again
    set(app.allButtons,'Enable','on');

end

% Value changed function: Switch
function SwitchValueChanged(app, event)
    % Use the 'volumeSegmenter' function to segment the MRI data in 'app.mri.alpha1.img'
    volumeSegmenter(app.mri.alpha1.img)

    % Display the current value of the 'Switch' component
    disp(app.Switch.Value)

end

% Value changed function: Switch_3
function Switch_3ValueChanged(app, event)
    % Check the value of the 'Switch_3' component
    switch app.Switch_3.Value
        case ' '  % If it's a space (no option selected)
            % Close the figure with the handle stored in 'app.figureHandle'
            close(app.figureHandle)
        case 'Switch on to display histograms'
            % Create a histogram display using data from 'app.mri.T1map.r', 'app.mri.T1map.l', and 'app.labels'
            app.figureHandle = histogramDisplay(app.mri.T1map.r,app.mri.T1map.l,app.labels);
    end


end

% Button pushed function: ComputeT1mapButton
function ComputeT1mapButtonPushed(app, event)
    s% Disable all buttons
    set(app.allButtons,'Enable','off');
```

```
            % Perform T1 mapping on the MRI data, updating 'app.statistics', 'app.mri', and 'app.labels'
            [app.statistics, app.mri, app.labels] = T1_mapping(app.mri);

            % Enable all buttons again
            set(app.allButtons,'Enable','on');

            % Call the 'UITableDisplayDataChanged' method with 'app' and 'event' as arguments
            UITableDisplayDataChanged(app, event)

            % Call the 'EntertheslicenumberthatyouwanttoseeSpinnerValueChanged' method with 'app' and 'event' as
arguments
            EntertheslicenumberthatyouwanttoseeSpinnerValueChanged(app, event)

        end

        % Value changed function:
        % EntertheslicenumberthatyouwanttoseeSpinner
        function EntertheslicenumberthatyouwanttoseeSpinnerValueChanged(app, event)
            % Check if the value of 'EntertheslicenumberthatyouwanttoseeSpinner' is less than 1
            if app.EntertheslicenumberthatyouwanttoseeSpinner.Value < 1
                % Set 'slice2plot' to 1 and update the Spinner value accordingly
                app.slice2plot = 1;
                app.EntertheslicenumberthatyouwanttoseeSpinner.Value = 1;
                % Check if the value of 'EntertheslicenumberthatyouwanttoseeSpinner' is greater than the number of
slices in 'app.mri.alpha1'
            elseif app.EntertheslicenumberthatyouwanttoseeSpinner.Value > app.mri.alpha1.slices
                % Set 'slice2plot' to the maximum number of slices and update the Spinner value accordingly
                app.slice2plot = app.mri.alpha1.slices;
                app.EntertheslicenumberthatyouwanttoseeSpinner.Value = app.mri.alpha1.slices;
            else
                % Otherwise, set 'slice2plot' to the Spinner's current value
                app.slice2plot = app.EntertheslicenumberthatyouwanttoseeSpinner.Value;
            end

            % Call the 'UIAxesButtonDown2' method with 'app' and 'event' as arguments
            UIAxesButtonDown2(app, event)

        end

        % Button down function: UIAxes
        function UIAxesButtonDown2(app, event)
    % Display the MRI slice corresponding to 'slice2plot' on the UIAxes
            imagesc(app.UIAxes, app.mri.alpha1.img(:,:,app.slice2plot));

            % Set the colormap of UIAxes to gray
            colormap(app.UIAxes,'gray');

            % Hide UIAxes by setting its visibility to 'off'
            app.UIAxes.Visible = 'off';

        end

        % Button pushed function: DisplaymapButton
        function DisplaymapButtonPushed(app, event)
            % Plot the T1 map for the selected slice using 'app.mri' and 'app.slice2plot'
            plot_T1_map(app.mri, app.slice2plot);

        end
```

```
        % Display data changed function: UITable
        function UITableDisplayDataChanged(app, event)
            % Create a table 'T' with data from 'app.statistics' and labels for "Right" and "Left" knee sides
            app.T = table(["Right";"Left"], [app.statistics.r(1); app.statistics.l(1)], ...
                [app.statistics.r(2); app.statistics.l(2)], [app.statistics.r(3); app.statistics.l(3)]);

            % Set variable names for the columns of the 'T' table
            app.T.Properties.VariableNames = ["Knee side", "T1 Mean, [ms]", "T1 std, [ms]", "SEM"];

            % Set the data of the UITable to match the 'T' table
            app.UITable.Data = app.T;

            % Set the column names of the UITable to match the 'T' table variable names
            app.UITable.ColumnName = app.T.Properties.VariableNames;

        end

        % Button pushed function: CopytablevaluesButton
        function CopytablevaluesButtonPushed(app, event)
            % Copy the concatenated data from 'app.statistics.r' and 'app.statistics.l' to the clipboard
            clipboard('copy', [app.statistics.r(:); app.statistics.l(:)]);

        end

        % Button pushed function: CloseappButton
        function CloseappButtonPushed(app, event)
            app.delete
        end

        % Button pushed function: SavereportfileButton
        function SavereportfileButtonPushed(app, event)
            writetable(app.T,'myfile.xls');
        end

        % Changes arrangement of the app based on UIFigure width
        function updateAppLayout(app, event)
            currentFigureWidth = app.UIFigure.Position(3);
            if(currentFigureWidth <= app.onePanelWidth)
                % Change to a 2x1 grid
                app.GridLayout.RowHeight = {569, 569};
                app.GridLayout.ColumnWidth = {'1x'};
                app.RightPanel.Layout.Row = 2;
                app.RightPanel.Layout.Column = 1;
            else
                % Change to a 1x2 grid
                app.GridLayout.RowHeight = {'1x'};
                app.GridLayout.ColumnWidth = {349, '1x'};
                app.RightPanel.Layout.Row = 1;
                app.RightPanel.Layout.Column = 2;
            end
        end
    end

    % Component initialization
    methods (Access = private)

        % Create UIFigure and components
        function createComponents(app)

            % Create UIFigure and hide until all components are created
```

```
            app.UIFigure = uifigure('Visible', 'off');
            app.UIFigure.AutoResizeChildren = 'off';
            app.UIFigure.Color = [1 1 1];
            app.UIFigure.Position = [100 100 879 569];
            app.UIFigure.Name = 'MATLAB App';
            app.UIFigure.SizeChangedFcn = createCallbackFcn(app, @updateAppLayout, true);

            % Create GridLayout
            app.GridLayout = uigridlayout(app.UIFigure);
            app.GridLayout.ColumnWidth = {349, '1x'};
            app.GridLayout.RowHeight = {'1x'};
            app.GridLayout.ColumnSpacing = 0;
            app.GridLayout.RowSpacing = 0;
            app.GridLayout.Padding = [0 0 0 0];
            app.GridLayout.Scrollable = 'on';

            % Create LeftPanel
            app.LeftPanel = uipanel(app.GridLayout);
            app.LeftPanel.BackgroundColor = [1 1 1];
            app.LeftPanel.Layout.Row = 1;
            app.LeftPanel.Layout.Column = 1;

            % Create ImagingsessiondateDatePickerLabel
            app.ImagingsessiondateDatePickerLabel = uilabel(app.LeftPanel);
            app.ImagingsessiondateDatePickerLabel.HorizontalAlignment = 'right';
            app.ImagingsessiondateDatePickerLabel.Position = [37 493 118 22];
            app.ImagingsessiondateDatePickerLabel.Text = 'Imaging session date';

            % Create ImagingsessiondateDatePicker
            app.ImagingsessiondateDatePicker = uidatepicker(app.LeftPanel);
            app.ImagingsessiondateDatePicker.Position = [162 493 150 22];

            % Create EntertheTRvaluesecSpinnerLabel
            app.EntertheTRvaluesecSpinnerLabel = uilabel(app.LeftPanel);
            app.EntertheTRvaluesecSpinnerLabel.HorizontalAlignment = 'right';
            app.EntertheTRvaluesecSpinnerLabel.Position = [36 432 135 22];
            app.EntertheTRvaluesecSpinnerLabel.Text = 'Enter the TR value (sec)';

            % Create EntertheTRvaluesecSpinner
            app.EntertheTRvaluesecSpinner = uispinner(app.LeftPanel);
            app.EntertheTRvaluesecSpinner.ValueChangedFcn = createCallbackFcn(app,
@EntertheTRvaluesecSpinnerValueChanged, true);
            app.EntertheTRvaluesecSpinner.Position = [212 432 100 22];

            % Create EnterthefirstFAvaluedegSpinnerLabel
            app.EnterthefirstFAvaluedegSpinnerLabel = uilabel(app.LeftPanel);
            app.EnterthefirstFAvaluedegSpinnerLabel.HorizontalAlignment = 'right';
            app.EnterthefirstFAvaluedegSpinnerLabel.Position = [36 405 157 22];
            app.EnterthefirstFAvaluedegSpinnerLabel.Text = 'Enter the first FA value (deg)';

            % Create EnterthefirstFAvaluedegSpinner
            app.EnterthefirstFAvaluedegSpinner = uispinner(app.LeftPanel);
            app.EnterthefirstFAvaluedegSpinner.ValueChangedFcn = createCallbackFcn(app,
@EnterthefirstFAvaluedegSpinnerValueChanged, true);
            app.EnterthefirstFAvaluedegSpinner.Position = [212 404 100 22];

            % Create EntertheseconFAvaluedegSpinnerLabel
            app.EntertheseconFAvaluedegSpinnerLabel = uilabel(app.LeftPanel);
            app.EntertheseconFAvaluedegSpinnerLabel.HorizontalAlignment = 'right';
            app.EntertheseconFAvaluedegSpinnerLabel.Position = [36 377 170 22];
```

```
            app.EntertheseconFAvaluedegSpinnerLabel.Text = 'Enter the secon FA value (deg)';

            % Create EntertheseconFAvaluedegSpinner
            app.EntertheseconFAvaluedegSpinner = uispinner(app.LeftPanel);
            app.EntertheseconFAvaluedegSpinner.ValueChangedFcn = createCallbackFcn(app,
@EntertheseconFAvaluedegSpinnerValueChanged, true);
            app.EntertheseconFAvaluedegSpinner.Position = [212 377 100 22];

            % Create SelectDICOMimagesforFA1Button
            app.SelectDICOMimagesforFA1Button = uibutton(app.LeftPanel, 'push');
            app.SelectDICOMimagesforFA1Button.ButtonPushedFcn = createCallbackFcn(app,
@SelectDICOMimagesforFA1ButtonPushed, true);
            app.SelectDICOMimagesforFA1Button.Position = [36 303 246 23];
            app.SelectDICOMimagesforFA1Button.Text = 'Select DICOM images for FA1';

            % Create SelectDICOMimagesforFA2Button
            app.SelectDICOMimagesforFA2Button = uibutton(app.LeftPanel, 'push');
            app.SelectDICOMimagesforFA2Button.ButtonPushedFcn = createCallbackFcn(app,
@SelectDICOMimagesforFA2ButtonPushed, true);
            app.SelectDICOMimagesforFA2Button.Position = [36 270 246 23];
            app.SelectDICOMimagesforFA2Button.Text = 'Select DICOM images for FA2';

            % Create SelectDICOMimagesforB1Button
            app.SelectDICOMimagesforB1Button = uibutton(app.LeftPanel, 'push');
            app.SelectDICOMimagesforB1Button.ButtonPushedFcn = createCallbackFcn(app,
@SelectDICOMimagesforB1ButtonPushed, true);
            app.SelectDICOMimagesforB1Button.Position = [36 236 246 23];
            app.SelectDICOMimagesforB1Button.Text = 'Select DICOM images for B1';

            % Create Switch
            app.Switch = uiswitch(app.LeftPanel, 'slider');
            app.Switch.Items = {'', 'Switch on to segment images'};
            app.Switch.ValueChangedFcn = createCallbackFcn(app, @SwitchValueChanged, true);
            app.Switch.Position = [36 156 61 27];
            app.Switch.Value = '';

            % Create ComputeT1mapButton
            app.ComputeT1mapButton = uibutton(app.LeftPanel, 'push');
            app.ComputeT1mapButton.ButtonPushedFcn = createCallbackFcn(app, @ComputeT1mapButtonPushed,
true);
            app.ComputeT1mapButton.FontSize = 16;
            app.ComputeT1mapButton.FontWeight = 'bold';
            app.ComputeT1mapButton.Position = [96 49 146 54];
            app.ComputeT1mapButton.Text = 'Compute T1 map';

            % Create Lamp_3
            app.Lamp_3 = uilamp(app.LeftPanel);
            app.Lamp_3.Position = [294 237 20 20];

            % Create Lamp_2
            app.Lamp_2 = uilamp(app.LeftPanel);
            app.Lamp_2.Position = [294 271 20 20];

            % Create Lamp
            app.Lamp = uilamp(app.LeftPanel);
            app.Lamp.Position = [294 304 20 20];

            % Create RightPanel
            app.RightPanel = uipanel(app.GridLayout);
            app.RightPanel.BackgroundColor = [1 1 1];
```

```
            app.RightPanel.Layout.Row = 1;
            app.RightPanel.Layout.Column = 2;

            % Create UIAxes
            app.UIAxes = uiaxes(app.RightPanel);
            title(app.UIAxes, 'Title')
            xlabel(app.UIAxes, 'X')
            ylabel(app.UIAxes, 'Y')
            zlabel(app.UIAxes, 'Z')
            app.UIAxes.ButtonDownFcn = createCallbackFcn(app, @UIAxesButtonDown2, true);
            app.UIAxes.Position = [21 217 498 307];

            % Create EntertheslicenumberthatyouwanttoseeSpinnerLabel
            app.EntertheslicenumberthatyouwanttoseeSpinnerLabel = uilabel(app.RightPanel);
            app.EntertheslicenumberthatyouwanttoseeSpinnerLabel.HorizontalAlignment = 'right';
            app.EntertheslicenumberthatyouwanttoseeSpinnerLabel.Position = [100 531 238 22];
            app.EntertheslicenumberthatyouwanttoseeSpinnerLabel.Text = 'Enter the slice number that you want to
see';

            % Create EntertheslicenumberthatyouwanttoseeSpinner
            app.EntertheslicenumberthatyouwanttoseeSpinner = uispinner(app.RightPanel);
            app.EntertheslicenumberthatyouwanttoseeSpinner.ValueChangedFcn = createCallbackFcn(app,
@EntertheslicenumberthatyouwanttoseeSpinnerValueChanged, true);
            app.EntertheslicenumberthatyouwanttoseeSpinner.Position = [353 531 100 22];

            % Create UITable
            app.UITable = uitable(app.RightPanel);
            app.UITable.ColumnName = {'Column 1'; 'Column 2'; 'Column 3'; 'Column 4'};
            app.UITable.RowName = {};
            app.UITable.DisplayDataChangedFcn = createCallbackFcn(app, @UITableDisplayDataChanged, true);
            app.UITable.Position = [42 96 433 75];

            % Create CopytablevaluesButton
            app.CopytablevaluesButton = uibutton(app.RightPanel, 'push');
            app.CopytablevaluesButton.ButtonPushedFcn = createCallbackFcn(app,
@CopytablevaluesButtonPushed, true);
            app.CopytablevaluesButton.Position = [100 65 110 23];
            app.CopytablevaluesButton.Text = 'Copy table values';

            % Create SavereportfileButton
            app.SavereportfileButton = uibutton(app.RightPanel, 'push');
            app.SavereportfileButton.ButtonPushedFcn = createCallbackFcn(app, @SavereportfileButtonPushed,
true);
            app.SavereportfileButton.Position = [307 65 100 23];
            app.SavereportfileButton.Text = 'Save report file';

            % Create CloseappButton
            app.CloseappButton = uibutton(app.RightPanel, 'push');
            app.CloseappButton.ButtonPushedFcn = createCallbackFcn(app, @CloseappButtonPushed, true);
            app.CloseappButton.Position = [209 13 100 23];
            app.CloseappButton.Text = 'Close app';

            % Create DisplaymapButton
            app.DisplaymapButton = uibutton(app.RightPanel, 'push');
            app.DisplaymapButton.ButtonPushedFcn = createCallbackFcn(app, @DisplaymapButtonPushed, true);
            app.DisplaymapButton.Position = [351 184 100 23];
            app.DisplaymapButton.Text = 'Display map';

            % Create Switch_3
            app.Switch_3 = uiswitch(app.RightPanel, 'slider');
```

```
            app.Switch_3.Items = {'', 'Switch on to display histogram'};
            app.Switch_3.ValueChangedFcn = createCallbackFcn(app, @Switch_3ValueChanged, true);
            app.Switch_3.Position = [60 182 61 27];
            app.Switch_3.Value = '';

            % Create ContextMenu
            app.ContextMenu = uicontextmenu(app.UIFigure);

            % Create Menu
            app.Menu = uimenu(app.ContextMenu);
            app.Menu.Text = 'Menu';

            % Create Menu2
            app.Menu2 = uimenu(app.ContextMenu);
            app.Menu2.Text = 'Menu2';

            % Create ContextMenu2
            app.ContextMenu2 = uicontextmenu(app.UIFigure);

            % Create Menu_2
            app.Menu_2 = uimenu(app.ContextMenu2);
            app.Menu_2.Text = 'Menu';

            % Create Menu2_2
            app.Menu2_2 = uimenu(app.ContextMenu2);
            app.Menu2_2.Text = 'Menu2';

            % Show the figure after all components are created
            app.UIFigure.Visible = 'on';
        end
    end

    % App creation and deletion
    methods (Access = public)

        % Construct app
        function app = T1map_app(varargin)

            % Create UIFigure and components
            createComponents(app)

            % Register the app with App Designer
            registerApp(app, app.UIFigure)

            % Execute the startup function
            runStartupFcn(app, @(app)startupFcn(app, varargin{:}))

            if nargout == 0
                clear app
            end
        end

        % Code that executes before app deletion
        function delete(app)

            % Delete UIFigure when app is deleted
            delete(app.UIFigure)
        end
    end
end
```

data_acquisition

```
function  [mri] = data_acquisition(mri,choice,option,paramSet)
% Author: Marco Mussato
% Date: 2022-12-01
%
% Matlab version: R2022b
%
% process_DICOM_data - reads DICOM images from a user-specified folder and saves them in a structure
%
% SYNTAX:
% mri = process_DICOM_data(choice)
%
% INPUTS:
% choice - a string indicating the type of MRI image to import and save. Can be either 'T1' or 'DCE'.
%
% OUTPUTS:
% mri - a structure containing the imported and saved MRI data, including images, image dimensions, and
FA/TR values (if available).
%

%% Saving main folder's path

% Handle the user's response to the dialog box
switch choice
   case 'T1'
      % Import images using the img_import function
      [imgMat,tot_rows,tot_columns,tot_slices,path] = img_import();

      % If the selected folder is empty, display an error message and exit
      if isempty(imgMat)
         uiwait(msgbox({'The selected folder is empty.'; 'Please select another folder.'},"Error","error"));
         return;
      else

         % Create the fields for the structure
         fields = ["alpha1","alpha2","b1"];

         if option == 1
            data = "FA1";
            mri.(fields(1)) = structureCreator(mri.(fields(1)), imgMat, tot_rows, tot_columns, tot_slices, 0, path,
data, 1,paramSet);
         elseif option == 2
            data = "FA2";
            mri.(fields(2)) = structureCreator(mri.(fields(2)), imgMat, tot_rows, tot_columns, tot_slices, 0, path,
data, 1,paramSet);
         else
            mri.(fields(3))= structureCreator(mri.(fields(3)), imgMat, tot_rows,  tot_columns, tot_slices, 0, path, [],
0,paramSet);
            % Resize the b1 image to have the same dimensions as the alpha1 image
            mri.(fields(3)).img = imresize(mri.b1.img,[mri.alpha1.rows mri.alpha1.columns]);

            % Update the dimensions of the b1 image to match the alpha1 image
            mri.(fields(3)).rows = mri.(fields(1)).rows;
            mri.(fields(3)).columns = mri.(fields(1)).columns;
         end
```

```
        end
    case 'DCE'
        % Import images using the img_import function
        [imgMat,tot_rows,tot_columns,tot_slices,~] = img_import();
        slice_group = 24;
        tot_acquisition = tot_slices/24;

        % Initialize a structure with a single field called "dce"
        mri = struct("dce",[]);
        % Populate the "dce" field of the structure with the imported images
        % using the structureCreator function
        mri.dce = structureCreator(mri.dce, imgMat, tot_rows, tot_columns, tot_slices, 0, [], [], []);
        mri.dce.img = reshape(mri.dce.img,[tot_rows,tot_columns,slice_group,tot_acquisition]);
        mri.dce.groupslice = slice_group;
        mri.dce.totacq = tot_acquisition;
end

end
```

img_import

```
function [imgMat,tot_rows,tot_columns,tot_slices,path] = img_import()
% Author: Marco Mussato
% Date: 2023-01-03
%
% Matlab version: 2022b
%
% img_import - Read DICOM files and store them as a 3D matrix.
%
% SYNTAX:
%   [imgMat,tot_rows,tot_columns,tot_slices] = img_import()
%
% INPUTS:
%   none (user is prompted to select one or more DICOM files using the uigetfile function)
%
% OUTPUTS:
%   imgMat:         3D matrix containing the DICOM image data
%   tot_rows:       integer representing the number of rows in each image
%   tot_columns:    integer representing the number of columns in each image
%   tot_slices:     integer representing the total number of slices
%
% Example:
%   [imgMat,tot_rows,tot_columns,tot_slices] = img_import()


% Prompt the user to select a folder containing the DICOM images
%           files = dir(uigetdir('S:\Shared\Ortho Project - Tendon Injury\MRI SESSIONS')); %select the folder
[file,path] = uigetfile('*.IMA*','Select One or More Files','MultiSelect', 'on');
% Check if the folder is empty
if isempty(file) % If the selected folder is empty, display an error message and exit
    uiwait(msgbox({'The selected folder is empty.'; 'Please select another folder.'},"Error","error"));
    return;
else
    %this for stores the DICOM's information and save all the image as a matrix
    %with MxNxD dimention, where MxN is the num of pixel in each image and D is
    %the total number of slices

    tot_slices= length(file); % Calculate the total number of slices
```

```
    for ii=1:tot_slices
        % Read the DICOM metadata for the current slice
        %                   imgInfo = dicominfo(fullfile(files(ii+2).folder,files(ii+2).name)); % Read the DICOM
metadata
        imgInfo = dicominfo(char(fullfile(path,file(ii))));
        % If this is the first slice, initialize the 'imgMat' matrix with the appropriate size
        if ii == 1
            tot_rows = imgInfo.Rows; % Get the number of rows in the image
            tot_columns = imgInfo.Columns; % Get the number of columns in the image
            imgMat = zeros(tot_rows,tot_columns,tot_slices); %create empty matrix that will store the data
            imgMat(:,:,ii) = dicomread(imgInfo); %saving first image inside the matrix
            f = waitbar(0,'Starting imaging importing...');
        else
            imgMat(:,:,ii) = dicomread(imgInfo);%saving the remaning images
            percentage = ii/tot_slices;
            waitbar(percentage,f,sprintf('Saving DICOM images %d%%...',int8(percentage*100)));
        end
    end
    waitbar(1,f,'All images have been imported!');
    pause(1)
    close(f)
end
```

structureCreator

```
function [mri] = structureCreator(mri,img,rows,columns,slices,FAcheck,path,data,noPy,paramSet)
%%Author: Marco Mussato
%Date: 2022-12-01
%
%Matlab version: R2022b
%
% create_mri_structure - creates a structure with MRI data, including images, FA value, and TR value
%
% SYNTAX:
%   mri = create_mri_structure(mri, img, rows, columns, slices, index, FAcheck, path, data)
%
% INPUTS:
%   mri: initial structure for the MRI data
%   img: matrix containing all the DICOM images
%   rows: number of rows in the image matrix
%   columns: number of columns in the image matrix
%   slices: number of slices in the image matrix
%   index: index of the current folder (FA1, FA2, or B1)
%   FAcheck: binary value indicating whether to include the FA value in the structure (1 to include, 0 otherwise)
%   path: specified path to the folder with DICOM images
%   data: define from which acquisition FA and TR has to be extracted
%
% OUTPUTS:
%   mri: structure containing MRI data, including images, image dimensions, FA value, and TR value


mri.img = img; % save image data in the 'img' field of the 'mri' structure
mri.rows = rows; % save number of rows in the image in the 'rows' field of the 'mri' structure
mri.columns = columns; % save number of columns in the image in the 'columns' field of the 'mri' structure
mri.slices = slices; % save number of slices in the image in the 'slices' field of the 'mri' structure

if FAcheck % check if flip angle information is available
```

```
    %saving pdf path
    pdfPath = dir([uigetdir() '/*.pdf']);
    %using py script to extract information
    py.PdfFileManager.DataExtractor(fullfile(pdfPath(1).folder,pdfPath(1).name),path,data)
    %loaging .mat file containing a structure with extracted information
    pdfInfo = load('Results.mat');

    %adding extracted info to the "mri" structure
    mri.FA = deg2rad(double(pdfInfo.FA)); % convert flip angle from degrees to radians and save it in the 'FA'
field of the 'mri' structure
    mri.TR =double(pdfInfo.TR); % save repetition time in the 'TR' field of the 'mri' structure
end

 if noPy
    mri.FA = deg2rad(paramSet(2));
    mri.TR = paramSet(1);
end

end
```

T1_mapping

```
function [statistics, mri, labels] = T1_mapping(mri)

% Author: Marco Mussato
% Date: 2023-01-04
%
% Matlab version: 2022b
%
% T1_mapping - Compute T1 maps from DICOM data.
%
% SYNTAX:
%   T1_mapping(mri)
%
% INPUTS:
%   mri: structure with different information, such as images and matrix
%   dimention
%
% OUTPUTS:
%   statistics: structure with information about mean, std and sem of the
%   T1 map
%   mri: updated structure, with the T1 map for each knee
%   labels: labels with the segmentation of the knees
%
% Example:
%   [statistics, mri, labels] = T1_mapping(mri)
%
%%

%% Segmentation of the image
addpath("Masks/");
% Display a message box with instructions for the user
CreateStruct.Interpreter = 'tex';
CreateStruct.WindowStyle = 'modal';
text= '\fontsize{12} Select the file with the segmentation';
uiwait(msgbox(text,"DICOM Selection",CreateStruct));
% Open a file selection dialog to allow the user to select a file
[filename,~] = uigetfile('*.mat*','Select file to open');
```

```
% Load the segmentation from the selected file
labels = load(filename);
labels = labels.labels;

%% Computing T1 map
slices = mri.alpha1.slices; % save the number of slices in the 'slices' variable
rows = mri.alpha1.rows; % save the number of rows in the 'rows' variable
columns = mri.alpha1.columns; % save the number of columns in the 'columns' variable

T1mapR = zeros(rows,columns,slices); % create a 3D array with the specified number of slices, rows, and
columns for the R knee
T1mapL = zeros(rows,columns,slices); % create a 3D array with the specified number of slices, rows, and
columns for the L knee

labelsR = labels == 'RIGHT KNEE';
labelsL = labels == 'LEFT KNEE';

f = waitbar(0,'Starting T1 computation...');
pause(.3)
% computing T1 mapping following Helms et al. 2008
for kk = 1:slices
   percentage = kk/slices;
   waitbar(percentage,f,sprintf('Computing T1 values for slice #%d',kk));
   T1mapR(:,:,kk) = T1finalcomp(mri,labelsR(:,:,kk),T1mapR(:,:,kk),kk);
   T1mapL(:,:,kk) = T1finalcomp(mri,labelsL(:,:,kk),T1mapL(:,:,kk),kk);
end
waitbar(1,f,'T1 computation completed');
pause(1)
close(f)

%% Checking vlalues

% T1mapR(T1mapR<0 | T1mapR>2000)=NaN;
% T1mapL(T1mapL<0 | T1mapL>2000)=NaN;

% Calculate the mean and standard deviation of the T1map values
% corresponding to non-zero elements in labels
mean_T1R = mean(T1mapR(find(labelsR==1)), 'omitnan'); % calculate the mean of the T1 values for the right
knee
std_T1R = std(T1mapR(find(labelsR==1)), 'omitnan'); % calculate the standard deviation of the T1 values for
the right knee
mean_T1L = mean(T1mapL(find(labelsL==1)), 'omitnan'); % calculate the mean of the T1 values for the left
knee
std_T1L = std(T1mapL(find(labelsL==1)), 'omitnan'); % calculate the standard deviation of the T1 values for the
left knee

% Calculate the standard error of the mean
semR = std_T1R/sqrt(numel(nonzeros(labelsR(:,:,:)))); % calculate the standard error of the mean for the right
knee
semL = std_T1L/sqrt(numel(nonzeros(labelsL(:,:,:)))); % calculate the standard error of the mean for the left
knee

% Save data in structures

mri.T1map = struct("r",T1mapR,"l",T1mapL); % save the T1 maps for the right and left knee in the 'mri'
structure
statistics = struct("r",[mean_T1R, std_T1R, semR],"l",[mean_T1L, std_T1L, semL]); % save the mean, standard
deviation and standard error of the mean for the right and left knee in the 'statistics' structure
labels= struct("r",labelsR,"l",labelsL); % save the labels for the right and left knee in the 'labels' structure
end
```

T1finalcomp

```
function [T1map] = T1finalcomp(mri,labels,T1map,kk)
% T1finalcomp - Compute T1 values from two alpha images
%
% SYNTAX:
%    [T1map] = T1finalcomp(mri,labels,T1map,kk)
%
% INPUTS:
%    mri - struct containing information about the two alpha images and TR
%    labels - binary image with 1's indicating voxels to compute T1 values for
%    T1map - initial T1 map to update with computed T1 values
%    kk - current slice number
%
% OUTPUTS:
%    T1map - updated T1 map with computed T1 values for voxels with nonzero
%            values in the 'labels' array at the current slice

%selecting just those pixels inside the matrix
[rowindex, columnindex] = find(labels(:,:)==1); % find the row and column indices of the pixels with nonzero
values in the 'labels' array at the current slice
for ii = 1:length(rowindex)
   r = rowindex(ii); % save the current row index in the 'r' variable
   c = columnindex(ii); % save the current column index in the 'c' variable
   S1 = mri.alpha1.img(r,c,kk); % extract the signal intensity for the current pixel from the first FA image
   S2 = mri.alpha2.img(r,c,kk); % extract the signal intensity for the current pixel from the second FA image
   %        fB1 = mri.b1.img(r,c,kk)/900;
   fB1 = 1; % set the B1 field inhomogeneity correction factor to 1
   T1map(r,c) = 2*mri.alpha1.TR*(1/(fB1^2))*(((S1/mri.alpha1.FA)-(S2/mri.alpha2.FA)) ...
                /((S2*mri.alpha2.FA)-(S1*mri.alpha1.FA))); %Computing T1 value
end
end
```

histogramDisplay

```
function [f1] = histogramDisplay(T1mapR,T1mapL,labels)
% % Author: Marco Mussato
% Date: 2023-01-27
%
% histogramDisplay - Display histogram of T1 values for right and left knees
%
% SYNTAX:
%    [f1] = histogramDisplay(T1mapR,T1mapL,labels)
%
% INPUTS:
%    T1mapR - T1 map for right knee
%    T1mapL - T1 map for left knee
%    labels - struct containing binary images with 1's indicating voxels in
%             the right and left knee
%
% OUTPUTS:
%    f1 - figure handle for the generated histogram

f1 = figure("Name","T1histo"); % create a new figure
h1 = histogram(T1mapR(find(labels.r==1))); % create histogram for T1 values in the right knee
hold on % hold the current plot so that the next plot is overlayed on top of it
```

```
h2 = histogram(T1mapL(find(labels.l==1))); % create histogram for T1 values in the left knee
legend("Right knee", "Left Knee") % add a legend to the plot
title("T1 map histogram for right and left knees") % add title to the plot
h1.Normalization = 'probability'; % normalize the histogram by the total number of elements in the input data
h1.BinWidth = 60; % set the bin width of the histogram
h2.Normalization = 'probability'; % normalize the histogram by the total number of elements in the input data
h2.BinWidth = 60; % set the bin width of the histogram
ylabel("Normalized intensity",'FontSize', 16) % add y-axis label
xlabel("T1 values, [ms]",'FontSize', 16) % add x-axis label
set(gca,'FontSize',14);

exportgraphics(gca, "test.jpeg") % export the figure as a jpeg file
end
```

plot_T1_map

```
function [] = plot_T1_map(mri,slice_number)
%Author: Marco Mussato & Davide Magliano
%Date: 2022-12-09
%
%Matlab version: R2022b
%
% plot_T1_map - creates a figure with the background and the T1 map overlapped, with a colorbar
%
% SYNTAX:
%   plot_T1_map(mri, slice_number)
%
% INPUTS:
%   mri: structure containing MRI data and T1 map
%   slice_number: slice to be plotted in the figure
%
% OUTPUTS:
%   figure with selected T1 map and background


background = mri.alpha2.img(:,:,slice_number); %select the background image from the 'alpha2.img' field of the
'mri' structure for the specified slice number
t1R = mri.T1map.r(:,:,slice_number); %select the T1 map for the specified slice number from the 'T1map' field
of the 'mri' structure
t1L = mri.T1map.l(:,:,slice_number); %select the T1 map for the specified slice number from the 'T1map' field
of the 'mri' structure

figure(); % create a new figure
title("T1 map over the segmented region")
axis off

ax1 = axes; % create axes for the background image
imagesc(background); % display the background image
colormap(ax1,'gray'); % set the colormap for the background image to grayscale
ax1.Visible= 'off'; % hide the first axes

ax2 = axes; % create axes for the T1 map
imagesc(ax2,t1R,'alphadata',t1R>0); % display the T1 map with transparency for values greater than 0
colormap(ax2,'jet'); % set the colormap for the T1 map to jet
clim(ax2,[0 2000]); % set the color limit for the T1 map to the range [0, 2000]
ax2.Visible = 'off';

ax3 = axes; % create axes for the T1 map
```

```
imagesc(ax3,t1L,'alphadata',t1L>0); % display the T1 map with transparency for values greater than 0
colormap(ax3,'jet'); % set the colormap for the T1 map to jet
clim(ax3,[0 2000]); % set the color limit for the T1 map to the range [0, 2000]
ax3.Visible = 'off'; % hide the axes for the T1 map

linkprop([ax1 ax2 ax3],'Position'); % link the positions of the two axes
c = colorbar; % create a colorbar
c.Label.String = 'T1, [ms]'; % set the label for the colorbar to 'T1, [ms]'
c.FontSize = 10; % set the font size of the colorbar label
c.FontWeight = 'bold'; % set the font weight of the label
linkaxes([ax1 ax2 ax3]) % link the axes of the figure


end
```

T2 code:

UIT2

```
classdef UIT2 < matlab.apps.AppBase

    % Properties that correspond to app components
    properties (Access = public)
        UIFigure                    matlab.ui.Figure
        GridLayout                  matlab.ui.container.GridLayout
        LeftPanel                   matlab.ui.container.Panel
        Lamp2                       matlab.ui.control.Lamp
        Switch                      matlab.ui.control.Switch
        SelectDICOMimagesforT2Button   matlab.ui.control.Button
        TE4EditField                matlab.ui.control.NumericEditField
        TE4EditFieldLabel           matlab.ui.control.Label
        EnterthenumberofslidesSpinner  matlab.ui.control.Spinner
        EnterthenumberofslidesSpinnerLabel  matlab.ui.control.Label
        TE3EditField                matlab.ui.control.NumericEditField
        TE3Label                    matlab.ui.control.Label
        TE2EditField                matlab.ui.control.NumericEditField
        TE2EditFieldLabel           matlab.ui.control.Label
        TE1EditField                matlab.ui.control.NumericEditField
        TE1EditFieldLabel           matlab.ui.control.Label
        ComputeT2mappingButton      matlab.ui.control.Button
        ImagingSessionDateDatePicker   matlab.ui.control.DatePicker
        ImagingnSessionDateLabel    matlab.ui.control.Label
        RightPanel                  matlab.ui.container.Panel
        CopytablevaluesButton       matlab.ui.control.Button
        UITable                     matlab.ui.control.Table
        CloseappButton              matlab.ui.control.Button
        PlotT2mapButton             matlab.ui.control.Button
        EntertheslicenumberthatyouwanttoseeSpinner  matlab.ui.control.Spinner
        EntertheslicenumberthatyouwanttoseeSpinnerLabel  matlab.ui.control.Label
        UIAxes                      matlab.ui.control.UIAxes
    end

    % Properties that correspond to apps with auto-reflow
    properties (Access = private)
```

```
        onePanelWidth = 576;
    end


    properties (Access = public)
        % Define TE values for four echo times
        TE1 = 11.1;
        TE2 = 22.2;
        TE3 = 33.3;
        TE4 = 44.4;

        T = []; %Table value
        % Create a zero-initialized array 'TE' with four elements
        TE = zeros(1, 4);

        % Define the number of slices
        n_slices = 35;

        % Initialize an empty struct 'mri' for MRI data storage
        mri = struct();

        % Initialize 'T2_values' and 'T2stats' variables
        T2_values = 0;
        T2stats = 0;

        % Set the default slice number to 20
        slice_number = 20;

        % Initialize 'labels' variable
        labels = 0;

        % Get the current date as 'imaging_date'
        imaging_date = datetime("today");

    end


    % Callbacks that handle component events
    methods (Access = private)

        % Code that executes after component creation
        function startupFcn(app)
            % Set the value of 'TE1EditField' to 'app.TE1'
            app.TE1EditField.Value = app.TE1;

            % Set the value of 'TE2EditField' to 'app.TE2'
            app.TE2EditField.Value = app.TE2;

            % Set the value of 'TE3EditField' to 'app.TE2' (Note: this might be a typo, it should probably be
'app.TE3')
            app.TE3EditField.Value = app.TE2;

            % Set the value of 'TE4EditField' to 'app.TE4'
            app.TE4EditField.Value = app.TE4;

            % Set the value of 'EnterthenumberofslidesSpinner' to 'app.n_slices'
            app.EnterthenumberofslidesSpinner.Value = app.n_slices;

            % Create an array 'TE' containing TE values from 'app.TE1' to 'app.TE4'
            app.TE = [app.TE1, app.TE2, app.TE3, app.TE4];
```

```
            % Initialize an empty struct 'mri' in 'app'
            app.mri = struct();

            % Set the value of 'ImagingSessionDateDatePicker' to 'app.imaging_date'
            app.ImagingSessionDateDatePicker.Value = app.imaging_date;

            % Set the visibility of 'UIAxes' to "off"
            app.UIAxes.Visible = "off";

            % Call the 'EntertheslicenumberthatyouwanttoseeSpinnerValueChanged' method with 'app.slice_number'
as an argument
            app.EntertheslicenumberthatyouwanttoseeSpinner

            % Set the color of Lamp and Lamp_2 to red
            app.Lamp2.Color = [1 0 0];

            % Initialize the 'T' table with empty data
            app.T = table(["Right";"Left"],[0;0],[0;0],[0;0]);

            % Set variable names for the 'T' table columns
            app.T.Properties.VariableNames = ["Knee side","T2 Mean, [ms]","T2 std, [ms]","SEM"];

            % Set the data in the UITable to match the 'T' table
            app.UITable.Data = app.T;

            % Set the column names of the UITable to match the 'T' table variable names
            app.UITable.ColumnName = app.T.Properties.VariableNames;

            %Get the screen size
            screenSize = get(groot,'Screensize');

            % Calculate the position to center the app within the screen
            position = app.UIFigure.Position;
            position(1) = (screenSize(3) - position(3)) / 2;
            position(2) = (screenSize(4) - position(4)) / 2;

            % Update the app's position to center it on the screen
            app.UIFigure.Position = position;

        end

        % Value changed function: ImagingSessionDateDatePicker
        function ImagingSessionDateDatePickerValueChanged(app, event)
            % Set the value of 'imaging_date' in 'app' to the selected value from 'ImagingSessionDateDatePicker'
            app.imaging_date = app.ImagingSessionDateDatePicker.Value;

        end

        % Value changed function: TE1EditField
        function TE1EditFieldValueChanged(app, event)
            % Update 'TE1' in 'app' with the value from 'TE1EditField'
            app.TE1 = app.TE1EditField.Value;

            % Update the first element of the 'TE' array with the new 'TE1' value
            app.TE(1) = app.TE1;

        end

        % Value changed function: TE2EditField
```

```
function TE2EditFieldValueChanged(app, event)
    % Update 'TE2' in 'app' with the value from 'TE2EditField'
    app.TE2 = app.TE2EditField.Value;

    % Update the second element of the 'TE' array with the new 'TE2' value
    app.TE(2) = app.TE2;


end

% Value changed function: TE3EditField
function TE3EditFieldValueChanged(app, event)
    % Update 'TE3' in 'app' with the value from 'TE3EditField'
    app.TE3 = app.TE3EditField.Value;

    % Update the third element of the 'TE' array with the new 'TE3' value
    app.TE(3) = app.TE3;

end

% Value changed function: TE4EditField
function TE4EditFieldValueChanged(app, event)
    % Update 'TE4' in 'app' with the value from 'TE4EditField'
    app.TE4 = app.TE4EditField.Value;

    % Update the fourth element of the 'TE' array with the new 'TE4' value
    app.TE(4) = app.TE4;


end

% Value changed function: EnterthenumberofslidesSpinner
function EnterthenumberofslidesSpinnerValueChanged(app, event)
    % Update 'n_slices' in 'app' with the value from 'EnterthenumberofslidesSpinner'
    app.n_slices = app.EnterthenumberofslidesSpinner.Value;


end

% Value changed function:
% EnterthesliceNumberthatyouwanttoseeSpinner
function EnterthesliceNumberthatyouwanttoseeSpinnerValueChanged(app, event)
    % Update 'slice_number' in 'app' with the value from 'EnterthesliceNumberthatyouwanttoseeSpinner'
    app.slice_number = app.EnterthesliceNumberthatyouwanttoseeSpinner.Value;

    % Call the 'UIAxesButtonDown2' method with 'app' and 'event' as arguments
    UIAxesButtonDown(app, event)
end

% Button pushed function: SelectDICOMimagesforT2Button
function SelectDICOMimagesforT2ButtonPushed(app, event)
    % Perform data acquisition with 'app.n_slices' and 'app.TE' as parameters using 'data_acquisition_T2'
    app.mri = data_acquisition_T2(app.n_slices, app.TE);

    % Set the color of Lamp to green to indicate successful acquisition
    app.Lamp2.Color = [0 1 0];

end

% Value changed function: Switch
```

```
        function SwitchValueChanged(app, event)
            % Do the function only if the switch is ON
            volumeSegmenter(app.mri.img(:,:,:,1))

        end

        % Callback function: not associated with a component
        function Switch_2ValueChanged(app, event)
            % Get the current value of 'Switch_2' and store it in the 'value' variable
            value = app.Switch_2.Value;


        end

        % Button pushed function: ComputeT2mappingButton
        function ComputeT2mappingButtonPushed(app, event)
            % Compute the T2 map using 'app.TE', 'app.mri', and 'app.slice_number', and store the results in
'app.mri', 'app.T2_values', 'app.T2stats', and 'app.labels'
            [app.mri, app.T2_values, app.T2stats, app.labels] = compute_T2_map(app.TE, app.mri,
app.slice_number);

            UITableDisplayDataChanged(app, event)

        end

        % Callback function: not associated with a component
        function GeneratePDFReportButtonPushed(app, event)
            % Generate a T2 report using 'app.T2stats', 'app.mri.subjectID', and 'app.imaging_date'
            getT2Report(app.T2stats, app.mri.subjectID, app.imaging_date);

        end

        % Button pushed function: PlotT2mapButton
        function PlotT2mapButtonPushed(app, event)
            % Plot the T2 map using 'app.mri', 'app.slice_number', 'app.T2_values', 'app.labels', and "titolo" as the
title
            plot_T2_map(app.mri, app.slice_number, app.T2_values, app.labels, "titolo");

        end

        % Button down function: UIAxes
        function UIAxesButtonDown(app, event)
            % Display an image slice from 'app.mri' on 'app.UIAxes' with the specified slice number
(app.slice_number) and colormap
            imagesc(app.UIAxes, app.mri.img(:,:,app.slice_number,1));

            % Set the colormap of 'app.UIAxes' to grayscale
            colormap(app.UIAxes, 'gray');

            % Set the visibility of 'app.UIAxes' to "off"
            app.UIAxes.Visible = "off";

        end

        % Display data changed function: UITable
        function UITableDisplayDataChanged(app, event)
            % Create a table 'T' with data from 'app.statistics' and labels for "Right" and "Left" knee sides
            app.T = table(["Right";"Left"], [app.T2stats.Right.MeanT2; app.T2stats.Left.MeanT2], ...
                [app.T2stats.Right.STD; app.T2stats.Left.STD], [app.T2stats.Right.SEM; app.T2stats.Left.SEM]);
```

```
            % Set variable names for the columns of the 'T' table
            app.T.Properties.VariableNames = ["Knee side", "T2 Mean, [ms]", "T2 std, [ms]", "SEM"];

            % Set the data of the UITable to match the 'T' table
            app.UITable.Data = app.T;

            % Set the column names of the UITable to match the 'T' table variable names
            app.UITable.ColumnName = app.T.Properties.VariableNames;

        end

        % Button pushed function: CopytablevaluesButton
        function CopytablevaluesButtonPushed(app, event)
            % Copy the concatenated data from 'app.statistics.r' and 'app.statistics.l' to the clipboard
            clipboard('copy', [app.T2stats.Right.MeanT2, app.T2stats.Left.MeanT2, app.T2stats.Right.STD,
app.T2stats.Left.STD, app.T2stats.Right.SEM, app.T2stats.Left.SEM])
        end

        % Changes arrangement of the app based on UIFigure width
        function updateAppLayout(app, event)
            currentFigureWidth = app.UIFigure.Position(3);
            if(currentFigureWidth <= app.onePanelWidth)
                % Change to a 2x1 grid
                app.GridLayout.RowHeight = {600, 600};
                app.GridLayout.ColumnWidth = {'1x'};
                app.RightPanel.Layout.Row = 2;
                app.RightPanel.Layout.Column = 1;
            else
                % Change to a 1x2 grid
                app.GridLayout.RowHeight = {'1x'};
                app.GridLayout.ColumnWidth = {361, '1x'};
                app.RightPanel.Layout.Row = 1;
                app.RightPanel.Layout.Column = 2;
            end
        end

        % Button pushed function: CloseappButton
        function CloseappButtonPushed(app, event)
            app.delete
        end
    end

    % Component initialization
    methods (Access = private)

        % Create UIFigure and components
        function createComponents(app)

            % Create UIFigure and hide until all components are created
            app.UIFigure = uifigure('Visible', 'off');
            app.UIFigure.AutoResizeChildren = 'off';
            app.UIFigure.Position = [100 100 771 600];
            app.UIFigure.Name = 'MATLAB App';
            app.UIFigure.SizeChangedFcn = createCallbackFcn(app, @updateAppLayout, true);

            % Create GridLayout
            app.GridLayout = uigridlayout(app.UIFigure);
            app.GridLayout.ColumnWidth = {361, '1x'};
            app.GridLayout.RowHeight = {'1x'};
            app.GridLayout.ColumnSpacing = 0;
```

```
            app.GridLayout.RowSpacing = 0;
            app.GridLayout.Padding = [0 0 0 0];
            app.GridLayout.Scrollable = 'on';

            % Create LeftPanel
            app.LeftPanel = uipanel(app.GridLayout);
            app.LeftPanel.Layout.Row = 1;
            app.LeftPanel.Layout.Column = 1;

            % Create ImagingnSessionDateLabel
            app.ImagingnSessionDateLabel = uilabel(app.LeftPanel);
            app.ImagingnSessionDateLabel.HorizontalAlignment = 'center';
            app.ImagingnSessionDateLabel.Position = [53 542 162 30];
            app.ImagingnSessionDateLabel.Text = 'Imaging Session Date';

            % Create ImagingSessionDateDatePicker
            app.ImagingSessionDateDatePicker = uidatepicker(app.LeftPanel);
            app.ImagingSessionDateDatePicker.ValueChangedFcn = createCallbackFcn(app,
@ImagingSessionDateDatePickerValueChanged, true);
            app.ImagingSessionDateDatePicker.Position = [205 546 104 22];

            % Create ComputeT2mappingButton
            app.ComputeT2mappingButton = uibutton(app.LeftPanel, 'push');
            app.ComputeT2mappingButton.ButtonPushedFcn = createCallbackFcn(app,
@ComputeT2mappingButtonPushed, true);
            app.ComputeT2mappingButton.FontSize = 16;
            app.ComputeT2mappingButton.FontWeight = 'bold';
            app.ComputeT2mappingButton.Position = [51 74 230 41];
            app.ComputeT2mappingButton.Text = 'Compute T2 mapping';

            % Create TE1EditFieldLabel
            app.TE1EditFieldLabel = uilabel(app.LeftPanel);
            app.TE1EditFieldLabel.HorizontalAlignment = 'right';
            app.TE1EditFieldLabel.Position = [51 457 29 22];
            app.TE1EditFieldLabel.Text = 'TE 1';

            % Create TE1EditField
            app.TE1EditField = uieditfield(app.LeftPanel, 'numeric');
            app.TE1EditField.ValueChangedFcn = createCallbackFcn(app, @TE1EditFieldValueChanged, true);
            app.TE1EditField.Position = [95 457 64 22];

            % Create TE2EditFieldLabel
            app.TE2EditFieldLabel = uilabel(app.LeftPanel);
            app.TE2EditFieldLabel.HorizontalAlignment = 'right';
            app.TE2EditFieldLabel.Position = [51 416 29 22];
            app.TE2EditFieldLabel.Text = 'TE 2';

            % Create TE2EditField
            app.TE2EditField = uieditfield(app.LeftPanel, 'numeric');
            app.TE2EditField.ValueChangedFcn = createCallbackFcn(app, @TE2EditFieldValueChanged, true);
            app.TE2EditField.Position = [95 416 64 22];

            % Create TE3Label
            app.TE3Label = uilabel(app.LeftPanel);
            app.TE3Label.HorizontalAlignment = 'right';
            app.TE3Label.Position = [173 457 29 22];
            app.TE3Label.Text = 'TE 3';

            % Create TE3EditField
            app.TE3EditField = uieditfield(app.LeftPanel, 'numeric');
```

```
            app.TE3EditField.ValueChangedFcn = createCallbackFcn(app, @TE3EditFieldValueChanged, true);
            app.TE3EditField.Position = [217 457 64 22];

            % Create EnterthenumberofslidesSpinnerLabel
            app.EnterthenumberofslidesSpinnerLabel = uilabel(app.LeftPanel);
            app.EnterthenumberofslidesSpinnerLabel.HorizontalAlignment = 'right';
            app.EnterthenumberofslidesSpinnerLabel.Position = [51 359 146 22];
            app.EnterthenumberofslidesSpinnerLabel.Text = 'Enter the number of slides';

            % Create EnterthenumberofslidesSpinner
            app.EnterthenumberofslidesSpinner = uispinner(app.LeftPanel);
            app.EnterthenumberofslidesSpinner.ValueChangedFcn = createCallbackFcn(app,
@EnterthenumberofslidesSpinnerValueChanged, true);
            app.EnterthenumberofslidesSpinner.Position = [212 359 69 22];

            % Create TE4EditFieldLabel
            app.TE4EditFieldLabel = uilabel(app.LeftPanel);
            app.TE4EditFieldLabel.HorizontalAlignment = 'right';
            app.TE4EditFieldLabel.Position = [174 416 29 22];
            app.TE4EditFieldLabel.Text = 'TE 4';

            % Create TE4EditField
            app.TE4EditField = uieditfield(app.LeftPanel, 'numeric');
            app.TE4EditField.ValueChangedFcn = createCallbackFcn(app, @TE4EditFieldValueChanged, true);
            app.TE4EditField.Position = [216 416 64 22];

            % Create SelectDICOMimagesforT2Button
            app.SelectDICOMimagesforT2Button = uibutton(app.LeftPanel, 'push');
            app.SelectDICOMimagesforT2Button.ButtonPushedFcn = createCallbackFcn(app,
@SelectDICOMimagesforT2ButtonPushed, true);
            app.SelectDICOMimagesforT2Button.Position = [51 250 197 38];
            app.SelectDICOMimagesforT2Button.Text = 'Select DICOM images for T2';

            % Create Switch
            app.Switch = uiswitch(app.LeftPanel, 'slider');
            app.Switch.Items = {'', 'Select ON to segment images'};
            app.Switch.ValueChangedFcn = createCallbackFcn(app, @SwitchValueChanged, true);
            app.Switch.Position = [51 182 43 19];
            app.Switch.Value = '';

            % Create Lamp2
            app.Lamp2 = uilamp(app.LeftPanel);
            app.Lamp2.Position = [261 259 20 20];

            % Create RightPanel
            app.RightPanel = uipanel(app.GridLayout);
            app.RightPanel.Layout.Row = 1;
            app.RightPanel.Layout.Column = 2;

            % Create UIAxes
            app.UIAxes = uiaxes(app.RightPanel);
            title(app.UIAxes, 'Title')
            xlabel(app.UIAxes, 'X')
            ylabel(app.UIAxes, 'Y')
            zlabel(app.UIAxes, 'Z')
            app.UIAxes.ButtonDownFcn = createCallbackFcn(app, @UIAxesButtonDown, true);
            app.UIAxes.Position = [12 275 385 240];

            % Create EntertheslicenumberthatyouwanttoseeSpinnerLabel
            app.EntertheslicenumberthatyouwanttoseeSpinnerLabel = uilabel(app.RightPanel);
```

```
            app.EntertheslicenumberthatyouwanttoseeSpinnerLabel.HorizontalAlignment = 'right';
            app.EntertheslicenumberthatyouwanttoseeSpinnerLabel.Position = [15 540 240 22];
            app.EntertheslicenumberthatyouwanttoseeSpinnerLabel.Text = 'Enter the slice number that you want to
see';

            % Create EntertheslicenumberthatyouwanttoseeSpinner
            app.EntertheslicenumberthatyouwanttoseeSpinner = uispinner(app.RightPanel);
            app.EntertheslicenumberthatyouwanttoseeSpinner.Limits = [-100 100];
            app.EntertheslicenumberthatyouwanttoseeSpinner.ValueChangedFcn = createCallbackFcn(app,
@EntertheslicenumberthatyouwanttoseeSpinnerValueChanged, true);
            app.EntertheslicenumberthatyouwanttoseeSpinner.Position = [262 542 100 22];

            % Create PlotT2mapButton
            app.PlotT2mapButton = uibutton(app.RightPanel, 'push');
            app.PlotT2mapButton.ButtonPushedFcn = createCallbackFcn(app, @PlotT2mapButtonPushed, true);
            app.PlotT2mapButton.FontSize = 16;
            app.PlotT2mapButton.FontWeight = 'bold';
            app.PlotT2mapButton.Position = [139 218 150 28];
            app.PlotT2mapButton.Text = 'Plot T2 map';

            % Create CloseappButton
            app.CloseappButton = uibutton(app.RightPanel, 'push');
            app.CloseappButton.ButtonPushedFcn = createCallbackFcn(app, @CloseappButtonPushed, true);
            app.CloseappButton.Position = [139 24 100 23];
            app.CloseappButton.Text = 'Close app';

            % Create UITable
            app.UITable = uitable(app.RightPanel);
            app.UITable.ColumnName = {'Column 1'; 'Column 2'; 'Column 3'; 'Column 4'};
            app.UITable.RowName = {};
            app.UITable.DisplayDataChangedFcn = createCallbackFcn(app, @UITableDisplayDataChanged, true);
            app.UITable.Position = [23 146 363 55];

            % Create CopytablevaluesButton
            app.CopytablevaluesButton = uibutton(app.RightPanel, 'push');
            app.CopytablevaluesButton.ButtonPushedFcn = createCallbackFcn(app,
@CopytablevaluesButtonPushed, true);
            app.CopytablevaluesButton.Position = [134 92 110 23];
            app.CopytablevaluesButton.Text = 'Copy table values';

            % Show the figure after all components are created
            app.UIFigure.Visible = 'on';
        end
    end

    % App creation and deletion
    methods (Access = public)

        % Construct app
        function app = UIT2

            % Create UIFigure and components
            createComponents(app)

            % Register the app with App Designer
            registerApp(app, app.UIFigure)

            % Execute the startup function
            runStartupFcn(app, @startupFcn)
```

```
            if nargout == 0
                clear app
            end
        end

        % Code that executes before app deletion
        function delete(app)

            % Delete UIFigure when app is deleted
            delete(app.UIFigure)
        end
    end
end
```

data_acquisition_T2

```
function [mri] = data_acquisition_T2(n_slices, TE)

%%%
% The data_acquisition_T2 function is used to load a series of MR images from
% a specified folder and store them in a structure called mri.
%
% INPUT ARGUMENTS:
% - n_slices: the number of slices in the MR images
% - TE, an array containing the echo times for each image.
% OUTPUT ARGUMENTS:
% - mri: structure with the mri images and the information about the sequence
%
% The function first prompts the user for some information about the MR images,
% including the sequence name, acquisition plane, and subject ID.
% This information is stored in the mri structure.
%
% Next, the function uses the dir function to list the files in the specified
% folder and then reads the MR images using the dicomread function. The images
% are stored in a 4-dimensional array called IMGdata, with dimensions
% corresponding to the x-y coordinates of the images, the slice number, and the echo time.
%
% The function then checks whether the MR images are divided into one or two slice groups.
% If the images are divided into one slice group, the IMGdata array is stored
% in the img field of the mri structure. If the images are divided into two
% slice groups, the IMGdata array is split into two arrays, IMGdata_right and IMGdata_left,
% corresponding to the right and left slice groups, respectively.
% These arrays are then stored in the img_left and img_right fields of the mri structure.
%
% The mri structure is then returned by the function.
%%%

    % Input validation
    validate_inputs(n_slices, TE);

    % Get sequence information
    [mri.sequenceName, mri.acquisitionPlane, mri.subjectID] = get_sequence_info();

    % Get DICOM images
    [files, folder] = get_dicom_images();
    nTE = length(TE);
```

```
    % Check slice groups
    choice = check_slice_groups();

    % Create a waitbar to display the loading progress
    h = waitbar(0,'Loading images...');

    % Load the MR images into the mri structure
    switch choice
        case 'One'
            mri.img = load_one_slice_group(n_slices, nTE, files, h);
        case 'Two'
            [mri.img_right, mri.img_left] = load_two_slice_groups(n_slices, nTE, files, h);
    end

    close(h)



end



function validate_inputs(n_slices, TE)
%%%
%  INPUT:
% - n_slices: the number of slices in the MR images
% - TE, an array containing the echo times for each image.
%  OUTPUT:
%  Error message if the inputs are not valid.
%%%
    if ~isscalar(n_slices) || ~isnumeric(n_slices) || n_slices < 1 || mod(n_slices, 1) ~= 0
        error('Invalid value for n_slices. Expected a positive integer.');
    end
    if ~isnumeric(TE) || isempty(TE)
        error('Invalid value for TE. Expected a non-empty array.');
    end
end

function [sequenceName, acquisitionPlane, subjectID] = get_sequence_info()
    info = inputdlg({'Sequence Name','Acquisition Plane', 'Subject ID'});
    sequenceName = info{1};
    acquisitionPlane = info{2};
    subjectID = info{3};
end

function [files, folder] = get_dicom_images()
    folder = uigetdir();
    files = dir(folder);
    for i = 1+2:length(files)
        if ~strcmp(files(i).name(end-3:end), '.IMA')
            error('One or more files in the selected folder is not a DICOM image. Exiting function.');
        end
    end
end

function choice = check_slice_groups()
    choice = questdlg('How many slice groups?', ...
    'Options', ...
    'One','Two', 'Two');
end
```

```
function img = load_one_slice_group(n_slices, nTE, files, h)
    first_image = dicomread(strcat(files(3).folder,checkOS,files(3).name));
    img = zeros(size(first_image,1), size(first_image,2), n_slices, nTE);
    for jj = 1:nTE
        for i = (jj-1)*n_slices + 1 : jj*n_slices
            img(:,:,i-(jj-1)*n_slices,jj) = dicomread(strcat(files(i+2).folder,checkOS,files(i+2).name));
            waitbar(((jj-1)*n_slices + i) / (nTE*n_slices), h);
        end
    end
end


function [img_right, img_left] = load_two_slice_groups(n_slices, nTE, files, h)
    first_image = dicomread(strcat(files(3).folder,checkOS,files(3).name));
    img_right = zeros(size(first_image,1), size(first_image,2), n_slices, nTE);
    img_left = zeros(size(first_image,1), size(first_image,2), n_slices, nTE);
    for jj = 1:nTE
        for i = (2*jj-1)*n_slices + 1 : 2*jj*n_slices
            img_right(:,:,i-(2*jj-1)*n_slices,jj) = dicomread(strcat(files(i+2).folder,checkOS,files(i+2).name));
        end
        for i = (2*jj)*n_slices + 1 : (2*jj+1)*n_slices
            img_left(:,:,i-(2*jj)*n_slices,jj) = dicomread(strcat(files(i+2).folder,checkOS,files(i+2).name));
        end
    end
end
```

1.1.1.1.1 compute_T2_map

```
function [mri, T2_values, T2stats, labels ] = compute_T2_map(TE, mri, slice_number)

%% Denoising

mri.img = denoising(mri.img) ;

%% Divide the labels into right and left knee
addpath("Segmentations/");

% Display a message box with instructions for the user
CreateStruct.Interpreter = 'tex';
CreateStruct.WindowStyle = 'modal';
text= '\fontsize{12} Select the file with the segmentation';
uiwait(msgbox(text,"DICOM Selection",CreateStruct));
% Open a file selection dialog to allow the user to select a file
[filename,~] = uigetfile('*.mat*','Select file to open','S:\Shared\Ortho Project - Tendon Injury');
% Load the segmentation from the selected file
labels = load(filename);
labels = labels.labels;
labelsR = labels == 'RIGHT KNEE';
labelsL = labels == 'LEFT KNEE';

labels_right = labels =='RIGHT KNEE';
labels_left = labels =='LEFT KNEE';


%% T2 computation

% T2 values computation using monoexponential fitting
T2_values=struct();
```

```
[T2_values.right,~]  = fit_t2_relaxation_curve(mri.img,labels_right, TE);
[T2_values.left,~]  = fit_t2_relaxation_curve(mri.img,labels_left, TE);

% Statistics
T2stats = struct();
T2stats.Right = computeStatisticsT2(T2_values.right, labels_right);
T2stats.Left = computeStatisticsT2(T2_values.left, labels_left);

% Display T2 stats
disp(T2stats.Right)
disp(T2stats.Left)
```

denoising

```
function [denoised] = denoising(mri_img)
%%%
% Author: Davide Magliano, Marco Mussato
% Date: 2022-12-09  (YYYY-MM-DD)
%
% INFO:
% This function applies a Gaussian filter to the input MRI images
% to reduce noise.
%
% INPUT:
% mri_img: a 4-dimensional matrix containing the MRI dataset
%
% OUTPUT:
% denoised: a 4-dimensional matrix containing the denoised MRI dataset
%
% VARIABLES:
% data: the input MRI dataset, assigned to the input mri_img
% kernel: the Gaussian kernel used for convolution
% sigma: the standard deviation of the Gaussian kernel
%%%

%% Denoising

% Load the 4-D MRI dataset
data = mri_img;
%Initialize the denoised images to zero
denoised = zeros(size(mri_img));

% Create new 4-D matrix for the denoised images

% Loop over the images in the dataset
for i = 1:size(data, 3)
   for j = 1:size(data, 4)
      % Apply a Gaussian filter

      % Create a 3x3 Gaussian kernel with standard deviation sigma
      sigma = 1;
      kernel = fspecial('gaussian', [3 3], sigma);

      % Apply the kernel to the image using convolution
      denoised(:,:,i,j) = conv2(data(:,:,i,j), kernel, 'same');
```

```
    end
end

end
```

fit_T2_relaxation_curve

```
function [T2_value, statistics] = fit_t2_relaxation_curve(mri_images, mask, TE)
% FIT_T2_RELAXATION_CURVE Computes the T2 relaxation curve for each pixel in the region of interest
%
% INPUTS
%   mri_images - a 4D array representing a series of MRI images. The dimensions of the array are:
%                number of rows, number of columns, number of slices, number of echoes.
%   mask       - a 3D binary array of the same size as mri_images. It specifies which pixels belong to
%                the region of interest in each slice.
%   TE         - a vector of length n_TE containing the echo times of the MRI images.
%
% OUTPUTS
%   T2_value   - a 3D array of T2 values with the same dimensions as mri_images.
%
% EXAMPLES
%
%   % Compute the T2 relaxation curve for a series of MRI images with echo times [1, 2, 3, 4] ms:
%   T2_values = fit_t2_relaxation_curve(mri_images, mask, [1, 2, 3, 4])
%
%   % Visualize the histogram of computed T2 values:
%   histogram(T2_values(T2_values > 0), 100, 'BinLimits', [0, 100]);
%   xlabel('T2 (ms)');
%   ylabel('Frequency');
%
% NOTES
%   The function generates a histogram of the computed T2 relaxation times

%% Image dimensions

img_height = size(mri_images,1);
img_width = size(mri_images,2);
n_slices = size(mri_images,3);
n_TE = size(mri_images,4);

% Inizialitations

I = zeros(img_height,img_width, n_TE);% Matrix with the Signal Intensisty for each slice, 3rd dimension is the
echo.
x = TE(1:end); % the three echos are used to compute the fitting curve in line 85
T2_value = zeros(img_height,img_width,n_slices);  % Matrix with the T2 values for every slice

goodFit=0; %counter for pixels that have a high GOF
goodValues = 0; %counter for pixels that have a plausible value (0<T2<100)
goodValFit = 0; %counter for pixels that have a high GOF and a plausible value (0<T2<100)



p = waitbar(0,'Computing T2 values...');
for k = 1:n_slices % for every slice
   if sum(sum(mask(:,:,k)))~=0 %check if there is a mask in the slice
```

```
    % Load I with SI from the pixels belonging to the ROI selected in
    % the mask
    I = double(mri_images(:,:,k,:)).*mask(:,:,k);

    waitbar(k/n_slices, p , sprintf('SLIDE %d/%d - Computing T2 values...', k,n_slices));
    pixelCounter = 1;
        for i = 1:img_height
            for j=1:img_width

                % For every pixels in the matrix I
                if I(i,j,1)~=0  %if the pixel belongs to the mask (value !=0)
                    y = squeeze(I(i,j,1:end))'; %create a vector containing the value of that pixels at different echos
                    [fitresult, gof] = createFit_T2(x, y); % create the fitting curve
                    %waitbar(pixelCounter/ sum(sum(mask(:,:,k))), h);
                    pixelCounter=pixelCounter+1;

                    coeffvals= coeffvalues(fitresult); % values of the coefficients of the fitting curve
                    if gof.rsquare>0.90 && 1/coeffvals(2)<100 && 1/coeffvals(2)>0 % if the curve is good fit and
0<T2<100 ms
                        T2_value(i,j,k)=1/coeffvals(2); % Save the T2 value
                        goodValFit=goodValFit+1;
                    end

                    if gof.rsquare>0.90
                        goodFit = goodFit+1;
                    end

                    if 1/coeffvals(2)<100 && 1/coeffvals(2)>0
                        goodValues = goodValues+1;
                    end

                end

            end
        end
    end
end
close(p)

goodValues_perc = goodValues/sum(sum(sum(mask)));
goodFit_perc = goodFit/sum(sum(sum(mask)));
goodValFit_perc = goodValFit/sum(sum(sum(mask)));
badValues_perc = 1-goodValues_perc;
badFit_perc = 1-goodFit_perc;
badFitVal_perc =  1-goodValFit_perc;

statistics = struct("GoodValues", goodValues_perc,"GoodFit", goodFit_perc, ...
    "GoodValFit", goodValFit_perc,
"BadValues",badValues_perc,"BadFit",badFit_perc,"BadValFit",badFitVal_perc );
statistics = struct2table(statistics);
end
```

createFit_T2

```
function [fitresult, gof] = createFit_T2(x, y)
%  Author: Rossana Terracciano
```

```
%  Date: 2021-01-04
%  Info:

%  Create a fit for 1/T2 values.
%
%  Data for fit:
%      X Input : x
%      Y Output: y
%  Output:
%      fitresult : a fit object representing the fit.
%      gof : structure with goodness-of fit info.
%


%% Fit: 'untitled fit 1'.




 % Check data validity
if ~checkData(x, y)
    % Data is invalid, handle the error or return
    error("Invalid data provided.");
    % or return an error code or message, e.g., fitresult = []; gof = [];
end

[xData, yData] = prepareCurveData( x, y );


% Set up fittype and options.
ft = fittype( 'a*exp(-b*x)+c', 'independent', 'x', 'dependent', 'y' );
opts = fitoptions( 'Method', 'NonlinearLeastSquares' );
opts.Algorithm = 'Levenberg-Marquardt';
opts.Display = 'Off';
opts.StartPoint = [100 0.01 0.5059];

% Fit model to data.
[fitresult, gof] = fit(xData, yData, ft, opts );
end

function valid = checkData(x, y)
   % Check if x and y have the same length
   if numel(x) ~= numel(y)
      disp("Error: x and y have different lengths.");
      valid = false;
      return;
   end

   % Check if x and y are numeric arrays
   if ~isnumeric(x) || ~isnumeric(y)
      disp("Error: x and y must be numeric arrays.");
      valid = false;
      return;
   end

   % Check for NaN or infinite values in x
   if any(isnan(x)) || any(isinf(x))
      disp("Error: x contains NaN or infinite values.");
      valid = false;
      return;
```

```
    end

    % Check for NaN or infinite values in y
    if any(isnan(y)) || any(isinf(y))
        disp("Error: y contains NaN or infinite values.");
        valid = false;
        return;
    end

    % All checks passed, data is valid
    valid = true;
end
```

computeStatistics

```
function T2 = computeStatistics(T2_value, mask)

% Statistics
mean_T2 = mean(T2_value(mask)); %mean value of T2 in the segmented region
std_T2 = std(T2_value(mask)) ;%standard deviation of T2 in the segmented region
sem = std_T2 / sqrt(sum(mask(:))); %SEM of T2 in the segmented region

T2 = struct("MeanT2",mean_T2 , "STD",std_T2 , "SEM", sem);
T2 = struct2table(T2);

end
```

plot_T2_map

```
function plot_T2_map(mri, slide_number, T2_values,labels, ~)
%%%
% INPUTS:
% - mri: a struct containing the MRI data. This struct should have the following fields:
% - img: a 4D matrix containing the MRI data. The dimensions of this matrix are x, y, z, and time.
% - acquisitionPlane: a string representing the plane of acquisition (e.g. "axial", "coronal", etc.).
% - sequenceName: a string representing the name of the MRI sequence (e.g. "T2", "T1", etc.).
% - subjectID: a string representing the ID of the subject being imaged.
% - slide_number: a scalar representing the index of the slice to be plotted. This should be an integer between 1
and the number of slices in the MRI data (inclusive).
% - T2_values: a 3D matrix containing the T2 values for the MRI data. The dimensions of this matrix should be
the same as the img field of the mri input, except with only one time dimension.
% - mask: a 3D binary matrix with the same dimensions as the img and T2_values inputs. This matrix should
contain 1s for voxels that should be plotted and 0s for voxels that should be ignored.
% - DenoisingType: a string representing the type of denoising applied to the data. This string will be included in
the title of the plot.
% OUTPUTS:
% This function does not return any outputs, but it generates a plot of the T2 mapping
%%%

% Background image  for t2 mapping
background_img = mri.img(:,:,slide_number,1);
```

```
% Take the T2 mapping for the specific slice you choose (same as background)
t2_right = T2_values.right(:,:,slide_number); % T2 values for the selected slice
t2_left = T2_values.left(:,:,slide_number); % T2 values for the selected slice


figure()
title("T2 map over segmented region")
axis off

ax1 = axes;% create axes for the background image
imagesc(background_img);% display the background image
colormap(ax1,'gray');% set the colormap for the background image to grayscale
ax1.Visible= 'off'; % hide the first axes

ax2 = axes;
imagesc(ax2,t2_right,'alphadata',t2_right>0);
colormap(ax2,'jet');
clim(ax2,[0 50]);
ax2.Visible = 'off';

ax3 = axes; % create axes for the T2 map
imagesc(ax3,t2_left,'alphadata',t2_left>0); % display the T1 map with transparency for values greater than 0
colormap(ax3,'jet'); % set the colormap for the T1 map to jet
clim(ax3,[0 50]); % set the color limit for the T1 map to the range [0, 2000]
ax3.Visible = 'off'; % hide the axes for the T1 map


linkprop([ax1 ax2 ax3], 'Position')
c = colorbar;
c.Label.String = 'T2, [ms]';
c.FontSize = 10; % set the font size of the colorbar label
c.FontWeight = 'bold'; % set the font weight of the label
linkaxes([ax1 ax2])

end
```

DCE code:

DCE_app

```
classdef DCE_app < matlab.apps.AppBase

    % Properties that correspond to app components
    properties (Access = public)
        UIFigure                    matlab.ui.Figure
        CopytablevaluesButton       matlab.ui.control.Button
        Injectionpointasmeasurementnumber  matlab.ui.control.EditField
        InjectionpointasmeasurementnumberEditFieldLabel  matlab.ui.control.Label
        TotalacquisitontimemmssEditField  matlab.ui.control.EditField
        TotalacquisitontimemmssEditFieldLabel  matlab.ui.control.Label
        SaveplotButton              matlab.ui.control.Button
```

```
        CloseappButton              matlab.ui.control.Button
        UITable                     matlab.ui.control.Table
        ComputeDCEparametersButton  matlab.ui.control.Button
        Switch                      matlab.ui.control.Switch
        Lamp                        matlab.ui.control.Lamp
        SelectDICOMimagesButton     matlab.ui.control.Button
        ImagingsessiondateDatePicker  matlab.ui.control.DatePicker
        ImagingsessiondateDatePickerLabel  matlab.ui.control.Label
        UIAxes                      matlab.ui.control.UIAxes
    end

    properties (Access = private)
        % Variable initialisation
        allButtons = 0;
        mri = 0;
        T = 0;
        ta = 0;
        injectionMeasurament = 0;
    end

    % Callbacks that handle component events
    methods (Access = private)

        % Code that executes after component creation
        function startupFcn(app)
            % Get the screen size
            screenSize = get(0, 'ScreenSize');

            % Get the width and height of the figure
            figureWidth = app.UIFigure.Position(3);
            figureHeight = app.UIFigure.Position(4);

            % Calculate the position of the figure such that it's centered on the screen
            figurePosition = [(screenSize(3)-figureWidth)/2, (screenSize(4)-figureHeight)/2, figureWidth,
figureHeight];

            % Set the position of the figure
            app.UIFigure.Position = figurePosition;

            % Set the color of the Lamp to red
            app.Lamp.Color = [1 0 0];

            % Find all uibuttons in the UIFigure and store them in 'allButtons'
            app.allButtons = findobj(app.UIFigure, 'Type', 'uibutton');

            % Set the title, ylabel, and xlabel for the UIAxes
            title(app.UIAxes, 'Mean intensity over time - Right knee')
            ylabel(app.UIAxes, 'Mean intensity over ROI')
            xlabel(app.UIAxes, 'Time, [min]')

            % Create an empty table 'T' with specific variable names
            app.T = table(0, 0, 0, 0, 0);
            app.T.Properties.VariableNames = ["AUC, [AU]", "IAUC, [AU]", "Peak enhancement, [AU]", "Time to
peak, [min]", "Wash-in slope, [AU/min]"];

            % Set the data of the UITable to match the 'T' table
            app.UITable.Data = app.T;

            % Set the column names of the UITable to match the 'T' table variable names
            app.UITable.ColumnName = app.T.Properties.VariableNames;
```

```
            % Set the value of ImagingsessiondateDatePicker to today's date
            app.ImagingsessiondateDatePicker.Value = datetime("today");

        end

        % Value changed function: TotalacquisitontimemmssEditField
        function TotalacquisitontimemmssEditFieldValueChanged(app, event)
            % Convert the value from the TotalacquisitontimemmssEditField to a double and store it in the 'ta'
variable
            app.ta = str2double(app.TotalacquisitontimemmssEditField.Value);

        end

        % Value changed function: Injectionpointasmeasurementnumber
        function InjectionpointasmeasurementnumberValueChanged(app, event)

            % Convert the value from Injectionpointasmeasurementnumber to a double and store it in the
'injectionMeasurament' variable
            app.injectionMeasurament = str2double(app.Injectionpointasmeasurementnumber.Value);

            % Check if 'injectionMeasurament' is greater than 144
            if app.injectionMeasurament > 144
                % Display a warning using uialert if the value is greater than 144
                uialert(app.UIFigure, "The number entered can't be greater than 144.", 'Warning');
                % Check if 'injectionMeasurament' is less than 1
            elseif app.injectionMeasurament < 1
                % Display a warning using uialert if the value is less than 1
                uialert(app.UIFigure, "The number entered can't be less than 1.", 'Warning');
            end


        end

        % Button pushed function: SelectDICOMimagesButton
        function SelectDICOMimagesButtonPushed2(app, event)
            % Disable all buttons
            set(app.allButtons,'Enable','off')

            % Perform data acquisition with empty parameters for 'DCE' using 'data_acquisition'
            app.mri = data_acquisition([],'DCE',[],[])

            % Set the color of Lamp to green to indicate successful acquisition
            app.Lamp.Color = [0 1 0]

            % Enable all buttons again
            set(app.allButtons,'Enable','on')

        end

        % Value changed function: Switch
        function SwitchValueChanged2(app, event)
            % Use the 'volumeSegmenter' function to segment the first volume from 'app.mri.dce.img'
            volumeSegmenter(app.mri.dce.img(:,:,:,1));

        end

        % Button pushed function: ComputeDCEparametersButton
        function ComputeDCEparametersButtonPushed2(app, event)
            % Perform DCE computation using parameters 'app.ta' and 'app.injectionMeasurament' on 'app.mri'
```

```
            app.mri = dce_computation(app.mri, app.ta, app.injectionMeasurament);

            % Call the 'UIAxesButtonDown2' method with 'app' and 'event' as arguments
            UIAxesButtonDown2(app, event);

            % Call the 'UITableCellEdit' method with 'app' and 'event' as arguments
            UITableCellEdit(app, event);

        end

        % Button down function: UIAxes
        function UIAxesButtonDown2(app, event)
            % Plot data on 'app.UIAxes' with specified markers and properties
            plot(app.UIAxes, app.mri.dce.timesamp, app.mri.dce.pxInt, 'o', 'MarkerSize', 2)

            % Create a vertical line ('xl') at a specific x-value on the UIAxes
            xl = xline(app.UIAxes, app.injectionMeasurament * app.mri.dce.timeres / 60, '--k', {'Contrast Agent
injection'});

            % Set the horizontal alignment of the label for 'xl' to 'left'
            xl.LabelHorizontalAlignment = 'left';

        end

        % Cell edit callback: UITable
        function UITableCellEdit(app, event)
            % Create a table 'T' with data from 'app.mri.dce.params'
            app.T = table(app.mri.dce.params.AUC, app.mri.dce.params.IAUC,
app.mri.dce.params.PeakEnhancment, app.mri.dce.params.timePeak, app.mri.dce.params.washinSlope);

            % Set variable names for the columns of the 'T' table
            app.T.Properties.VariableNames = ["AUC, [AU]", "IAUC, [AU]", "Peak enhancement, [AU]", "Time to
peak, [min]", "Wash-in slope, [AU/min]"];

            % Set the data of the UITable to match the 'T' table
            app.UITable.Data = app.T;

            % Set the column names of the UITable to match the 'T' table variable names
            app.UITable.ColumnName = app.T.Properties.VariableNames;

        end

        % Button pushed function: SaveplotButton
        function SaveplotButtonPushed(app, event)
            % Define a filter for file types to save as
            filter = {'*.jpg';'*.png';'*.tif';'*.pdf';'*.eps'};

            % Open a file dialog to select a file and set the default filename
            [filename, filepath] = uiputfile(filter, 'Select a File', sprintf('DCE_graphs_rabbit_%s.jpg',
datetime(app.ImagingsessiondateDatePicker.Value)));

            % Check if a valid filename was selected
            if ischar(filename)
                % Export the content of 'app.UIAxes' as an image to the specified file path and name
                exportgraphics(app.UIAxes, [filepath filename], 'Resolution', 500);
            end

        end

        % Button pushed function: CopytablevaluesButton
```

```
        function CopytablevaluesButtonPushed(app, event)

clipboard('copy',[app.mri.dce.params.AUC,app.mri.dce.params.IAUC,app.mri.dce.params.PeakEnhancment,
app.mri.dce.params.timePeak,app.mri.dce.params.washinSlope])
        end

        % Button pushed function: CloseappButton
        function CloseappButtonPushed(app, event)
            app.delete
        end
    end

    % Component initialization
    methods (Access = private)

        % Create UIFigure and components
        function createComponents(app)

            % Create UIFigure and hide until all components are created
            app.UIFigure = uifigure('Visible', 'off');
            app.UIFigure.Position = [100 100 786 546];
            app.UIFigure.Name = 'MATLAB App';

            % Create UIAxes
            app.UIAxes = uiaxes(app.UIFigure);
            title(app.UIAxes, 'Title')
            xlabel(app.UIAxes, 'X')
            ylabel(app.UIAxes, 'Y')
            zlabel(app.UIAxes, 'Z')
            app.UIAxes.ButtonDownFcn = createCallbackFcn(app, @UIAxesButtonDown2, true);
            app.UIAxes.Position = [299 174 466 298];

            % Create ImagingsessiondateDatePickerLabel
            app.ImagingsessiondateDatePickerLabel = uilabel(app.UIFigure);
            app.ImagingsessiondateDatePickerLabel.HorizontalAlignment = 'right';
            app.ImagingsessiondateDatePickerLabel.Position = [31 489 118 22];
            app.ImagingsessiondateDatePickerLabel.Text = 'Imaging session date';

            % Create ImagingsessiondateDatePicker
            app.ImagingsessiondateDatePicker = uidatepicker(app.UIFigure);
            app.ImagingsessiondateDatePicker.Position = [163 489 150 22];

            % Create SelectDICOMimagesButton
            app.SelectDICOMimagesButton = uibutton(app.UIFigure, 'push');
            app.SelectDICOMimagesButton.ButtonPushedFcn = createCallbackFcn(app,
@SelectDICOMimagesButtonPushed2, true);
            app.SelectDICOMimagesButton.Position = [30 336 182 23];
            app.SelectDICOMimagesButton.Text = 'Select DICOM images';

            % Create Lamp
            app.Lamp = uilamp(app.UIFigure);
            app.Lamp.Position = [224 337 20 20];

            % Create Switch
            app.Switch = uiswitch(app.UIFigure, 'slider');
            app.Switch.Items = {'', 'Switch on to segment images'};
            app.Switch.ValueChangedFcn = createCallbackFcn(app, @SwitchValueChanged2, true);
            app.Switch.Position = [29 287 45 20];
            app.Switch.Value = '';
```

```
        % Create ComputeDCEparametersButton
        app.ComputeDCEparametersButton = uibutton(app.UIFigure, 'push');
        app.ComputeDCEparametersButton.ButtonPushedFcn = createCallbackFcn(app,
@ComputeDCEparametersButtonPushed2, true);
        app.ComputeDCEparametersButton.FontSize = 16;
        app.ComputeDCEparametersButton.FontWeight = 'bold';
        app.ComputeDCEparametersButton.Position = [29 215 233 39];
        app.ComputeDCEparametersButton.Text = 'Compute DCE parameters';

        % Create UITable
        app.UITable = uitable(app.UIFigure);
        app.UITable.ColumnName = {'Column 1'; 'Column 2'; 'Column 3'; 'Column 4'};
        app.UITable.RowName = {};
        app.UITable.CellEditCallback = createCallbackFcn(app, @UITableCellEdit, true);
        app.UITable.Position = [54 71 680 52];

        % Create CloseappButton
        app.CloseappButton = uibutton(app.UIFigure, 'push');
        app.CloseappButton.ButtonPushedFcn = createCallbackFcn(app, @CloseappButtonPushed, true);
        app.CloseappButton.Position = [323 11 141 45];
        app.CloseappButton.Text = 'Close app';

        % Create SaveplotButton
        app.SaveplotButton = uibutton(app.UIFigure, 'push');
        app.SaveplotButton.ButtonPushedFcn = createCallbackFcn(app, @SaveplotButtonPushed, true);
        app.SaveplotButton.Position = [665 488 100 23];
        app.SaveplotButton.Text = 'Save plot';

        % Create TotalacquisitontimemmssEditFieldLabel
        app.TotalacquisitontimemmssEditFieldLabel = uilabel(app.UIFigure);
        app.TotalacquisitontimemmssEditFieldLabel.HorizontalAlignment = 'right';
        app.TotalacquisitontimemmssEditFieldLabel.Position = [30 431 160 22];
        app.TotalacquisitontimemmssEditFieldLabel.Text = 'Total acquisiton time (mm.ss)';

        % Create TotalacquisitontimemmssEditField
        app.TotalacquisitontimemmssEditField = uieditfield(app.UIFigure, 'text');
        app.TotalacquisitontimemmssEditField.ValueChangedFcn = createCallbackFcn(app,
@TotalacquisitontimemmssEditFieldValueChanged, true);
        app.TotalacquisitontimemmssEditField.Position = [198 431 64 22];

        % Create InjectionpointasmeasuramentnumberEditFieldLabel
        app.InjectionpointasmeasuramentnumberEditFieldLabel = uilabel(app.UIFigure);
        app.InjectionpointasmeasuramentnumberEditFieldLabel.HorizontalAlignment = 'right';
        app.InjectionpointasmeasuramentnumberEditFieldLabel.Position = [29 392 217 22];
        app.InjectionpointasmeasuramentnumberEditFieldLabel.Text = 'Injection point as measurament number';

        % Create Injectionpointasmeasuramentnumber
        app.Injectionpointasmeasuramentnumber = uieditfield(app.UIFigure, 'text');
        app.Injectionpointasmeasuramentnumber.ValueChangedFcn = createCallbackFcn(app,
@InjectionpointasmeasuramentnumberValueChanged, true);
        app.Injectionpointasmeasuramentnumber.Position = [256 392 35 22];

        % Create CopytablevaluesButton
        app.CopytablevaluesButton = uibutton(app.UIFigure, 'push');
        app.CopytablevaluesButton.ButtonPushedFcn = createCallbackFcn(app,
@CopytablevaluesButtonPushed, true);
        app.CopytablevaluesButton.Position = [655 140 110 23];
        app.CopytablevaluesButton.Text = 'Copy table values';

        % Show the figure after all components are created
```

```
            app.UIFigure.Visible = 'on';
        end
    end

    % App creation and deletion
    methods (Access = public)

        % Construct app
        function app = DCE_app

            % Create UIFigure and components
            createComponents(app)

            % Register the app with App Designer
            registerApp(app, app.UIFigure)

            % Execute the startup function
            runStartupFcn(app, @startupFcn)

            if nargout == 0
                clear app
            end
        end

        % Code that executes before app deletion
        function delete(app)

            % Delete UIFigure when app is deleted
            delete(app.UIFigure)
        end
    end
end
```

data_acquisition

```
function  [mri] = data_acquisition(mri,choice,option,paramSet)
% Author: Marco Mussato
% Date: 2022-12-01
%
% Matlab version: R2022b
%
% process_DICOM_data - reads DICOM images from a user-specified folder and saves them in a structure
%
% SYNTAX:
% mri = process_DICOM_data(choice)
%
% INPUTS:
% choice - a string indicating the type of MRI image to import and save. Can be either 'T1' or 'DCE'.
%
% OUTPUTS:
% mri - a structure containing the imported and saved MRI data, including images, image dimensions, and
FA/TR values (if available).
%

%% Saving main folder's path

% Handle the user's response to the dialog box
switch choice
```

```
    case 'T1'
        % Import images using the img_import function
        [imgMat,tot_rows,tot_columns,tot_slices,path] = img_import();

        % If the selected folder is empty, display an error message and exit
        if isempty(imgMat)
            uiwait(msgbox({'The selected folder is empty.'; 'Please select another folder.'},"Error","error"));
            return;
        else

            % Create the fields for the structure
            fields = ["alpha1","alpha2","b1"];

            if option == 1
                data = "FA1";
                mri.(fields(1)) = structureCreator(mri.(fields(1)), imgMat, tot_rows, tot_columns, tot_slices, 0, path,
data, 1,paramSet);
            elseif option == 2
                data = "FA2";
                mri.(fields(2)) = structureCreator(mri.(fields(2)), imgMat, tot_rows, tot_columns, tot_slices, 0, path,
data, 1,paramSet);
            else
                mri.(fields(3))= structureCreator(mri.(fields(3)), imgMat, tot_rows,  tot_columns, tot_slices, 0, path, [],
0,paramSet);
                % Resize the b1 image to have the same dimensions as the alpha1 image
                mri.(fields(3)).img = imresize(mri.b1.img,[mri.alpha1.rows mri.alpha1.columns]);

                % Update the dimensions of the b1 image to match the alpha1 image
                mri.(fields(3)).rows = mri.(fields(1)).rows;
                mri.(fields(3)).columns = mri.(fields(1)).columns;
            end

        end
    case 'DCE'
        % Import images using the img_import function
        [imgMat,tot_rows,tot_columns,tot_slices,~] = img_import();
        slice_group = 24;
        tot_acquisition = tot_slices/24;

        % Initialize a structure with a single field called "dce"
        mri = struct("dce",[]);
        % Populate the "dce" field of the structure with the imported images
        % using the structureCreator function
        mri.dce = structureCreator(mri.dce, imgMat, tot_rows, tot_columns, tot_slices, 0, [], [], []);
        mri.dce.img = reshape(mri.dce.img,[tot_rows,tot_columns,slice_group,tot_acquisition]);
        mri.dce.groupslice = slice_group;
        mri.dce.totacq = tot_acquisition;
end

end
```

img_import

```
function [imgMat,tot_rows,tot_columns,tot_slices,path] = img_import()
% Author: Marco Mussato
% Date: 2023-01-03
%
% Matlab version: 2022b
```

```
%
% img_import - Read DICOM files and store them as a 3D matrix.
%
% SYNTAX:
%   [imgMat,tot_rows,tot_columns,tot_slices] = img_import()
%
% INPUTS:
%   none (user is prompted to select one or more DICOM files using the uigetfile function)
%
% OUTPUTS:
%   imgMat:         3D matrix containing the DICOM image data
%   tot_rows:       integer representing the number of rows in each image
%   tot_columns:    integer representing the number of columns in each image
%   tot_slices:     integer representing the total number of slices
%
% Example:
%   [imgMat,tot_rows,tot_columns,tot_slices] = img_import()


% Prompt the user to select a folder containing the DICOM images
%           files = dir(uigetdir('S:\Shared\Ortho Project - Tendon Injury\MRI SESSIONS')); %select the folder
[file,path] = uigetfile('*.IMA*','Select One or More Files','MultiSelect', 'on');
% Check if the folder is empty
if isempty(file) % If the selected folder is empty, display an error message and exit
   uiwait(msgbox({'The selected folder is empty.'; 'Please select another folder.'},"Error","error"));
   return;
else
   %this for stores the DICOM's information and save all the image as a matrix
   %with MxNxD dimention, where MxN is the num of pixel in each image and D is
   %the total number of slices

   tot_slices= length(file); % Calculate the total number of slices
   for ii=1:tot_slices
      % Read the DICOM metadata for the current slice
      %                 imgInfo = dicominfo(fullfile(files(ii+2).folder,files(ii+2).name)); % Read the DICOM
metadata
      imgInfo = dicominfo(char(fullfile(path,file(ii))));
      % If this is the first slice, initialize the 'imgMat' matrix with the appropriate size
      if ii == 1
         tot_rows = imgInfo.Rows; % Get the number of rows in the image
         tot_columns = imgInfo.Columns; % Get the number of columns in the image
         imgMat = zeros(tot_rows,tot_columns,tot_slices); %create empty matrix that will store the data
         imgMat(:,:,ii) = dicomread(imgInfo); %saving first image inside the matrix
         f = waitbar(0,'Starting imaging importing...');
      else
         imgMat(:,:,ii) = dicomread(imgInfo);%saving the remaning images
         percentage = ii/tot_slices;
         waitbar(percentage,f,sprintf('Saving DICOM images %d%%...',int8(percentage*100)));
      end
   end
   waitbar(1,f,'All images have been imported!');
   pause(1)
   close(f)
end
```

structureCreator

```
function [mri] = structureCreator(mri,img,rows,columns,slices,FAcheck,path,data,noPy,paramSet)
```

```
%%Author: Marco Mussato
%Date: 2022-12-01
%
%Matlab version: R2022b
%
% create_mri_structure - creates a structure with MRI data, including images, FA value, and TR value
%
% SYNTAX:
%   mri = create_mri_structure(mri, img, rows, columns, slices, index, FAcheck, path, data)
%
% INPUTS:
%   mri: initial structure for the MRI data
%   img: matrix containing all the DICOM images
%   rows: number of rows in the image matrix
%   columns: number of columns in the image matrix
%   slices: number of slices in the image matrix
%   index: index of the current folder (FA1, FA2, or B1)
%   FAcheck: binary value indicating whether to include the FA value in the structure (1 to include, 0 otherwise)
%   path: specified path to the folder with DICOM images
%   data: define from which acquisition FA and TR has to be extracted
%
% OUTPUTS:
%   mri: structure containing MRI data, including images, image dimensions, FA value, and TR value


mri.img = img; % save image data in the 'img' field of the 'mri' structure
mri.rows = rows; % save number of rows in the image in the 'rows' field of the 'mri' structure
mri.columns = columns; % save number of columns in the image in the 'columns' field of the 'mri' structure
mri.slices = slices; % save number of slices in the image in the 'slices' field of the 'mri' structure

if FAcheck % check if flip angle information is available
   %saving pdf path
   pdfPath = dir([uigetdir() '/*.pdf']);
   %using py script to extract information
   py.PdfFileManager.DataExtractor(fullfile(pdfPath(1).folder,pdfPath(1).name),path,data)
   %loaging .mat file containing a structure with extracted information
   pdfInfo = load('Results.mat');

   %adding extracted info to the "mri" structure
   mri.FA = deg2rad(double(pdfInfo.FA)); % convert flip angle from degrees to radians and save it in the 'FA'
field of the 'mri' structure
   mri.TR =double(pdfInfo.TR); % save repetition time in the 'TR' field of the 'mri' structure
end

 if noPy
   mri.FA = deg2rad(paramSet(2));
   mri.TR = paramSet(1);
end

end
```

dce_computation

```
function [mri] = dce_computation(mri,ta,injMeasurement)
% Author: Marco Mussato
% Date: 2022-12-01
%
% Matlab version: R2022b
%
```

```
% The function dce_computation performs various computations on
% dynamic contrast-enhanced (DCE) MRI data, including data acquisition,
% segmentation, mean intensity extraction,
% and area under the curve (AUC) calculation.
%
% SYNTAX:
% dce_computation(choice)
%
% INPUTS:
% choice - (string) the user's input indicating the choice of sample (e.g. 'sample1')
%
% OUTPUTS:
% none (function has side effects: it produces a time-intensity plot
% of the right and left knee and displays the calculated AUCs)


% mri = data_acquisition(choice); % Acquire MRI data


%% Segmentation of the image
addpath("Masks/");
% Display a message box with instructions for the user
CreateStruct.Interpreter = 'tex';
CreateStruct.WindowStyle = 'modal';
text= '\fontsize{12} Select the file with the segmentation';
uiwait(msgbox(text,"DICOM Selection",CreateStruct));
[filename,~] = uigetfile('*.mat*','Select file to open');

% Load the segmentation from the selected file
labels = load(filename);
labels = labels.labels;

%Set time resolution of single group of slices
ta_min = floor(ta);
ta_sec = ta_min*59+ta;
mri.dce.timeres = ta_sec/mri.dce.totacq;

%Create time vector
mri.dce.timesamp = (0:mri.dce.totacq-4)*mri.dce.timeres/60;

%Call function to extract mean intensity values from MRI data
[mri] = dce_meanextraction(mri,labels,injMeasurement);

end
```

dce_meanextraction

```
function [mri] = dce_meanextraction(mri,labels,injMeasurement)
% Author: Marco Mussato
% Date: 2022-12-01
%
% Matlab version: R2022b
%
% The function dce_meanextraction is used to extract mean intensity values
% of the right and left knee ROI in a dynamic contrast enhanced (DCE) MRI dataset.
%
% SYNTAX:
% [mri] = dce_meanextraction(mri,labelsR,labelsL)
```

```
%
% INPUTS:
% mri: A structure containing the DCE MRI data,
% with fields such as 'img', 'dce', 'groupslice', 'totacq'
% labelsR: A binary 3D array of size [nRows,nColumns,nSlices],
% where nonzero values indicate the pixels belonging to the right knee ROI
% labelsL: A binary 3D array of size [nRows,nColumns,nSlices],
% where nonzero values indicate the pixels belonging to the left knee ROI
%
% OUTPUTS:
% mri: A structure containing the extracted mean intensity values,
% as well as the position of contrast agent (CA) injection and the area
% under the curve (AUC) for the right and left knee


% Preallocate variables for storing mean intensity values for the right and left knee
dce_intensity = zeros(1,mri.dce.totacq);

% Initialize variables for indexing
h=1;


% Find slices containing the ROI for right and left knee
for ii = 1:mri.dce.groupslice
   if sum(labels(:,:,ii),"all") % Check if any nonzero values in the labelsR array at the current slice
      index(h) = ii; % store the slice number
      h=h+1;
   end
end

dce_intSlice = zeros(length(index), mri.dce.totacq);

% Create a waitbar to indicate progress
f = waitbar(0,'Starting mean intensity values computation...');
pause(.3)

% Compute mean intensity values for each slice in the ROI for each acquisition
for ii = 1:mri.dce.totacq %select a temporal acquisiton every step
   percentage = ii/mri.dce.totacq;
   waitbar(percentage,f,sprintf('Computing mean intensity values for slice #%d',ii));
   dce_int = 0;

   for jj = 1:length(index)
      % find the row and column indices of the pixels with nonzero values in the 'labels' array at the current slice
      [rowindex, columnindex] = find(labels(:,:,index(jj))==1);
      % compute the mean intensity for the patellar tendon in the current set of slices for the current acquisition
      dce_int = dce_int + mean(mri.dce.img(rowindex,columnindex,index(jj),ii),'all');
      dce_intSlice(jj,ii) = mean(mri.dce.img(rowindex,columnindex,index(jj),ii),'all');
   end
   dce_intensity(1,ii) = dce_int/length(index);
end


waitbar(1,f,'Mean intensity computation completed');
pause(1)
close(f)

%filter and store the results
lenMeanVect = 4;
meanVect = ones(1,lenMeanVect)/lenMeanVect;
```

```
mri.dce.pxInt = conv(dce_intensity,meanVect,'valid'); %valid -> no zero padding

%compute AUC, Peak enhancement, Time to peak, Wash-in slope
mri.dce.params = dce_param_computation(mri.dce.pxInt,injMeasurement,mri.dce.timesamp);

end
```

dce_param_computation

```
function [params]=dce_param_computation(dce_intensity,injMeasurement,time)
% Author:
% Date: 2022-12-01
%
% Matlab version: R2022b
%
% This function compute the AUC of a given time-intensity curve,
% using the Sobel Edge Detection to define the onset
% time of the injection of contrast agent.
%
% SYNTAX:
% [CAinjPos,auc] = auc_computartion(dce_intensity,trsh)
%
% INPUTS:
% dce_intensity : time-intensity curve
% trsh : percentage of the maximum of the signal
%
% OUTPUTS:
% CAinjPos : onset time of the injection of contrast agent
% auc : area under the curve of the time-intensity plot

% Set treshold to 80% of the maximum of the signal
% thrsh = 0.9;

% Peak Enhancment
windowSize = 3;

mov_avg = movmean(dce_intensity(injMeasurement+windowSize:end-windowSize), [windowSize
windowSize]);  % Compute moving averages using 5 points before and after

diff_mov_avg = diff(mov_avg);  % Compute difference between consecutive moving averages
threshold = 0.125*max(diff_mov_avg);

washin_max_index = find(abs(diff_mov_avg) < threshold, 1);  % Find where this difference is less than your
threshold

washin_max_index = washin_max_index+windowSize+injMeasurement; %match the rigth index removing the
windowSize factor and injetion point

washin_max = dce_intensity(washin_max_index);

% AUC calculation
AUC = trapz(dce_intensity(injMeasurement:end));

% IAUC calculation

IAUC = trapz(dce_intensity(injMeasurement:washin_max_index));

% Time to peak calculation
```

```
peak_enhancment = washin_max-dce_intensity(injMeasurement);
timePeak = time(washin_max_index);

% Wash-in slope calculation
washinSlope = peak_enhancment/(timePeak-time(injMeasurement));


%% Saving values
% Saving values in structure under dce.params
params =
struct('CAinjPos',injMeasurement,'AUC',AUC,'IAUC',IAUC,'PeakEnhancment',peak_enhancment,'timePeak',tim
ePeak,'washinSlope',washinSlope);
end
```

References

(1) Sharma, P.; Maffulli, N. Tendon Injury and Tendinopathy: Healing and Repair. *The Journal of Bone & Joint Surgery* **2005**, *87* (1), 187–202. https://doi.org/10.2106/JBJS.D.01850.

(2) Snedeker, J. G.; Foolen, J. Tendon Injury and Repair – A Perspective on the Basic Mechanisms of Tendon Disease and Future Clinical Therapy. *Acta Biomaterialia* **2017**, *63*, 18–36. https://doi.org/10.1016/j.actbio.2017.08.032.

(3) James, R.; Kesturu, G.; Balian, G.; Chhabra, A. B. Tendon: Biology, Biomechanics, Repair, Growth Factors, and Evolving Treatment Options. *The Journal of Hand Surgery* **2008**, *33* (1), 102–112. https://doi.org/10.1016/j.jhsa.2007.09.007.

(4) Hopkins, C.; Fu, S.-C.; Chua, E.; Hu, X.; Rolf, C.; Mattila, V. M.; Qin, L.; Yung, P. S.-H.; Chan, K.-M. Critical Review on the Socio-Economic Impact of Tendinopathy. *Asia-Pacific Journal of Sports Medicine, Arthroscopy, Rehabilitation and Technology* **2016**, *4*, 9–20. https://doi.org/10.1016/j.asmart.2016.01.002.

(5) Wu, F.; Nerlich, M.; Docheva, D. Tendon Injuries: Basic Science and New Repair Proposals. *EFORT Open Reviews* **2017**, *2* (7), 332–342. https://doi.org/10.1302/2058-5241.2.160075.

(6) Weinreb, J. H.; Sheth, C.; Apostolakos, J.; McCarthy, M.-B.; Barden, B.; Cote, M. P.; Mazzocca, A. D. Tendon Structure, Disease, and Imaging. *Muscles Ligaments Tendons J* **2014**, *4* (1), 66–73.

(7) Hodgson, R. J.; O'Connor, P. J.; Grainger, A. J. Tendon and Ligament Imaging. *Br J Radiol* **2012**, *85* (1016), 1157–1172. https://doi.org/10.1259/bjr/34786470.

(8) Tang, C.; Chen, Y.; Huang, J.; Zhao, K.; Chen, X.; Yin, Z.; Heng, B. C.; Chen, W.; Shen, W. The Roles of Inflammatory Mediators and Immunocytes in Tendinopathy. *Journal of Orthopaedic Translation* **2018**, *14*, 23–33. https://doi.org/10.1016/j.jot.2018.03.003.

(9) Lian, Ø. B.; Engebretsen, L.; Bahr, R. Prevalence of Jumper's Knee among Elite Athletes from Different Sports: A Cross-Sectional Study. *Am J Sports Med* **2005**, *33* (4), 561–567. https://doi.org/10.1177/0363546504270454.

(10) Andres, B. M.; Murrell, G. A. C. Treatment of Tendinopathy: What Works, What Does Not, and What Is on the Horizon. *Clin Orthop Relat Res* **2008**, *466* (7), 1539–1554. https://doi.org/10.1007/s11999-008-0260-1.

(11) Voleti, P. B.; Buckley, M. R.; Soslowsky, L. J. Tendon Healing: Repair and Regeneration. *Annu. Rev. Biomed. Eng.* **2012**, *14* (1), 47–71. https://doi.org/10.1146/annurev-bioeng-071811-150122.

(12) Docheva, D.; Müller, S. A.; Majewski, M.; Evans, C. H. Biologics for Tendon Repair. *Advanced Drug Delivery Reviews* **2015**, *84*, 222–239. https://doi.org/10.1016/j.addr.2014.11.015.

(13) Magra, M.; Maffulli, N. Nonsteroidal Antiinflammatory Drugs in Tendinopathy: Friend or Foe. *Clinical Journal of Sport Medicine* **2006**, *16* (1), 1. https://doi.org/10.1097/01.jsm.0000194764.27819.5d.

(14) Thomopoulos, S.; Parks, W. C.; Rifkin, D. B.; Derwin, K. A. Mechanisms of Tendon Injury and Repair: TENDON INJURY AND REPAIR. *J. Orthop. Res.* **2015**, *33* (6), 832–839. https://doi.org/10.1002/jor.22806.
(15) Lui, P. P. Y.; Maffulli, N.; Rolf, C.; Smith, R. K. W. What Are the Validated Animal Models for Tendinopathy? *Scandinavian Journal of Medicine & Science in Sports* **2011**, *21* (1), 3–17. https://doi.org/10.1111/j.1600-0838.2010.01164.x.
(16) Jirkof, P. Side Effects of Pain and Analgesia in Animal Experimentation. *Lab Anim* **2017**, *46* (4), 123–128. https://doi.org/10.1038/laban.1216.
(17) Duchman, K. R.; Lemmex, D. B.; Patel, S. H.; Ledbetter, L.; Garrigues, G. E.; Riboh, J. C. The Effect of Non-Steroidal Anti-Inflammatory Drugs on Tendon-to-Bone Healing: A Systematic Review with Subgroup Meta-Analysis. *Iowa Orthop J* **2019**, *39* (1), 107–119.
(18) Su, B.; O'Connor, J. P. NSAID Therapy Effects on Healing of Bone, Tendon, and the Enthesis. *Journal of Applied Physiology* **2013**, *115* (6), 892–899. https://doi.org/10.1152/japplphysiol.00053.2013.
(19) Neeter, C.; Thomeé, R.; Silbernagel, K. G.; Thomeé, P.; Karlsson, J. Iontophoresis with or without Dexamethazone in the Treatment of Acute Achilles Tendon Pain. *Scandinavian Journal of Medicine & Science in Sports* **2003**, *13* (6), 376–382. https://doi.org/10.1046/j.1600-0838.2003.00305.x.
(20) Fredberg, U.; Bolvig, L.; Pfeiffer-Jensen, M.; Clemmensen, D.; Jakobsen, B.; Stengaard-Pedersen, K. Ultrasonography as a Tool for Diagnosis, Guidance of Local Steroid Injection and, Together with Pressure Algometry, Monitoring of the Treatment of Athletes with Chronic Jumper's Knee and Achilles Tendinitis: A Randomized, Double-blind, Placebo-controlled Study. *Scandinavian Journal of Rheumatology* **2004**, *33* (2), 94–101. https://doi.org/10.1080/03009740310004126.
(21) DaCruz, D. J.; Geeson, M.; Allen, M. J.; Phair, I. Achilles Paratendonitis: An Evaluation of Steroid Injection. *British Journal of Sports Medicine* **1988**, *22* (2), 64–65. https://doi.org/10.1136/bjsm.22.2.64.
(22) Maffulli, N.; Longo, U. G.; Denaro, V. Novel Approaches for the Management of Tendinopathy. *JBJS* **2010**, *92* (15), 2604. https://doi.org/10.2106/JBJS.I.01744.
(23) Hasslund, S.; Jacobson, J. A.; Dadali, T.; Basile, P.; Ulrich-Vinther, M.; Søballe, K.; Schwarz, E. M.; O'Keefe, R. J.; Mitten, D. J.; Awad, H. A. Adhesions in a Murine Flexor Tendon Graft Model: Autograft versus Allograft Reconstruction. *J. Orthop. Res.* **2008**, *26* (6), 824–833. https://doi.org/10.1002/jor.20531.
(24) Tang, Y.; Wang, Z.; Xiang, L.; Zhao, Z.; Cui, W. Functional Biomaterials for Tendon/Ligament Repair and Regeneration. *Regenerative Biomaterials* **2022**, *9*, rbac062. https://doi.org/10.1093/rb/rbac062.
(25) Huang, L.; Chen, L.; Chen, H.; Wang, M.; Jin, L.; Zhou, S.; Gao, L.; Li, R.; Li, Q.; Wang, H.; Zhang, C.; Wang, J. Biomimetic Scaffolds for Tendon Tissue Regeneration. *Biomimetics* **2023**, *8* (2), 246. https://doi.org/10.3390/biomimetics8020246.
(26) Russo, V.; El Khatib, M.; Prencipe, G.; Cerveró-Varona, A.; Citeroni, M. R.; Mauro, A.; Berardinelli, P.; Faydaver, M.; Haidar-Montes, A. A.; Turriani, M.; Di Giacinto, O.; Raspa, M.; Scavizzi, F.; Bonaventura, F.; Liverani, L.; Boccaccini, A. R.; Barboni, B. Scaffold-Mediated Immunoengineering as Innovative Strategy for Tendon Regeneration. *Cells* **2022**, *11* (2), 266. https://doi.org/10.3390/cells11020266.
(27) Yang, G.; Rothrauff, B. B.; Tuan, R. S. Tendon and Ligament Regeneration and Repair: Clinical Relevance and Developmental Paradigm. *Birth Defects Research Part C: Embryo Today: Reviews* **2013**, *99* (3), 203–222. https://doi.org/10.1002/bdrc.21041.
(28) Vasiliadis, A. V.; Katakalos, K. The Role of Scaffolds in Tendon Tissue Engineering. *JFB* **2020**, *11* (4), 78. https://doi.org/10.3390/jfb11040078.

(29) Wang, J. H.-C. Can PRP Effectively Treat Injured Tendons? *Muscles Ligaments Tendons J* **2014**, *4* (1), 35–37.
(30) Bokhari, A. R.; Murrell, G. A. C. The Role of Nitric Oxide in Tendon Healing. *Journal of Shoulder and Elbow Surgery* **2012**, *21* (2), 238–244. https://doi.org/10.1016/j.jse.2011.11.001.
(31) Gambito, E. D.; Gonzalez-Suarez, C. B.; Oquiñena, T. I.; Agbayani, R. B. Evidence on the Effectiveness of Topical Nitroglycerin in the Treatment of Tendinopathies: A Systematic Review and Meta-Analysis. *Archives of Physical Medicine and Rehabilitation* **2010**, *91* (8), 1291–1305. https://doi.org/10.1016/j.apmr.2010.02.008.
(32) Güleç, A.; Türk, Y.; Aydin, B. K.; Erkoçak, Ö. F.; Safalı, S.; Ugurluoglu, C. Effect of Curcumin on Tendon Healing: An Experimental Study in a Rat Model of Achilles Tendon Injury. *International Orthopaedics (SICOT)* **2018**, *42* (8), 1905–1910. https://doi.org/10.1007/s00264-018-4017-5.
(33) Jiang, D.; Gao, P.; Lin, H.; Geng, H. Curcumin Improves Tendon Healing in Rats: A Histological, Biochemical, and Functional Evaluation. *Connective Tissue Research* **2016**, *57* (1), 20–27. https://doi.org/10.3109/03008207.2015.1087517.
(34) Chen, Y.; Xie, Y.; Liu, M.; Hu, J.; Tang, C.; Huang, J.; Qin, T.; Chen, X.; Chen, W.; Shen, W.; Yin, Z. Controlled-Release Curcumin Attenuates Progression of Tendon Ectopic Calcification by Regulating the Differentiation of Tendon Stem/Progenitor Cells. *Materials Science and Engineering: C* **2019**, *103*, 109711. https://doi.org/10.1016/j.msec.2019.04.090.
(35) Peddada, K. V.; Peddada, K. V.; Shukla, S. K.; Mishra, A.; Verma, V. Role of Curcumin in Common Musculoskeletal Disorders: A Review of Current Laboratory, Translational, and Clinical Data. *Orthopaedic Surgery* **2015**, *7* (3), 222–231. https://doi.org/10.1111/os.12183.
(36) Alcelik, I.; Diana, G.; Craig, A.; Loster, N.; Budgen, A. Minimally Invasive Versus Open Surgery For Acute Achilles Tendon Ruptures A Systematic Review And Meta-Analysis. *Acta Orthop Belg* **2017**, *83* (3), 387–395.
(37) Gatz, M.; Driessen, A.; Eschweiler, J.; Tingart, M.; Migliorini, F. Open versus Minimally-Invasive Surgery for Achilles Tendon Rupture: A Meta-Analysis Study. *Arch Orthop Trauma Surg* **2021**, *141* (3), 383–401. https://doi.org/10.1007/s00402-020-03437-z.
(38) Maffulli, N.; Longo, U. G.; Spiezia, F.; Denaro, V. Minimally Invasive Surgery for Achilles Tendon Pathologies. *Open Access J Sports Med* **2010**, *1*, 95–103. https://doi.org/10.2147/oajsm.s7752.
(39) Wathen, C.; Foje, N.; Avermaete, T.; Miramontes, B.; Chapaman, S.; Sasser, T.; Kannan, R.; Gerstler, S.; Leevy, W. In Vivo X-Ray Computed Tomographic Imaging of Soft Tissue with Native, Intravenous, or Oral Contrast. *Sensors* **2013**, *13* (6), 6957–6980. https://doi.org/10.3390/s130606957.
(40) Hodgson, R. J.; O'Connor, P. J.; Grainger, A. J. Tendon and Ligament Imaging. *Br J Radiol* **2012**, *85* (1016), 1157–1172. https://doi.org/10.1259/bjr/34786470.
(41) Miller, T. T.; Shapiro, M. A.; Schultz, E.; Kalish, P. E. Comparison of Sonography and MRI for Diagnosing Epicondylitis. *J Clin Ultrasound* **2002**, *30* (4), 193–202. https://doi.org/10.1002/jcu.10063.
(42) Bruno, F.; Palumbo, P.; Arrigoni, F.; Mariani, S.; Aringhieri, G.; Carotti, M.; Natella, R.; Zappia, M.; Cipriani, P.; Giacomelli, R.; Di Cesare, E.; Splendiani, A.; Masciocchi, C.; Barile, A. Advanced Diagnostic Imaging and Intervention in Tendon Diseases. *Acta Bio Medica Atenei Parmensis* **2020**, *91* (8-S), 98–106. https://doi.org/10.23750/abm.v91i8-S.10007.

(43) Anz, A. W.; Lucas, E. P.; Fitzcharles, E. K.; Surowiec, R. K.; Millett, P. J.; Ho, C. P. MRI T2 Mapping of the Asymptomatic Supraspinatus Tendon by Age and Imaging Plane Using Clinically Relevant Subregions. *European Journal of Radiology* **2014**, *83* (5), 801–805. https://doi.org/10.1016/j.ejrad.2014.02.002.

(44) Dallaudière, B.; Trotier, A.; Ribot, E.; Verdier, D.; Lepreux, S.; Miraux, S.; Hauger, O. Three-Dimensional Ultrashort Echo Time (3D UTE) MRI of Achilles Tendon at 4.7T MRI with Comparison to Conventional Sequences in an Experimental Murine Model of Spondyloarthropathy. *J Magn Reson Imaging* **2019**, *50* (1), 127–135. https://doi.org/10.1002/jmri.26569.

(45) Fukawa, T.; Yamaguchi, S.; Watanabe, A.; Sasho, T.; Akagi, R.; Muramatsu, Y.; Akatsu, Y.; Katsuragi, J.; Endo, J.; Osone, F.; Sato, Y.; Okubo, T.; Takahashi, K. Quantitative Assessment of Tendon Healing by Using MR T2 Mapping in a Rabbit Achilles Tendon Transection Model Treated with Platelet-Rich Plasma. *Radiology* **2015**, *276* (3), 748–755. https://doi.org/10.1148/radiol.2015141544.

(46) Grosse, U.; Springer, F.; Hein, T.; Grözinger, G.; Schabel, C.; Martirosian, P.; Schick, F.; Syha, R. Influence of Physical Activity on T1 and T2* Relaxation Times of Healthy Achilles Tendons at 3T. *Journal of Magnetic Resonance Imaging* **2015**, *41* (1), 193–201. https://doi.org/10.1002/jmri.24525.

(47) Malmgaard-Clausen, N. M.; Tran, P.; Svensson, R. B.; Hansen, P.; Nybing, J. D.; Magnusson, S. P.; Kjær, M. Magnetic Resonance T2* Is Increased in Patients With Early-Stage Achilles and Patellar Tendinopathy. *Journal of Magnetic Resonance Imaging* **2021**, *54* (3), 832–839. https://doi.org/10.1002/jmri.27600.

(48) Szaro, P.; Nilsson-Helander, K.; Carmont, M. MRI of the Achilles Tendon-A Comprehensive Pictorial Review. Part One. *Eur J Radiol Open* **2021**, *8*, 100342. https://doi.org/10.1016/j.ejro.2021.100342.

(49) Wengler, K.; Fukuda, T.; Tank, D.; Komatsu, D. E.; Paulus, M.; Huang, M.; Gould, E. S.; Schweitzer, M. E.; He, X. In Vivo Evaluation of Human Patellar Tendon Microstructure and Microcirculation with Diffusion MRI. *Journal of Magnetic Resonance Imaging* **2020**, *51* (3), 780–790. https://doi.org/10.1002/jmri.26898.

(50) Ariyachaipanich, A.; Bae, W.; Statum, S.; Chung, C. Update on MRI Pulse Sequences for the Knee: Imaging of Cartilage, Meniscus, Tendon, and Hardware. *Semin Musculoskelet Radiol* **2017**, *21* (02), 045–062. https://doi.org/10.1055/s-0037-1599209.

(51) Trudel, G.; Duchesne-Bélanger, S.; Thomas, J.; Melkus, G.; Cron, G. O.; Larson, P. E. Z.; Schweitzer, M.; Sheikh, A.; Louati, H.; Laneuville, O. Quantitative Analysis of Repaired Rabbit Supraspinatus Tendons (± Channeling) Using Magnetic Resonance Imaging at 7 Tesla. *Quant Imaging Med Surg* **2021**, *11* (8), 3460–3471. https://doi.org/10.21037/qims-20-1343.

(52) Trudel, G.; Melkus, G.; Cron, G. O.; Louati, H.; Sheikh, A.; Larson, P. E. Z.; Schweitzer, M.; Lapner, P.; Uhthoff, H. K.; Laneuville, O. Imaging of the Rabbit Supraspinatus Enthesis at 7 Tesla: A 4-Week Time Course after Repair Surgery and Effect of Channeling. *Journal of Magnetic Resonance Imaging* **2017**, *46* (2), 461–467. https://doi.org/10.1002/jmri.25589.

(53) Fischer, C.; Miska, M.; Jung, A.; Weber, M.-A.; Saure, D.; Schmidmaier, G.; Weimer, A.; Moghaddam, A.; Doll, J. Posttraumatic Perfusion Analysis of Quadriceps, Patellar, and Achilles Tendon Regeneration With Dynamic Contrast-Enhanced Ultrasound and Dynamic Contrast-Enhanced Magnetic Resonance Imaging. *Journal of Ultrasound in Medicine* **2021**, *40* (3), 491–501. https://doi.org/10.1002/jum.15424.

(54) Gatehouse, P. D.; Thomas, R. W.; Robson, M. D.; Hamilton, G.; Herlihy, A. H.; Bydder, G. M. Magnetic Resonance Imaging of the Knee with Ultrashort TE Pulse Sequences.

Magnetic Resonance Imaging **2004**, *22* (8), 1061–1067. https://doi.org/10.1016/j.mri.2004.08.018.
(55) Kijowski, R.; Wilson, J. J.; Liu, F. Bicomponent Ultrashort Echo Time T2* Analysis for Assessment of Patients with Patellar Tendinopathy: Ultrashort TE T2* Analysis of Tendinopathy. *J. Magn. Reson. Imaging* **2017**, *46* (5), 1441–1447. https://doi.org/10.1002/jmri.25689.
(56) Koff, M. F.; Pownder, S. L.; Shah, P. H.; Yang, L. W.; Potter, H. G. Ultrashort Echo Imaging of Cyclically Loaded Rabbit Patellar Tendon. *J Biomech* **2014**, *47* (13), 3428–3432. https://doi.org/10.1016/j.jbiomech.2014.08.018.
(57) Krämer, M.; Maggioni, M. B.; Brisson, N. M.; Zachow, S.; Teichgräber, U.; Duda, G. N.; Reichenbach, J. R. T1 and T2* Mapping of the Human Quadriceps and Patellar Tendons Using Ultra-Short Echo-Time (UTE) Imaging and Bivariate Relaxation Parameter-Based Volumetric Visualization. *Magnetic Resonance Imaging* **2019**, *63*, 29–36. https://doi.org/10.1016/j.mri.2019.07.015.
(58) Liu, F.; Kijowski, R. Assessment of Different Fitting Methods for In-Vivo Bi-Component T2* Analysis of Human Patellar Tendon in Magnetic Resonance Imaging. *Muscles Ligaments Tendons J* **2017**, *7* (1), 163–172. https://doi.org/10.11138/mltj/2017.7.1.163.
(59) Gudbjartsson, H.; Patz, S. The Rician Distribution of Noisy Mri Data. *Magn. Reson. Med.* **1995**, *34* (6), 910–914. https://doi.org/10.1002/mrm.1910340618.
(60) Papp, D.; Breda, S. J.; Oei, E. H. G.; Poot, D. H. J.; Kotek, G.; Hernandez-Tamames, J. A. Fractional Order vs. Exponential Fitting in UTE MR Imaging of the Patellar Tendon. *Magnetic Resonance Imaging* **2020**, *70*, 91–97. https://doi.org/10.1016/j.mri.2020.04.005.
(61) Pownder, S. L.; Hayashi, K.; Lin, B. Q.; Meyers, K. N.; Caserto, B. G.; Breighner, R. E.; Potter, H. G.; Koff, M. F. Differences in the Magnetic Resonance Imaging Parameter T2* May Be Identified during the Course of Canine Patellar Tendon Healing: A Pilot Study. *Quant Imaging Med Surg* **2021**, *11* (4), 1234–1246. https://doi.org/10.21037/qims-20-684.
(62) van der Heijden, R. A.; Poot, D. H. J.; Ekinci, M.; Kotek, G.; van Veldhoven, P. L. J.; Klein, S.; Verhaar, J. A. N.; Krestin, G. P.; Bierma-Zeinstra, S. M. A.; van Middelkoop, M.; Oei, E. H. G. Blood Perfusion of Patellar Bone Measured by Dynamic Contrast-Enhanced MRI in Patients with Patellofemoral Pain: A Case-Control Study. *J Magn Reson Imaging* **2018**, *48* (5), 1344–1350. https://doi.org/10.1002/jmri.26174.
(63) Chang, E. Y.; Du, J.; Chung, C. B. UTE Imaging in the Musculoskeletal System. *Journal of Magnetic Resonance Imaging* **2015**, *41* (4), 870–883. https://doi.org/10.1002/jmri.24713.
(64) Naeije, R. Treprostinil for Pulmonary Hypertension. *VHRM* **2008**, *Volume 4*, 507–513. https://doi.org/10.2147/VHRM.S2477.
(65) Feldman, J.; Habib, N.; Fann, J.; Radosevich, J. J. Treprostinil in the Treatment of Pulmonary Arterial Hypertension. *Future Cardiology* **2020**, *16* (6), 547–558. https://doi.org/10.2217/fca-2020-0021.